Master Thesis in Energy
Study specialization: Renewable Energy - Environmental Consequences of Renewable Energy

Influence of Offshore Wind Farms on Primary Production in the North Sea

Ingvild Øijorden

June 2016

UNIVERSITY OF BERGEN
GEOPHYSICAL INSTITUTE

Abstract

The less studied environmental consequences of power production from offshore wind energy on the marine ecosystem dynamics, are studied through investigation of response on primary production. An idealized wind farm parameterization is developed based on a theoretical approach by (Brostrom, 2008), giving a two-dimensional wind stress pattern of reduced wind stress downstream of a wind farm. The method is modified to simulate a number of offshore wind farms in the North Sea with a variable wind forcing. The wind farm parameterization is developed for the well known bio-physical model ECOSMO (ECOSystem MOdel). The wind stress field forcing the model is modified by the wind farm parameterization, giving a modified wind stress field of reduced wind stress downstream of wind farms. Different model runs for year 2008, including the parameterization with different maximum wind stress deficit and for different setup of wind farms in the North Sea, are compared to a reference run. The primary producers Flagellates and Diatoms are investigated and the physical state variables temperature and salinity are used to study stratification and mixing of the North Sea during the year.

The wind farm parameterization creates the desired wind stress deficit pattern from (Brostrom, 2008) for different wind speeds and directions, where larger wind farms results in a stronger and wider wake. Modelled annual total primary production in the North Sea for year 2008 is only weakly effected by wind farm implementation by a few percent increase in production. However greater geographical variations in primary production are found. Both areas of increased and decreased production due to wind farm implementation in the North Sea are found for daily, monthly and yearly means, of order 80 % change in production. The large geographical change in distribution of primary production is expected to effect higher trophic levels.

Acknowledgements

I wish to thank my supervisor Peter Haugan and my assistant supervisor Corinna Schrum for giving me the opportunity to study an interesting and less studied topic.

I thank Peter Haugan for great help with ideas for the wind farm parameterization code and helpful corrections on the final text. I also thank Corrina Schrum for giving me the opportunity to use the numerical model ECOSMO and for discussing the model and dynamics of the North Sea.

Rocio Castano Primo deserves a great thanks for providing the ECOSMO scripts in addition to helpful shell scripts and for indispensable help with matlab, ECOSMO runs and post-processing of output data. I also thank Ute Daewel and Corinna Schrum for help with technical modelling issues.

Finally I wish to thank my fellow students for five good years at Geofysen, with long lunches, coffee breaks and especially the ice cream breaks in the sun. I also thank my family and friends for help and support during this year.

Contents

List of Figures

List of Tables

List of Abbreviations

CPU	Central Processing Unit
DOM	Dissolved organic matter
ECOSMO	ECOSystem MOdel
HAMSOM	HAMburg Shelf Ocean Model
KE	Kinetic energy
MABL	Marine atmospheric boundary layer
METRAS	MEsoscale TRAnsport and Stream model
MLD	Mixed layer depth
NPZD	Nutrient, Phytoplankton, Zooplankton, Detritus
NW	North-west
OML	Oceanic mixed layer
OWE	Offshore wind energy
OWF	Offshore wind farm
PEA	Potential energy anomaly
TKE	Turbulence kinetic energy
TVD	Total Variation Diminishing
WOA	World Ocean Atlas
WRF	Weather Research Forecasting model

Chapter 1

Introduction

At the United Nations Climate Change Conference in December 2015, a global agreement was made to avoid the global temperature from rising more than 1.5-2 °C. For the worlds countries to be able to cut their emissions, renewable energy is reckoned as one of the main contributors in making this goal achievable (Eurostat, 2015). A legally binding target of at least 27 % renewable energy by 2030, was set by the European Union in 2014. Wind energy is expected to take a large share of the electricity generation, where the majority of planned offshore wind farms (OWF) are located in the North Sea (European Wind Energy Association, 2015).

In Europe the North Sea (Fig. 1.1) is a preferable area for extraction of offshore wind energy (OWE) due to reliable wind supply and shallow water depth. However in the busy North Sea, an increasing number of OWFs will meet conflicting activities, such as shipping, oil and gas extraction, fisheries, cables and pipelines, military activities, sand extraction and nature conservations (Jongbloed et al., 2014). The study by Jongbloed et al. (2014) examined the effects of OWE on the marine users mentioned above. It was shown possible for OWE to co-exist with nature conservation and wild life under certain conditions. For the other mentioned activities co-existence with OWE was shown to be limited or non-existent.

Environmental consequences of OWF, including nature conservations and wild life, has been studied to some extent. The study by Bailey et al. (2014) evaluated environmental impacts of OWF and claimed that the main environmental consequences related to OWE are noise from pile driving, risk of collisions, changes to benthic and pelagic

habitats, alternations to food webs, pollution from increased vessel traffic and release of pollution from seabed sediments. Noise from pile driving seemed to have the largest impact on marine mammals in the form of migrating away from the construction cite. Suspended particulate matter has been observed in wakes downstream of wind turbines. This can lead to reduced light conditions and affect the local primary production (Vanhellemont and Ruddick, 2014). Still there are many unknown aspects related to response of marine species and population level impacts. As Bailey et al. (2014) concluded, there is a need of investigating biological impacts in a population context, including natural variations and anthropogenic drivers like fisheries.

Other consequences of extended use of OWE are possible changes to the local and global meteorology. Paskyabi and Fer (2012) found that several large wind farms located within the same area can possibly create changes in temperature, distribution of clouds and precipitation. To closely examine the effects of OWFs on the local wind climate is therefore important. This is done through studies of wake effects downstream of a wind farm, e.g. (Christiansen and Hasager, 2005; Calaf et al., 2010; Fitch et al., 2012, 2013; Boettcher et al., 2015).

The motivation for this thesis was to get more knowledge about the less studied environmental consequences of OWFs, regarding possible changes in the marine ecosystem. The focus was to get an understanding of the ocean response to changes in wind forcing due to OWFs in the North Sea and to investigate the changes in primary production and physical state variables with possible effect on ecosystem dynamics. Fitch et al. (2012) studied the effect of OWF implementation on the atmospheric boundary layer, while Brostrom (2008); Paskyabi and Fer (2012); Paskyabi (2015); Ludewig (2015) investigated response of OWF implementation on the upper ocean. However, as far as we know, effects on marine ecosystems have not yet been modelled using a coupled bio-physical numerical model. In this thesis a well known ocean model ECOSMO (ECOSystem MOdel) was used to investigate the state of the North Sea including a wind farm parameterization. A wind farm parameterization based on a theoretical method by (Brostrom, 2008), was developed to create wind stress deficit due to a number of wind farms in the North Sea. Earlier the theoretical method has only been used to investigate one idealized wind farm, but here developed for use in a numerical model forced by real

wind conditions. The parameterization is simplified and describes an idealized wind stress deficit by wind farms, not including changes in turbulence intensity. However the aim of this study is to investigate the basic response of the upper ocean to development of OWFs in the North Sea and possible consequences on primary production.

This thesis consists of a chapter describing the necessary background information, a chapter giving a general description of the numerical model ECOSMO and a chapter providing the wind farm parameterization with validation and model setup for the runs of ECOSMO used in this thesis. Then the results are presented and discussed followed by a conclusion and outlook for further work.

Figure 1.1: Map of the North Sea (Halava, 2010).

Chapter 2

Background and theory

2.1 Characteristics of atmosphere-ocean interactions

2.1.1 Marine atmospheric boundary layer

The atmospheric boundary layer is defined as the part of the troposphere that is directly influenced by the presence of the surface of the earth (Stull, 1989). The marine atmospheric boundary layer (MABL) is directly influenced by the ocean surface and is mainly divided in two regions, the constant flux layer interacting with the ocean surface and the overlying free atmosphere. The constant flux layer, also called the surface layer, is primarily dominated by small-scale turbulent eddies that are responsible for the momentum, heat and moisture transport (Toba and Jones, 2001). Turbulent motion is the fluctuating part of a velocity flow that are deviating from the mean flow, which together gives the total velocity. Kinetic energy (KE) is continuously transmitted to smaller scales of motion until molecular viscosity resists the motion and dissipates the energy to heat (Mann, 2006).

2.1.1.1 Shear stress

Important in the MABL is the flux of momentum across the ocean surface. This rate of transport of momentum from the wind to the ocean currents is called the surface shear stress, a drag force per unit area at the sea surface (Toba and Jones, 2001). The surface waves also transport horizontal momentum from the wind to the ocean. Breaking waves

transfers KE to the underlying water. Estimates of the rate of transport of KE from the wind to the ocean are given by τu_s, where u_s is the drift speed of the surface water and τ is the wind stress on the sea surface given by Equation 2.1, where V_a is the wind speed, often 10 m above the mean sea surface, and c_{da} is the drag coefficient that increases with wind speed (Thorpe, 2007). The density of air, ρ_a, is here included in Equation 2.2.

$$\tau = c_{da} V_a |V_a|, \tag{2.1}$$

A constant drag coefficient is often used, however Equation 2.2 represents wind stress dependent on wind speed (Schrum and Backhaus, 1999).

$$c_{da} = \rho_a (1.18 + 0.016|V_a|) 10^{-3} \tag{2.2}$$

2.1.1.2 Velocity profile

The velocity profile in the surface layer usually changes logarithmically with height, as the wind speed becomes zero near the surface due to frictional drag. Above the boundary layer the free atmosphere is not affected by frictional drag and the winds are nearly geostrophic (Stull, 1989). Conversion from geostrophic winds to 10 m wind speed was used in the wind farm parameterization developed for this thesis presented in Section 4.1. Equations for the conversion is therefore given in this section.

The velocity profile depends on surface stress and surface roughness, given by Equation 2.3, where u_z is the velocity at height z, u_* is the friction velocity, κ is the von karman constant of value 0.4 and z_0 is the roughness length dependent on wind- and sea conditions (Stull, 1989).

$$u_z = \frac{u_*}{\kappa} ln(\frac{z}{z_0}) \tag{2.3}$$

The relation between the upper level winds and surface winds are described by formulas from dimensional analysis given in (Holmes, 2015). The geostrophic drag coefficient C_g is given by Equation 2.4 where U_g is the geostrophic wind. The Rossby number R_0 is the ratio of the inertial to Coriolis forces given by Equation 2.5, where f is the Coriolis parameter. f is given by $f = 2\Omega sin\lambda$ where Ω is the Earth's rotation rate of $7.2 \times 10^{-5} s^{-1}$ and λ is the latitude (Marshall and Plumb, 2007). Full-scale measurements

gave the relationship in Equation 2.6 proposed by Davenport (1963).

$$C_g = \frac{u_*}{U_g}, \tag{2.4}$$

$$R_0 = \frac{U_g}{f z_0} \tag{2.5}$$

$$C_g = 0.16 R_0^{-0.09}, \tag{2.6}$$

From these equations an expression for the friction velocity including the geostrophic wind is derived, given by Equation 2.7.

$$u_* = 0.16 U_g (\frac{U_g}{f z_0})^{-0.09} \tag{2.7}$$

The Charnock relation for aerodynamic roughness length produces a drag coefficient that increases with wind speed, Equation 2.8 (Toba and Jones, 2001).

$$z_0 = a_c \frac{u_*^2}{g} \tag{2.8}$$

The empirical constant, a_c, is usually 0.018 for the open ocean and about 0.016 for near-coastal areas. The latter is used in this thesis for the North Sea. Combining Equation 2.7 and 2.8 gives a relation for u_* including U_g given by Equation 2.9.

$$u_* = (0.16 U_g (\frac{U_g g}{0.016 f})^{-0.09})^{\frac{1}{0.82}} \tag{2.9}$$

The logarithmic wind Equation 2.3 combined with the Charnock relation (Eq. 2.8) gives wind speed at a reference height 10 m given by Equation 2.10.

$$u_{10} = \frac{u_*}{\kappa} ln \frac{10 g}{0.016 u_*^2} \tag{2.10}$$

Equation 2.9 and 2.10 can be used to calculate wind speed at 10 m height from geostrophic wind speed (Toba and Jones, 2001).

2.1.2 Oceanic Mixed Layer

The oceanic mixed layer (OML) is the upper ocean boundary layer which is affected by the overlying atmosphere through air-sea interactions. The layer is stirred by winds and convection and has relatively uniform properties in the vertical. The main input of energy from the atmosphere to the ocean is the wind stress. This energy mainly goes into driving surface gravity waves and the turbulent motions within the OML (Thorpe, 2007).

Below the OML the temperature decreases with depth and at the depth where the range of change in temperature is large, is called the thermocline. The density increases below the OML and the pycnocline is located where the rate of change in density is large (Stewart, 2008).

The mixed layer depth (MLD) varies throughout the day and year because of variation in ocean heat gain and mixing energy gain. Loss of oceanic energy at the surface can be explained by evaporation and long-wave radiation. These factors are approximately constant during a day, thus the diurnal difference is caused by the ocean heat gain which is zero during the night and having a maximum value at noon. Seasonal differences are characterized by a deepening of the OML during winter, this because of increased turbulence due to greater wind speed and because of downward mixing by convection due to cooling of surface water. In spring a diurnal and seasonal thermocline is developed and during spring and summer the depth of the seasonal thermocline is decreasing as the upper OML becomes more stable. The diurnal OML decreases in this period. In late summer and towards winter the seasonal thermocline grows deeper and the diurnal OML tends to disappear (Mann, 2006).

There are different methods available for calculation of the MLD based on the physical parameters, temperature, salinity and density. A gradient method requires the profiles of the chosen parameter to have sharp gradients (de Boyer Montégut et al., 2004). A difference criterion depends on a critical value of the chosen parameter. In G. Monterey (1997) the different thresholds was given as the difference from the ocean surface of 0.5 °C as the temperature criterion, 0.125 [sigma units] as a density criterion and a variable density change corresponding to a temperature change of 0.5 °C. Density, ρ is usually measured in $[kgm^{-3}]$ and is often referred to as sigma-T (σ_T), a dimensionless number

given by $\rho - 1000$, referred to as sigma units (Thorpe, 2007). In the North Sea a gradient method is a suitable approach, with a threshold of a temperature gradient larger than 0.5 °C (Schrum et al., 2003).

To get information about how strong the stratification is, potential energy anomaly (PEA), ϕ, $[Jm^{-3}]$ given by Equation 2.11, can be used to calculate the amount of work required to have complete mixing per unit of volume of the OML.

$$\phi = \frac{1}{H}\int_{-h}^{\eta}(\bar{\rho} - \rho)gz\mathrm{d}z \tag{2.11}$$

In Equation 2.11 H is the depth of the water column (H=h+η), h is the sea bed, η is the sea surface elevation, ρ is the density of the water column, $\bar{\rho}$ is the depth averaged density, g is the gravitational acceleration and z is the vertical coordinate (de Boer et al., 2008).

2.2 Characteristics of the North Sea

The North Sea is a shelf sea, which makes the topography (Fig. 2.1) important when investigating properties of the water columns. It is characterized having the deepest area outside the coast of Norway, the Norwegian Trench, by shallow areas from the shallow Dogger Bank towards the coast of the continental Europe and the south part of the British Isles, while deeper grounds are found north of Dogger Bank offshore of the north parts of Britain (Rodhe et al., 2006).

2.2.1 Hydro- and thermodynamics

The North Sea is a freshwater influenced sea with inflow from freshwater runoff and net surplus of precipitation. It has open boundaries to the Atlantic Ocean through the wide northern boundary and the English Channel in south-west, with inflow of saline water. This results in a mean salinity of around 34 PSU (Schrum and Backhaus, 1999). The North Sea is therefore characterized by strong fronts and gradients between fresh and saline water (Barthel et al., 2012). The circulation in the North Sea is cyclonic and the water is renewed within one year, on average (Rodhe et al., 2006). The prevailing wind direction controls the general circulation (Fig. 2.2). Westerly winds gives the cyclonic

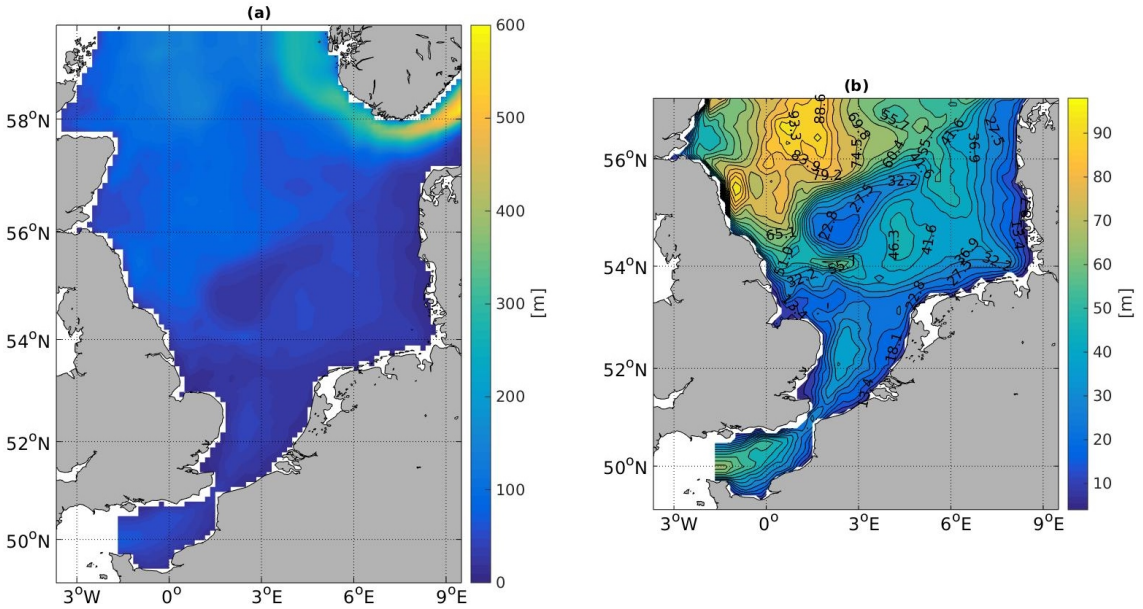

Figure 2.1: Modelled topography of the North Sea [m] from the numerical model ECOSMO, where a) includes the deep Norwegian Trench and b) shows more detailed topography of central and south North Sea.

circulation, while occasionally the circulation reverses with easterly winds and states of stagnation appears for north-westerly and south-easterly winds (Sündermann and Pohlmann, 2011). Tidal waves enter through the open northern boundary, travels south along the British Isles, follows along the Dutch, German and Danish coast and leaves the sea along the Norwegian coast. Tidal waves also enter through the English Channel south in the North Sea. Tide-topography interaction creates a cyclonic residual circulation and induce turbulent mixing (Nauw et al., 2015).

The thermodynamics of the North Sea is characterized by a positive net heat flux to the ocean in summer, where the oceanic heat content is increasing. During winter a slow release to the atmosphere is taking place. The water in the North Sea, except the Norwegian Trench, is then totally mixed by convection, and the release of heat continues until the end of the cooling period (Schrum and Backhaus, 1999). Due to heating in summer and less wind intensity, the central North Sea becomes stratified, while along the coast in the southern and western North Sea the tidal-induced turbulent mixing is strong enough to maintain the vertical mixing throughout the year (Rodhe et al., 2006).

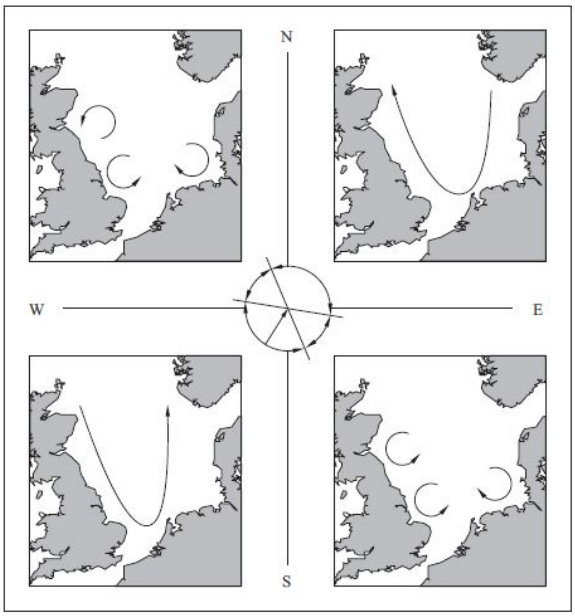

Figure 2.2: Wind driven circulation in the North Sea for different prevailing wind directions. Lower left panel shows a cyclonic circulation from south-westerly winds, upper right panel shows the reverse circulation for north-easterly winds and the upper left and lower right panels shows state of stagnation (Sündermann and Pohlmann, 2011).

The boundaries between the stratified deeper water and the tidal-induced mixed water at the continental shelves are called tidal fronts (Mann, 2006).

2.2.2 Primary production and physical impact

Phytoplankton are at the bottom of the food chain, as primary producers. Primary production is dependent on light and nutrients. In the North Sea the production is supported by the inflow of nutrient rich water from the Atlantic Ocean and from anthropogenic nutrients added in the south. Little nutrients are lost to sedimentation or deep water transport, because of the shallow depth, high oxygen level and winter convection, which returns remineralized nutrients to the water column. In winter the hours of daylight are limited and in the well mixed water limited phytoplankton are located in the euphotic zone. Therefore decay and remineraliztion processes dominate, primary production is low and the nutrient level increase (Rodhe et al., 2006). Sverdrup (1953) developed a critical depth hypothesis describing the onset of spring bloom as a function of depth of mixing. The compensation depth is the depth where respiration and produc-

tion is in balance and the critical depth is the depth where the integrated production equals the integrated respiration in the water column above the given depth (Slagstad, 1992). In spring when the increased heating and decreased wind mixing creates a shallow enough seasonal MLD, and the critical depth exceeds the depth of the MLD, a spring bloom occurs of rapid increase in primary production (Rodhe et al., 2006).

In areas where the water is fully mixed by tidal streams, the primary production is held large through the summer, compared to production in seasonally stratified areas. The euphotic zone in the well mixed water is held nutrient rich by tidal-induced bottom stress. In stratified water the euphotic zone can become nutrient depleted after the spring bloom (Rodhe et al., 2006).

Intra- and inter annual variations in stratification, timing and intensity of phytoplankton bloom in the North Sea was investigated by Nielsen and John (2003), showing substantial variations within and between years, dependent on the meteorological forcing. Year 1997 with strong stability had low values of mean-depth chlorophyll concentrations, while year 1998 with weak stability had high depth-mean chlorophyll concentrations as a result of increased phytoplankton biomass and a continued input of nutrients. Events of higher wind intensity or cooling, resulted in increased level of entrained nutrient rich water into the euphotic zone.

2.3 Offshore wind energy

With the demand of a larger share of renewable energy in Europe, OWE in the North Sea has had a rapid growth (Bailey et al., 2014). Stronger and more stable wind resources are found offshore, because of a lower surface roughness at the sea than over land. This results in a lower turbulence intensity and wind shear, favouring OWE extraction over onshore wind farms (Manwell et al., 2010). An OWF consists of a number of wind turbines in an array. A wind turbine has three main parts, a tower, a nacelle on top of the tower containing the generator, and the rotor, normally with tree blades attached to a hub on the nacelle (Thomsen, 2012).

Wind turbines are designed to extract kinetic energy from the wind. The energy extracted is measured by the thrust coefficient C_T. It is transformed into electrical energy,

determined by the power coefficient C_P, non-productive drag that produces turbulence kinetic energy (TKE) and mechanical and electrical losses (Fitch et al., 2012). Due to the atmospheric loss of kinetic energy, the wind passing through the turbine slows down. The decrease in wind speed and increase in turbulence intensity are characteristic for the air flow behind the wind turbine and are called the wind wake effect. Turbines within the same wind farm will be affected by the wind wakes from the other turbines and the power output of turbines in the wake area will be reduced. Wind farms located close to each other will also be affected by this phenomenon called wind shadowing (Burton, 2011). Behind the turbines the wind wake is being diffused at the boundaries by turbulence, while the rate of diffusion is determined by the stability of the atmosphere. The wake effect downstream of a wind farm is therefore dependent on the wind speed, the atmospheric stability and number of turbines in operation (Christiansen and Hasager, 2005).

A power curve of a wind turbine (Fig. 2.3) represents the turbine performances of expected power output as a function of wind speed. It is separated in different parts by

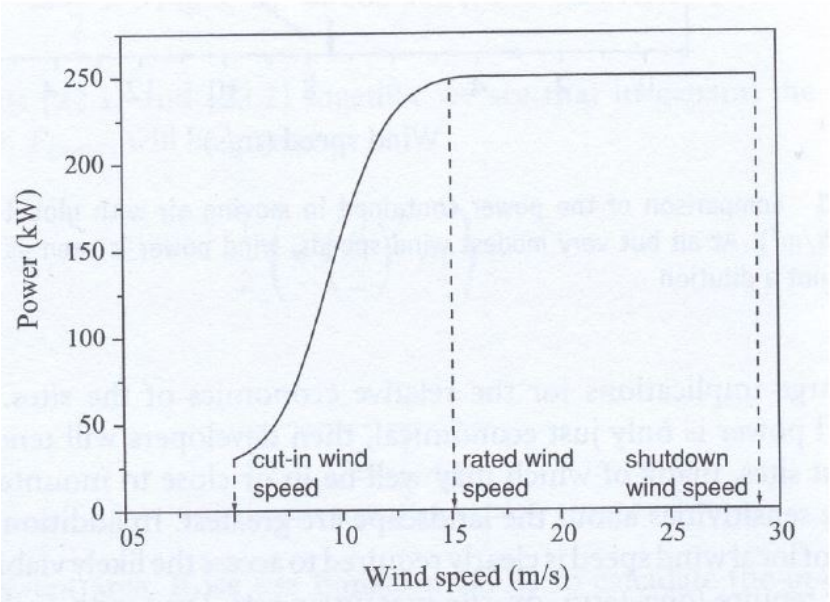

Figure 2.3: Schematic representation of a power curve showing cut-in, rated and cut-out wind speed (Coley, 2011).

the cut-in wind speed, rated wind speed and cut-out wind speed. Below cut-in speed the winds are too small to produce energy and above cut-out speed the loads on the

turbine are too large to have it in operation due to safety reasons. The power increases with wind speed between cut-in and rated speed. At rated speed the turbine has reached its rated power, a limit for the electrical generator. For wind speeds between the rated and cut-out speed the power is held constant at rated power, usually by adjusting the blade angle, called active pitch control (Das, 2014).

2.3.1 Extracting power

The kinetic energy of the wind, KE, is dependent on the highly variable wind velocity **v**, (Eq. 2.12) which controls the power output P_{out}, (Eq. 2.13) (Ehrlich, 2013). A is the circular rotor area, m is the mass of air passing through A, ρ is the air density and C_P is the power coefficient.

$$KE = \frac{1}{2} m\mathbf{v}^2 \tag{2.12}$$

$$P_{out} = \frac{1}{2} C_p A \rho \mathbf{v}^3 \tag{2.13}$$

Assuming that only the air mass passing through the rotor disk is affected by the turbine and that it is isolated from the surrounding air, a stream-tube is considered (Fig. 2.4). This concept is called the energy extracting actuator disk. Because of the slowing of the wind within the stream-tube the mass flow rate has to be conserved. The cross-sectional area is increasing, being smaller upstream of the disk and larger downstream. Upstream of the disk the static pressure is increasing due to the slowing wind and the

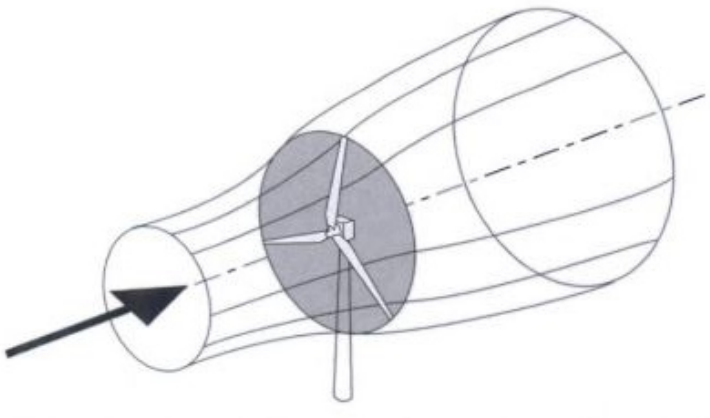

Figure 2.4: Energy extracting stream-tube of a wind turbine (Burton, 2011).

following decrease in KE. At the actuator disk the KE is extracted and the pressure drops. Downstream of the disk the velocity and static pressure is reduced. The pressure downstream has to reach equilibrium with the atmospheric pressure which requires KE. From the pressure difference across the disk follows a rate of change of momentum. The pressure difference is given by Bernoulli's equation upstream and downstream (explained in (Burton, 2011). The Lanchester-Betz limit gives the maximum value possible for the power coefficient, given when dP/da = 0 or dC_P/da = 0. Then the axial flow indicator factor, a = 1/3 and $C_{P,max}$ = 16/27 = 0.593 (Burton, 2011). Because of the cone shaped wake as a result of the actuator disk concept, the ocean is not affected by the wind wake until it has a radius larger than the turbine hub-height (Christiansen and Hasager, 2005).

2.4 Wind farm parameterizations

To be able to study OWF implementation in numerical models, different parameterizations simulating effects of wind power extraction have been developed.

Brostrom (2008) studied the effect of a large OWF on the upper ocean response by investigating changes in wind stress on the ocean surface. Changes in wind stress downstream of an OWF has been studied to a lesser degree than the structure of wind turbines in OWFs and wake effects within a wind farm related to optimization of power production. Brostrom (2008) stated that the upper ocean response is based on the size and extent of the reduction in wind stress at the sea surface. Using a theoretical approach considering the form and strength of the wind drag, two simple forms of wind stress was investigated in the study, given by Equation 2.14a and 2.14b.

$$\tau_x = \tau_{x0} - \Delta\tau_x e^{-(2y/L)^2}, \tag{2.14a}$$

$$\tau_x = \tau_{x0} - \Delta\tau_x e^{-(2y/(0.8L+0.2x))^2} \quad max\,(e^{-(1-x)/L}x/L, 0) \tag{2.14b}$$

Equation 2.14a gives a wind stress that is homogeneous in x-direction while Equation 2.14b gives a two-dimensional wind stress pattern, where τ_{x0} is the undisturbed wind stress, $\Delta\tau_x$ represents the change in wind stress induced by the wind farm and L is the characteristic size of the wind farm. This is an idealized case where a constant wind

speed and direction is considered, with the wind stress in x-direction. For the two dimensional case a zero wind deficit at the upwind end of the wind farm and a maximum deficit at the end of the wind farm was assumed. Downwind of the wind farm the wind stress deficit was assumed to decline with a characteristic length scale L (Brostrom, 2008).

Brostrom (2008) showed that as a result of the presence of a large OWF a change in the oceanic circulation pattern surrounding the wind farm could be found. The size of the wind farm was shown to be important, as patterns of upwelling and downwelling was found when the size of the wind farm was equal to or larger than the internal Rossby radius of deformation, the length scale where the effects of rotation becomes as important as those of stratification (Marshall and Plumb, 2007). This was given as a result of a much larger curl of the wind stress in the presence of a large wind farm, than what is naturally seen in the open ocean. As a result a change in nutrient supply and local ecosystem was expected (Brostrom, 2008).

A study by Paskyabi and Fer (2012) included wave effects to the method of Brostrom (2008). To study the circulation close to a wind farm, the characteristic length of the wind farm and wind-wave and wave-current momentum was included in the shallow-water equations. The result corresponded well with the result of Brostrom (2008). The near-surface Ekman current, the volume transport 45° to the right of the wind when the friction and Coriolis force is in balance (Brown et al., 2001), was affected in the vicinity of a wind farm, showing strong up- and downwelling. The wave effects were shown to be strongly related to the upper ocean response, by increasing the magnitude of the pycnocline displacement. Paskyabi (2015) investigated the OWF wake effect on stratification and coastal upwelling using wake models. The result also implied that disturbances in the wind field could influence the upwelling and stratification pattern.

Fitch et al. (2012) created a new wind farm parameterization for the Weather Research Forecasting Model (WRF). The parameterization was based on calculation of drag by wind turbines. The total KE extracted from the wind field was given by the thrust coefficient C_T and transferred into electrical energy, losses and non-productive drag. The electrical energy was measured by the power coefficient C_P, the mechanical and electrical losses were neglected and all the non-productive drag was assumed to

produce TKE. The TKE was therefore given by $C_{TKE} = C_T - C_P$. The calculations of the effect of a wind farm on the wind field is described in detail by Fitch et al. (2012) and briefly summarized here. The rate of loss of KE from one turbine was integrated over the rotor area and the horizontal grid cell. The total rate of change of KE in a grid cell was calculated for the horizontal wind component, since the vertical component was assumed not to be affected by wind turbine drag. The two equations representing the rate of change and loss of KE was combined, which gave a momentum tendency term and further a term representing the power extracted by turbines transferred into electrical energy and a term for the power transferred into TKE (Fitch et al., 2012).

The wind farm parameterization used by Ludewig (2015) is similar to the one used by Fitch et al. (2012). It is based on Beth's theory and the actuator disk concept explained in Section 2.3.1. The rotor thrust T' (Eq. 2.15), is based on the formulation of the thrust coefficient C_T, given by the rotor thrust, T', over maximum thrust, T_{max}, where A' is the area at the rotor disk and $\mathbf{v}_1$ is the wind speed for undisturbed flow far in front of the wind turbine.

$$T' = C_T T_{max} = \frac{1}{2} C_T \rho A' \mathbf{v}_1^2 \tag{2.15}$$

Wind turbines was parameterized by multiplying the rotor thrust, T', by a wind turbine mask, the area per grid cell covered by rotor disks, and added to the momentum equation as a deficit term. A detailed explanation of the wind turbine parameterization is given in (Ludewig, 2015).

This parameterization was used in the meteorological MEsoscale TRAnsport and Stream model (METRAS) and the result was used to force the HAMburg Shelf Ocean Model (HAMSOM). Since HAMSOM is forced by wind stress and not by wind speed, the wind speed was used to calculate wind stress by the formula given in (Ludewig, 2015) as $\boldsymbol{\tau} = c_{da} \frac{\rho_a}{\rho_{ref}} |\boldsymbol{v}| 10^3$, where ρ_a is the density of air and ρ_{ref} is the density of sea water. [1]

[1] We noted that the formula for wind stress used in (Ludewig, 2015) does not correspond to the formula given in the literature explained by Equation 2.1, as a velocity component is missing. We also noted that among the equations given in (Fitch et al., 2012) the equation for drag of force is given by $\mathbf{F}_{drag} = \frac{1}{2} C_T(|\mathbf{V}|)\rho|\mathbf{V}|\mathbf{V}A$, including an extra velocity component giving a different dimension than what is found in the literature. The drag force is given by $F = \frac{1}{2} C_D \rho A \mathbf{V}^2$ [N] (Ehrlich, 2013).

Chapter 3

Numerical model: ECOSMO

This chapter provides a description of the numerical model used in this thesis, a fully coupled bio-physical model ECOSMO (ECOSystem MOdel) (Daewel and Schrum, 2013; Barthel et al., 2012; Schrum et al., 2006; Schrum and Backhaus, 1999), which was applied to the coupled system North Sea–Baltic Sea. The coupled model consists of a physical model, a 3D hydrodynamic model, and a biogeochemical, NPZD (Nutrient, Phytoplankton, Zooplankton, Detritus), model. The physical and biochemical models were coupled online using the same grid and solved simultaneously with a 20 minute time step (Daewel and Schrum, 2013). In this thesis a model run for one year was investigated and the study area was the North Sea. The full model will be explained in this chapter. The focus further on will be on wind farm representation and processes related to the North Sea. The model runs for this thesis, for year 2008 including a wind farm parameterization, will be described in Section 4.4.

3.1 Physical model

The hydrodynamic module of ECOSMO builds on the free-surface 3D baroclinic coupled sea-ice model HAMSOM (HAMburg Shelf Ocean Model), which has successfully been used to investigate hydro- and thermodynamics of several shelf seas, described in detail by Schrum and Backhaus (1999). The model equations are solved on a staggered Arakawa-C grid (Fig. 3.1) (Arakawa and Lamb, 1977) with fixed layer thickness, except the free surface with a variable thickness of the first layer. A spherical grid was used with

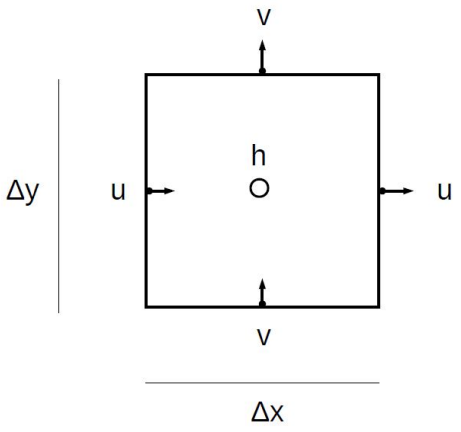

Figure 3.1: An unstaggered grid defines the variables in the same point of the grid, while the variables in a staggered grid are defined at different points and therefore has a higher resolution. The staggered Arakawa-C grid calculates variables of pressure, density and surface elevation (h) at the center of the grid and the velocities (u,v) staggered by half a grid distance (Collins et al., 2013).

a horizontal resolution of 6' in north-south direction and 10' in west-east direction (degrees minutes). The resolution for the 20 vertical levels was 5 m in the upper 40 m, 8 m up to 88 m depth and an decreasing resolution below, to resolve stratification. The calculation of turbulent vertical exchange processes are done by an algebraic first order k-ϵ model, which combines the equation for turbulent kinetic energy (k) and its dissipation rate (ϵ) (Schrum, 1997; Pohlmann, 1996). The developed version of ECOSMO (Daewel and Schrum, 2013) includes a Total Variation Diminishing (TVD) advection scheme, instead of the more diffusive upwind advection scheme used by Schrum et al. (2006). The modified scheme is a combination of the first-order upwind scheme and the second-order Lax-Wendroff scheme with superbee limiter, making it a TVD (Harten, 1983). A more detailed description of the scheme and the implementation in ECOSMO is found in (Barthel et al., 2012).

3.2 Ecosystem model

The basis of the ecosystem model are interactions between 16 state variables for the biological parameterization for the North Sea and Baltic Sea. Eleven state variables resolve the three main nutrient cycles which limit phytoplankton production in the North Sea, the nitrogen-, phosphorus- and silicate cycle. Primary production is limited by light and the nutrients phosphate (PO_4), nitrogen (NO_3, NH_4) and silicate (SiO_2) and is represented by the three functional phytoplankton groups diatoms, flagellates and cyanobacteria. The latter is needed to represent nitrogen fixation by cyanobacteria in

the Baltic Sea. Based on their feeding behaviour two functional zooplankton groups are estimated, microzooplankton and macrozooplankton (herbivorous, omnivorous). Other state variables are oxygen (O_2), detrius (D), dissolved organic matter (DOM) and tree sediment pools. The sediment pools are important for the highly stratified Baltic Sea, however for the North Sea Schrum et al. (2006) stated that for the turbulent shelf sea the sedimentations processes could be neglected. This was verified by Daewel and Schrum (2013) since in winter the seasonal sedimentation in the central North Sea is re-suspended. The DOM was shown to be important not only for the Baltic sea, but also for the North Sea by allowing for recycling of nutrients in the euphotic zone. The interactions between the variables are described by the flow of nutrients and biomass calculated by Redfield stoichiometry, a fixed relationship between carbon, nitrogen and phosphorous in marine phytoplankton, cited after Redfield (1934). A schematic diagram of the state variable interactions is shown in Fig. 3.2 (Daewel and Schrum, 2013).

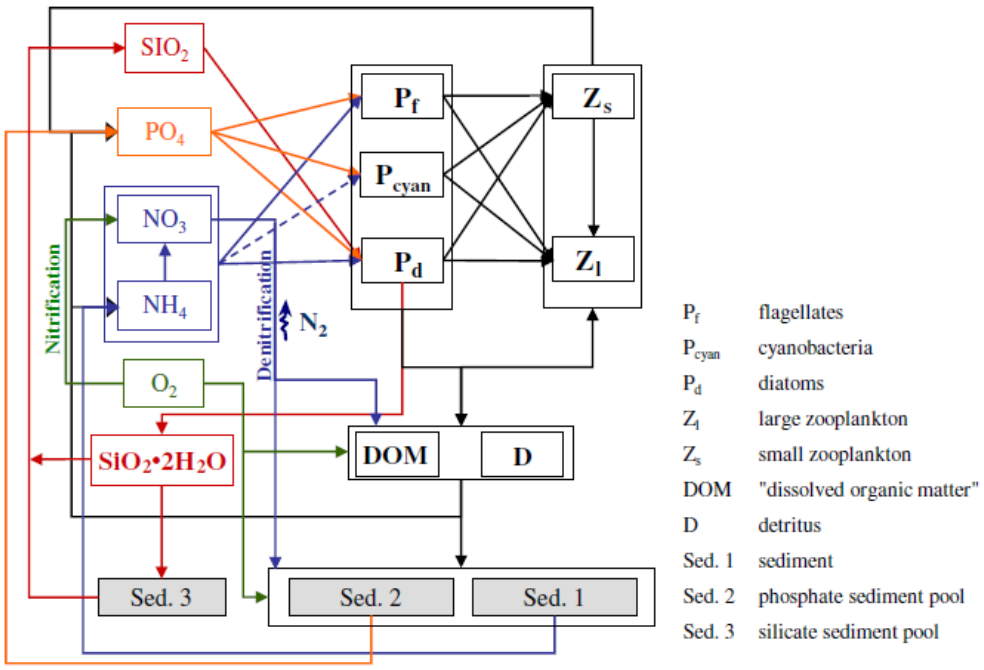

Figure 3.2: Graphic description of the interactions between the variables in the ecological model.The colors represent the different flows of groups of variables; blue represents nitrogen, green represents oxygen, orange represents phosphorous, red represents silica and black represents organic carbon (Daewel and Schrum, 2013).

3.3 ECOSMO model setup

The ECOSMO was created to continuously integrate from 1948-2008 in Daewel and Schrum (2013), where the initial and boundary conditions are explained in detail and are here summarized. The model domain is influenced by the free surface, the open boundary to the North Atlantic Ocean and river runoff at the land-ocean interface. NCEP /NCAR re-analysis data (Kalnay et al., 1996) provided atmospheric boundary conditions at the free surface with a time step of 6 h. Atmospheric nitrogen wet deposition was given by daily averaged values from year 2000 from a Community Multiscale Air Quality model (Matthias et al., 2008). The open boundaries were forced by daily sea surface elevation from a coarser diagnostic model for the North Atlantic Ocean (Backhaus and Hainbucher, 1987) and tidal variations was added including the eight dominant tidal components with a time step of 20 minutes (Daewel and Schrum, 2013). Salinity at the boundary was given by climatological gridded data from Janssen et al. (1999) and annual variations from ICES database (http://www.ices.dk) was added. Temperature at the boundary was given by a Sommerfeld radiation condition (Orlanski, 1976). Fields of nutrients at the boundary were provided from the World Ocean Atlas (WOA) (Conkright et al., 2002). Freshwater river runoff and nutrient loads were collected from different sources to force the model (Daewel and Schrum, 2013). The climatological data for temperature and salinity (Janssen et al., 1999) and the WOA data for nutrients (Conkright et al., 2002) mentioned above was used to initialize the model.

Chapter 4

Wind Farm Parameterization

This chapter provides a description of the wind farm parameterization implemented in ECOSMO including a code description and validation of the parameterization with some examples of different wind forcing, to illustrate the effect of the wind farm parameterization on the wind stress field. The setup of the different model runs performed is described.

To be able to use ECOSMO to simulate the North Sea containing a number of wind farms of different size, a parameterization estimating the reduction in wind stress due to the wind farms was developed. The wind farm parameterizations presented in Section 2.4 were considered. The method by Fitch et al. (2012) is the most realistic representation of a wind farm, since it is based on the drag of each wind turbine and includes the part of the extracted energy that goes into TKE. Both Fitch et al. (2012) and Ludewig (2015) used an atmospheric model, where Ludewig (2015) used the modified wind field to force the ocean model HAMSOM. In this thesis only the ocean model ECOSMO is used. The theoretical method by Brostrom (2008) based on Equation 2.14b, which gives a two-dimensional wind stress pattern of reduced wind stress, was chosen for this thesis. It provides a simple and physically consistent formula, and a theoretical link to earlier idealized studies. It seems appropriate for application to realistic wind farms, in combination with results from (Ludewig, 2015).

A parameterization of wind stress deficit due to current operational OWFs in the North Sea was created and implemented as a subroutine of ECOSMO. Wind stress components, speed and direction fields from ECOSMO was used as input for the parameter-

ization and the output to be used for further calculations in ECOSMO was the modified wind stress fields. The fortran code for the parameterization is found in Appendix A.1 and is described in detail in the next section.

4.1 Code description

A loop was created to run over a file with information on the wind farms to be calculated. The farm characteristics for each wind farm, the area [km^2] and center point position in latitude and longitude decimal degrees, was gathered from (Global Database, 2016). For simplicity when applying the method by Brostrom (2008), the farms were assumed to have a quadratic form, i.e., a length scale is defined as the square root of the wind farm area.

Information on the ECOSMO model domain was collected from the model scripts and the north-west (NW) corner position was used as a reference for the locations of the wind farms. The NW-corner of the grid was converted from decimal minutes to decimal degrees. The center point coordinates of each wind farm were given by the number of grids from the NW corner position of the model domain. The grid coordinates of the wind farms were given by the difference in latitude and longitude between the farm and the NW-corner, divided by the latitudinal and longitudinal grid spacing in ECOSMO.

The value of wind speed and direction at the center point coordinates were obtained from the input fields. The cut-in and cut-out wind speed of wind turbines were included by only making calculations for the wind speeds within a production range from 3.5 to 25 ms^{-1}. The wind direction was added 180 degrees, hence zero degrees represents wind from east, 90 degrees winds from north, 180 degrees winds from west and 270 degrees winds from south, before the direction was converted to radians. The unmodified wind stress magnitude was calculated for all grid points outside the wind farm loop by $\tau_x = \sqrt{\tau_{xx}^2 + \tau_{yy}^2}$. Within the loop the wind stress field was modified for each wind farm.

The maximum change in wind stress induced by a wind farm was needed for the calculation of Equation 2.14b from (Brostrom, 2008). This change was calculated using results from Ludewig (2015), where the effect of an OWF on the wind field was estimated in METRAS, using three different geostrophic wind speeds as forcing; 5, 8 and 16

ms^{-1}. From the plotted result in (Ludewig, 2015) (figure in Appendix A.2) the maximum and minimum 10-m wind speed for the three different cases were used to calculate the change in wind speed due to a wind farm. The constant wind speed in front of the farm was used instead of the maximum value shown in the figure because of an overshooting right in front of the farm. Equation 2.1 and 2.2 were used to calculate the wind stress for each 10-m wind speed and the difference between the maximum and minimum wind stress was calculated.

A relation between the initial geostrophic wind speed and the resulting change in wind stress was created. Since the wind speed used in ECOSMO is 10-m wind speed, and not geostrophic wind as used in (Ludewig, 2015), a relation between the change in wind stress and 10-m wind speed was required to be able to calculate the change in wind stress for every wind speed. Equation 2.9 and 2.10 were used to calculate 10-m wind speed, U_{10}, from the three different geostrophic wind speeds from Ludewig (2015). Curve fitting in matlab was used to find the resulting relation given by Equation 4.1.

$$\Delta\tau_x = 0.001334\, U_{10}^{2.061} \tag{4.1}$$

A strong correlation close to 1 was found for both a linear and a power curve. Ludewig (2015) assumed the relation to be nearly linear, however both the undisturbed and disturbed wind stress are proportional to v^2 from Equation 2.1 and 2.2. Based on this and the slightly stronger correlation, the relation for change in wind stress was also assumed to be proportional to v^2. Uncertainties were present since the relation was based only on three data points of the 10-m wind speeds 3.9, 6.1 and 11.1 ms^{-1} and extended up to 26 ms^{-1}. Because of the large maximum wind stress deficit which may occur from the formula, the deficit was required to be smaller than the wind stress itself. The maximum change in wind stress, $\Delta\tau_x$, used in the calculation of the reduced wind stress pattern (Eg. 4.1), is further referred to as the maximum specified wind stress deficit, while the resulting maximum modelled change in wind stress, $\Delta\tau$, is referred to as the resulting maximum wind stress deficit.

To calculate the pattern of wind stress downstream of a wind farm, Equation 2.14b from (Brostrom, 2008) was used. This wind stress formula was created for a constant

wind stress field. Some developments had to be made to be able to use the formula on a real and time varying wind stress field. For each unmodified wind stress magnitude and direction and for each wind farm a coordinate system was created with x-axis along the wind direction and y-axis orthogonal to it referred to as x' and y' respectively. This coordinate system is further referred to as wind farm coordinates. Each wind farm was assumed to be oriented having one of the sides orthogonal to the wind direction and the x'-axis through the center (Fig. 4.1). A characteristic length of the farms was calculated as the square root of the farm area. This length was used to calculate the origin of the wind farm coordinates for each farm by trigonometry and thus needed to be converted to the number of grid points that the characteristic length covers.

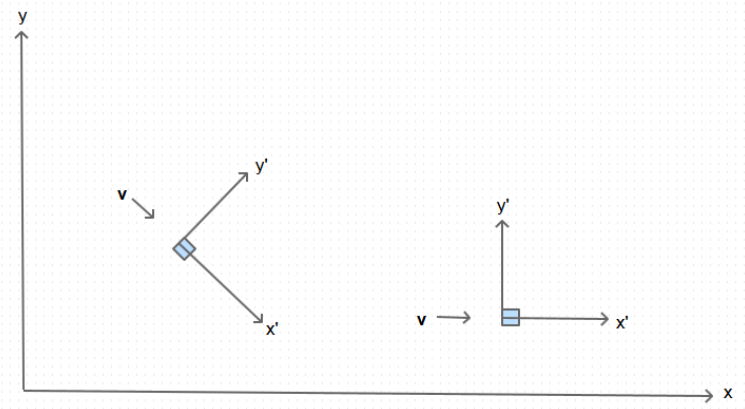

Figure 4.1: Schematic representation of the wind farm coordinate-system compared to the model grid for two different wind conditions. The wind direction is given by **v** and the box represents the wind farm.

A loop over the ECOSMO model domain consisting of 177 × 207 grid cells, was created to transform all grid coordinates into wind farm coordinates using counter-clockwise coordinate transformation. Spherical coordinates were used in ECOSMO, with constant grid steps in the north-south direction and grid steps in the west-east direction dependent on the latitude. The length of each step [m] in the wind farm coordinate system was calculated using the length of each grid step from ECOSMO. Equation 2.14b consist of a damping term to get the wanted shape of the wake. The formula for modification of wind stress used in the parameterization is given by Equation 4.2.

$$\tau_x = \tau_x - \Delta\tau_x e^{-(\frac{2y}{(0.8L+0.2x)})^2} \quad max\,(e^{\frac{1-x}{L}}\frac{x}{L}, 0) \tag{4.2}$$

The maximum term was modified with a positive exponent, also used by Paskyabi and Fer (2012), compared to the formula given in (Brostrom, 2008).

Since the wind stress deficit induced by a wind farm was assumed to be zero upwind of the wind farm (Brostrom, 2008), Equation 4.2 was calculated only for grid cells with x'-coordinate larger than zero and therefore only the first term in the maximum function was used. As the wind stress deficit calculated in wind farm coordinates was the output of the subroutine, it had to be decomposed to model grid coordinates by trigonometry.

The wind farm parameterization explained above, including the maximum specified wind stress deficit based on results from (Ludewig, 2015), is the main parameterization used in this thesis, called P1. A similar parameterization, P2, was created by changing the maximum specified reduction in wind stress deficit $\Delta\tau_x$ to the same as was used by Brostrom (2008) and Paskyabi and Fer (2012), to better compare the results of this thesis with previous studies. The maximum specified reduction of wind stress in P2 was given by Equation 4.3.

$$\Delta\tau_x = 0.5\tau_{x0} \tag{4.3}$$

4.2 Cases of wind farm setup

The wind farm parameterization was calculated for two different cases of wind farm setup in the North Sea. The main case used was representing the present situations in the North Sea including 37 operational wind farms. Another case was representing a future situation including all wind farms in the North Sea that are operational, under construction and in the planning phase, 86 in total (Global Database, 2016). Fig. 4.2 shows the location of the center point of the wind farms in the North Sea, for a) the operational wind farms in 2015 and for b) the future scenario of wind farms in the North Sea. The size of the farms are not included in this graphical representation.

For the operational wind farms in 2015 the size of the wind farms were from 2 to 146 km^2, while the future case included wind farms from 2 to 599 km^2. The model grid cells are about 10x10 km^2. Most of the wind farms in the case with present wind farms were smaller than the grid cell, while in the future case of wind farms in the North Sea more wind farms had a larger area than a grid cell. In the parameterization the size

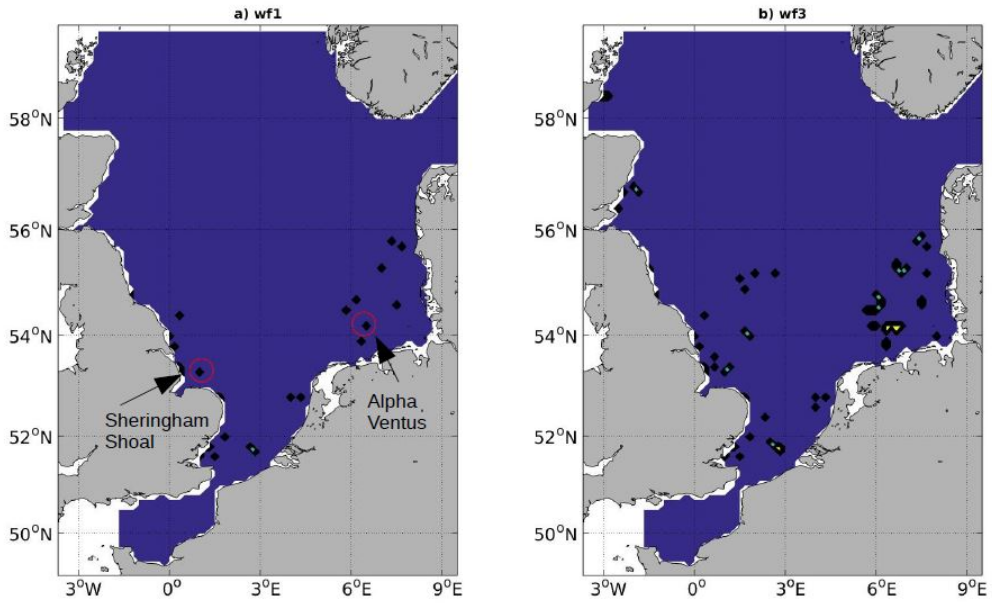

Figure 4.2: Locations of the wind farms in the North Sea for a) the present wind farm distribution and b) the future wind farm distribution.

of the wind farms are represented by the characteristic length scale, which represents the scale of the wind farm and thereby the area where wind energy is extracted. The wind stress downstream of the wind farm area was reduced based on the characteristic length scale in Equation 4.2. For wind farms of smaller size than a grid cell, the value of wind stress reduction will be set to a larger area than the wind farm itself, and may therefore be overestimated in the grid cell where the wind farm is located. However the resulting maximum reduction of wind stress in the wind farm area and the reduction of wind stress in grid cells downstream of the wind farm is dependent on the characteristic length scale.

4.3 Validation

The parameterization code was first tested in matlab and a fortran compiler for constant wind conditions. The wind stress was calculated using the Equations 2.1 and 2.2. This test was done separately from ECOSMO to see that the parameterization code calculated the desired wind stress deficit pattern based on (Brostrom, 2008) and to see

that the modifications done to use the method for different wind speeds and directions gave the desired result. The same exercise was done after the code was implemented in ECOSMO. Runs with constant wind forcing were created to show the changes induced by the wind farms for different wind conditions in the model domain. Both wind farm parameterizations with different maximum specified wind stress deficit, P1 and P2, and the two different cases of wind farm distribution in the North Sea were tested. The values representing the wind forcing for each test is given in Table 4.1.

Run	cwf-1a	cwf-1b	cwf-2a	cwf-2b	cwf-2c	cwf-3a	cwf-3b	cwf-3c
OWF parameterization	P1	P1	P1	P1	P1	P2	P2	P2
OWF setup	op	op	op	op	all	op	op	all
Wind speed [ms^{-1}]	7	10	7	10	10	7	10	10
Wind direction [Deg]	210	210	315	315	315	315	315	315
Wind stress x-dir [Nm^{-2}]	-0.07	-0.14	0.05	0.1	0.1	0.05	0.1	0.1
Wind stress y-dir [Nm^{-2}]	-0.04	-0.08	-0.05	-0.1	-0.1	-0.05	-0.1	-0.1

Table 4.1: The constant wind forcing for the cwf runs, where zero degrees represents wind from east, 90 degrees wind from north, 180 degrees wind from west and 270 degrees wind from south.

The runs including the constant wind forcing show clear patterns of wind stress deficit downstream of the location of the wind farms. Figure 4.3 shows the total wind stress over the North Sea for the runs cwf-1a and cwf-1b. The direction is held constant at 210 degrees while the wind speed is 7 and 10 ms^{-1} respectively. In cwf-1a the resulting maximum value of wind stress is 0.0806 Pa and the minimum value is 0.0498 Pa. The resulting maximum deficit is 0.0308 Pa and gives in a wind stress of 61.8 % of the initial wind stress left after the reduction, a reduction of 38.2 %. In cwf-1b the resulting maximum wind stress deficit is 0.0622 Pa, a reduction of 38.6 %.

Figure 4.4 shows the total wind stress over the North Sea for the runs cwf-2a, cwf-2b and cwf-2c. The direction is held constant at 315 degrees while the wind speed is 7, 10 and 10 ms^{-1} respectively. In cwf-2c all the planned wind farms in the North Sea is included, together with the already existing wind farms used in the previous runs. In cwf-2a the resulting maximum deficit is 0.0249 Pa, a 35.2 % reduction. In cwf-2b the

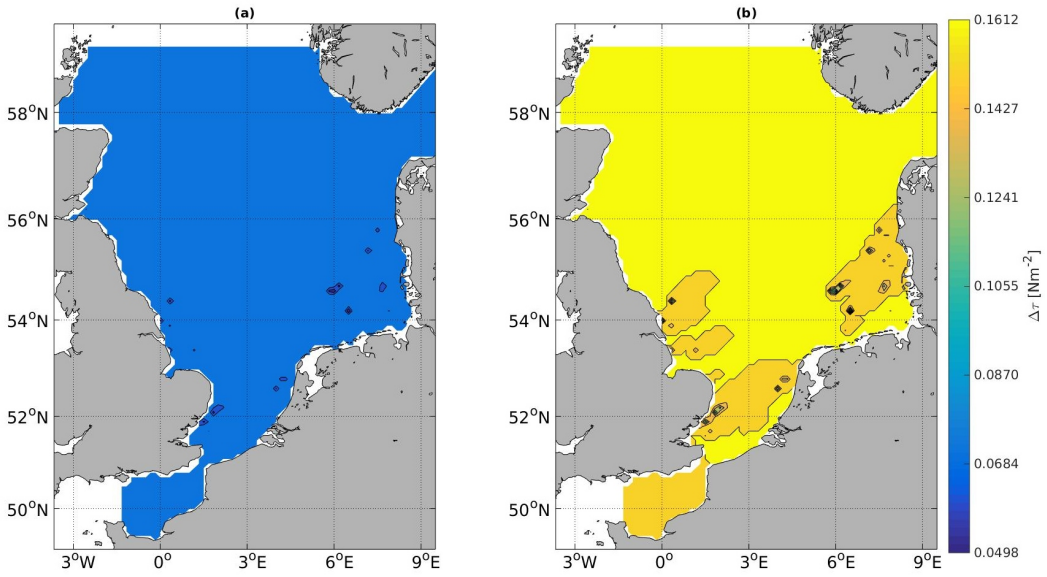

Figure 4.3: Wind stress $[Nm^{-2}]$ using P1 from a) run cwf-1a with 7 ms^{-1} wind speed and b) run cwf-1b with 10 ms^{-1} wind speed, showing wind stress deficit pattern downstream of OWFs.

resulting maximum deficit is 0.0497 Pa, a reduction of 35.2 %. In cwf-2c the resulting maximum deficit is 0.1050 Pa, a reduction of 74.2 %.

For the alternative wind farm parameterization, P2, Figure 4.5 shows the total wind stress over the North Sea area for the runs cwf-3a, cwf-3b and cwf-3c. The wind forcing is the same as for cwf-2. In cwf-3a the resulting maximum deficit is 0.0124 Pa, a reduction of 17.6 %. In cwf-3b the resulting maximum deficit is 0.0249 Pa, a 17.6 % reduction. In cwf-3c the resulting maximum deficit is 0.0750 Pa, a reduction of 53.0 %.

The results from the runs with constant wind forcing are summarized in Table 4.2, including the resulting maximum and minimum wind stress of the different runs.

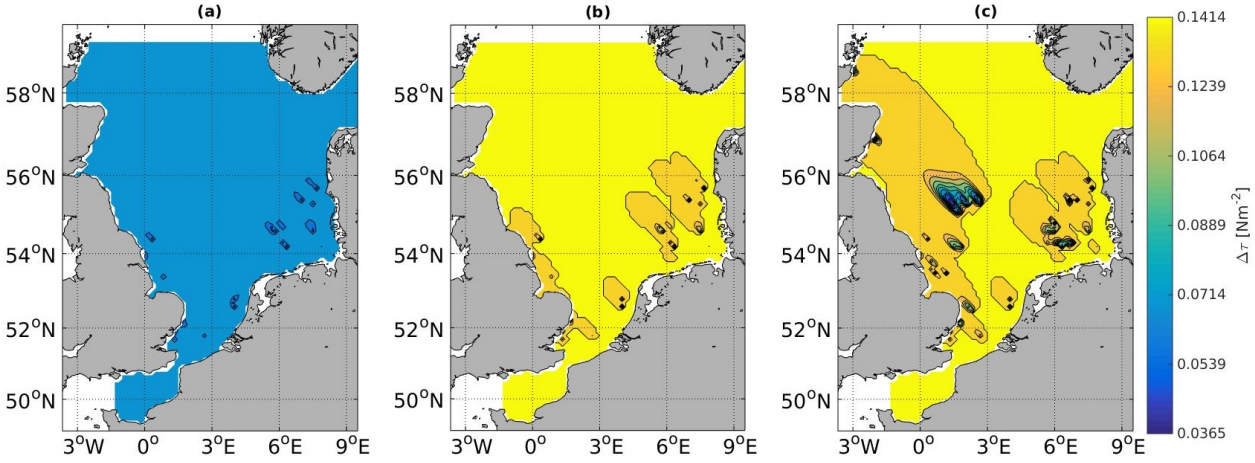

Figure 4.4: Wind stress $[Nm^{-2}]$ using P1 from a) run cwf-2a with 7 ms^{-1} wind speed, b) run cwf-2b with 10 ms^{-1} wind speed and c) run cwf-2c with 10 ms^{-1} wind speed for the current case of OWF setup, all showing wind stress deficit pattern downstream of OWFs.

Run	cwf-1a	cwf1-b	cwf-2a	cwf-2b	cwf-2c	cwf-3a	cwf-3b	cwf-3c
Max τ $[Nm^{-2}]$	0.0806	0.1612	0.0707	0.1414	0.1414	0.0707	0.1414	0.1414
Min τ $[Nm^{-2}]$	0.0498	0.099	0.0458	0.0917	0.0365	0.0583	0.1166	0.0664
Max $\Delta\tau$ $[Nm^{-2}]$	0.0308	0.0622	0.0249	0.0497	0.1050	0.0124	0.0249	0.075
Max $\Delta\tau$ [%]	38.2	38.6	35.2	35.2	74.2	17.6	17.6	53

Table 4.2: Resulting wind stress and wind stress deficit $[Nm^{-2}]$ of runs with constant wind forcing, cwf-1 to cwf-3.

These examples show that the parameterization calculates the wind stress deficit pattern downstream of the wind farm locations similar to (Brostrom, 2008). Larger wind speed gives a more extended wake and the directions are calculated correctly, with winds from east for zero degrees and winds from north for 90 degrees. It is showed that a small change in wind speed does only give a small change in the resulting maximum wind stress deficit. However wind farms of larger size included in cwf-2c and cwf-3c at Dogger Bank and outside the coast of Scotland shows an increase in the resulting maximum wind stress deficit and a larger extent of the wake area. This is consistent with findings in (Ludewig, 2015), where a larger wind farm resulted in a wider and stronger

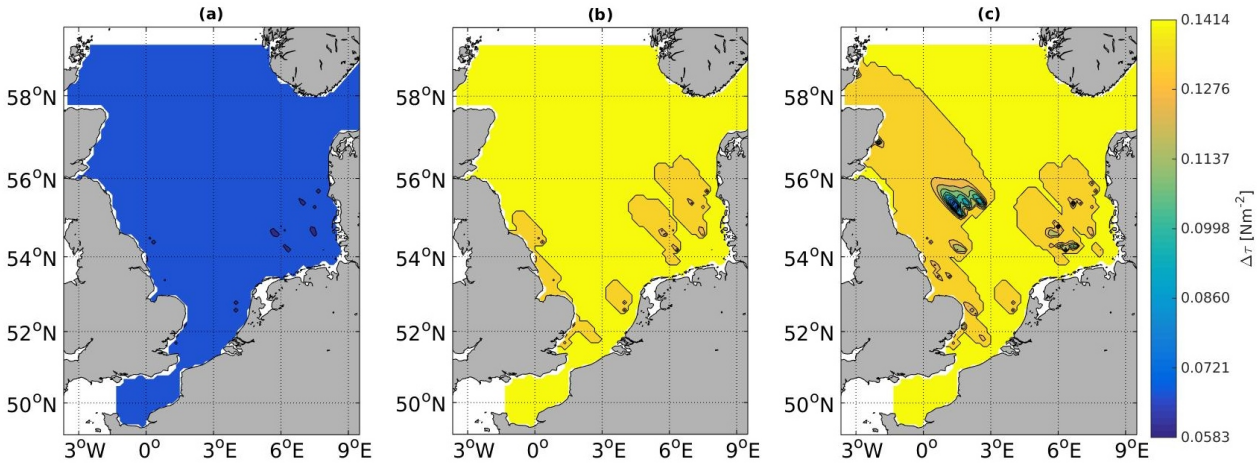

Figure 4.5: Wind stress $[Nm^{-2}]$ using P2 from a) run cwf-3a with 7 ms^{-1} wind speed, b) run cwf-3b with 10 ms^{-1} wind speed and c) run cwf-3c with 10 ms^{-1} wind speed for the future case of OWF setup, all showing wind stress deficit pattern downstream of wind farms.

wind wake. It was therefore concluded that the wind farm parameterizations calculated the desired pattern of wind stress deficit. [1]

When comparing the two wind farm parameterizations with different maximum specified deficit in wind stress, $\Delta\tau_x$, it is seen that the method created based on METRAS-results from (Ludewig, 2015), P1, results in a larger maximum wind stress deficit, $\Delta\tau$, than P2 based on Brostrom (2008) and Paskyabi and Fer (2012). The wind farm parameterization P2 used a maximum specified deficit of 50 % of the wind stress in all cases. The calculated change in maximum specified wind stress based on (Ludewig, 2015) was almost as large as the undisturbed wind stress, up to a 100 % deficit which most likely are overestimated numbers. Hence the parameterization P1 gives a larger resulting maxi-

[1] At later analysis the wind stress deficit for real wind forcing showed to give some small areas of slightly larger wind stress in the runs including the wind farm parameterization, than in the reference run. This was visible for some of the days with low wind speed in summer. The cause of this was not found conclusively. Hopefully this increase in wind stress does not effect the result, because it is found in summer with lower wind speeds, where the effect of the wind stress on the ocean is small. The wind farm parameterization is anyway turned off if the wind speed is below the cut-in speed of 3.5 ms^{-1}. One possible reason may be geographical variations in the unmodified wind field. If the unmodified wind stress downstream of the wind farm is smaller than the reduced wind stress based on the wind forcing in the grid cell containing the center point of the farm, the wind stress downstream of wind farms will in this case become larger than the unmodified wind stress.

mum deficit than P2 and it is expected that run wf1 including P1 will possibly give lager effects on dynamics of primary production in the North Sea than run wf2, including P2.

The idea behind creating a maximum specified wind stress deficit based on METRAS-results, in addition to the 50 % maximum deficit, was to be able to compare the response on the upper ocean for different maximum specified wind stress deficit. Since wind farm parameterization P1 used a maximum specified wind stress deficit of almost 100 % , different strengths of reduction was compared. The method behind P1 was based on modelled atmospheric wind speed deficit due to a wind farm. The parameterization created in this thesis was therefore based on another parameterization for wind farms and only on three data points as mentioned in the code description. Thus the method is uncertain. However this is an idealized and simplified parameterization of wind farms, which in this study is meant to investigate the idealised impact from wind farms on the upper ocean and general response on the marine ecosystem from reduced wind stress.

4.4 Setup of model runs

In this thesis the model runs of ECOSMO including the wind farm parameterization had similar setup as described in Section 3.3. The model was run for one year, 2008, being a year of high wind speed (Geyer et al., 2015) and the most recent year available with input data in ECOSMO. The simulations were run from climatology, described in Section 3.3, with a spinup time of two years, which was sufficient for the well mixed North Sea. The time step of the model was 20 min and the time step of the atmospheric forcing was 6 h (Daewel and Schrum, 2013), hence the modified wind stress was calculated every 6 h. The model runs were run sequentially on one Central Processing Unit (CPU) instead of parallel on 18 CPUs, which is normally used for ECOSMO. This was necessary to be able to run the model including the wind farm parameterization. As a consequence the computational time for a run over one year was 6 hours, instead of 1 hour for the parallel run on 18 processors.

The variables investigated in this thesis were primary production by Flagellates and Diatoms and the physical variables temperature and salinity. Vertically averaged values and 3d-fields, with values for each vertical level, were calculated in the postprocess-

ing of the model output for daily, weekly, monthly and yearly averaged values. The 3d-fields were used for calculation of stratification of the water masses and for vertically integrated values of primary production. The output of the postprocessing was given in $[mgCm^{-3}day^{-1}]$ for production. For some calculations the unit was converted to $[gCm^{-2}day^{-1}]$ for vertically integrated values or $[gCm^{-2}year^{-1}]$ for vertical and temporal integrated values. Temperature was given in [°C] and salinity in [PSU].

Different runs of ECOSMO were created (Tab. 4.3). As explained in the previous section, the code including the wind farm parameterization was first run for the first 6 hours of the year with different constant wind forcings, named cwf. The runs for the whole year 2008 was forced by the variable wind field used to force ECOSMO, explained in Section 3.3. A reference run without the wind farm parameterization, nwf, was created and used for comparison with the simulations of influence of wind farms on the ocean. The main run including the wind farm parameterization created for this thesis, P1, was named wf1. A run including the wind farm parameterization with the same maximum specified wind stress deficit, $\Delta\tau_x$, as used by Brostrom (2008) and Paskyabi and Fer (2012), P2, was named wf2. In these two runs the wind farm parameterizations were calculated for the operational wind farms in the North Sea in 2015. A second run including wind farm parameterization P1, wf3, was calculated for the future case of wind farm implementation in the North Sea, including all the planned wind farms. The runs representing the North Sea influenced by wind farm implementation was compared to the reference run with undisturbed conditions.

Run	Wind forcing	OWF parameterization	OWF setup
cwf	constant	P1/P2	operational/all
nwf	undisturbed	-	-
wf1	disturbed	P1	operational
wf2	disturbed	P2	operational
wf3	disturbed	P1	all

Table 4.3: The different model runs of ECOSMO.

Chapter 5

Results

This chapter presents the results of general ocean response on large-scale power production from offshore wind farms. First comparison between the main run including operational wind farms in the North Sea, wf1, with the reference run of undisturbed conditions, nwf, is shown. The difference between the two runs is calculated by subtracting the values of run wf1 from nwf for all variables investigated, hence positive change represents smaller values in wf1 and negative change represents larger values in wf1, compared to nwf. When explaining the differences between the two runs, coastlines and names of areas in the North Sea (Fig. 1.1) are used. Modelled changes in primary production by Flagellates and Diatoms are presented, followed by physical state parameters relevant for driving primary production and the ecosystem in the North Sea, primarily related to wind-induced turbulent mixing. Model results are first presented for undisturbed conditions in the reference run nwf, then for conditions disturbed by the modified wind field in the main run wf1. An alternative wind farm parameterization P2 used in run wf2, and a future wind farm scenario in the North Sea used in run wf3, are also presented and compared to the main run, wf1. Further interpretation and discussion of physical processes including upwelling are included in Chapter 6.

5.1 Primary production by Flagellates and Diatoms run wf1

5.1.1 Annual spatial change

This section presents the modelled yearly averaged primary production in 2008 by Flagellates and Diatoms, to show the general changes in phytoplankton production.

Annual vertically integrated primary production by Flagellates and Diatoms are shown in Fig. 5.1 for the runs nwf (a and d), wf1 (b and e) and the difference between the two runs (c and f), where the upper panel shows production by Flagellates and the lower panel shows production by Diatoms. Large production by Flagellates in run nwf (Fig.

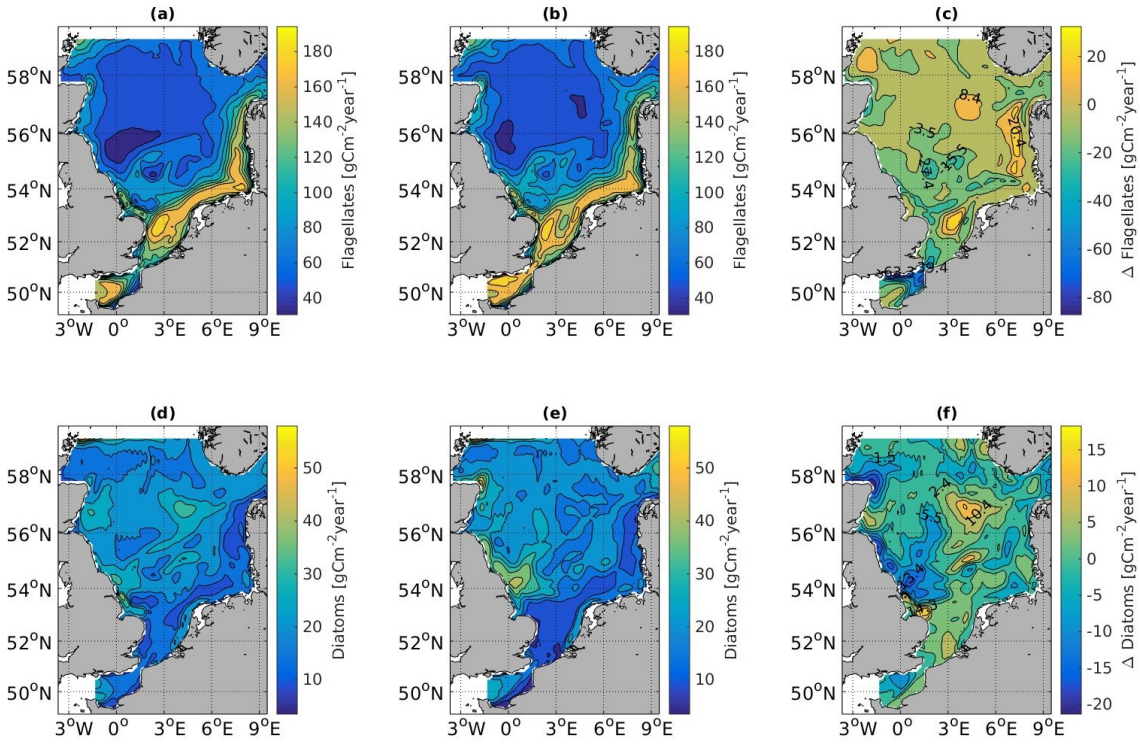

Figure 5.1: Annual vertically integrated distribution of primary production $[gCm^{-2}year^{-1}]$ by a) Flagellates run nwf, b) Flagellates run wf1, c) the difference in Flagellates between the two runs (nwf-wf1), d) Diatoms run nwf, e) Diatoms run wf1 and f) the difference in Diatoms between the two runs.

5.1a) is found along the European continental coast, in the central and northern part of the Southern Bight. High production is also found at the shallow parts off the British coast, south-west of Dogger Bank, and significant production is also found surrounding

the shallow Dogger Bank. The maximum production in a 10×10 grid cell of the model domain is 194.2 $gCm^{-2}year^{-1}$. The total averaged production by Flagellates in the North Sea is 86.2 $gCm^{-2}year^{-1}$ for run nwf and 88.9 $gCm^{-2}year^{-1}$ for run wf1. In run wf1 (Fig. 5.1b) similar pattern of production as in run nwf is shown, with a maximum production of 189.3 $gCm^{-2}year^{-1}$. However a clear pattern of change in distribution of production between the two runs is shown in figure (Fig. 5.1c). A larger production in run wf1, represented by the negative values, is found over Dogger Bank stretching southwards to the shallow British coast and towards the Helgoland Bight. Larger production is also found south in Southern Bight and north of Denmark and Jutland Bank. Less production in run wf1, represented by positive values, is found north in the Southern Bight and off the coast of Denmark and Germany, north of Helgoland Bight. The maximum decrease in production in a grid cell is 32.4 $gCm^{-2}year^{-1}$ and the maximum increase is 87.2 $gCm^{-2}year^{-1}$ in wf1. Hence in addition to the increased total averaged production in run wf1, the distribution of primary production is also changed.

The annual vertically integrated production by Diatoms for run nwf (Fig. 5.1d), shows large production off the British coast west of Dogger Bank and further south along the shallow coast. Large production is also found at the large bank north-east of Dogger bank and off the coast of Scotland. The maximum production in a grid cell is 57.9 $gCm^{-2}year^{-1}$. A smaller production is found along the continental European coast and along the British coast in the the Southern Bight. The total averaged production by Diatoms in the North Sea is 20.6 $gCm^{-2}year^{-1}$ for run nwf and 20.8 $gCm^{-2}year^{-1}$ for run wf1. In run wf1 (Fig. 5.1e) a similar pattern is shown, with a maximum production in a grid cell of 57 $gCm^{-2}year^{-1}$, however the difference between the two runs (Fig. 5.1f) shows less production in the Southern Bight and north-east of it, at the shallow British coastal waters and at the Little Fisher Bank north-east of Dogger Bank in run wf1. Larger production in run wf1 is found south and west of Dogger Bank along the coast of the British Isles and off the coast of Scotland. Offshore of Denmark and Germany patterns of larger and smaller production in run wf1 are shown. The maximum decreased production in one grid cell is 18.3 $gCm^{-2}year^{-1}$ and the maximum increased production is 21.3 $gCm^{-2}year^{-1}$ in run wf1.

Vertically integrated annual primary production for year 2008 for Flagellates (Fig.

5.1a) and Diatoms (Fig. 5.1d) both show larger primary production than for year 1984 simulated by Schrum et al. (2006), where the maximum primary production by Flagellates was about 140 $gCm^{-2}year^{-1}$ and for Diatoms 50 $gCm^{-2}year^{-1}$.

5.1.2 Seasonal temporal change

To get information on how the annual primary production is distributed throughout the year, time series of total averaged primary production in the North Sea of daily vertically averaged primary production is investigated. Seasonal dynamics of temporal values of total averaged primary production in the North Sea from daily vertically averaged values of Diatoms and Flagellates for year 2008, is presented for run wf1 and the reference run nwf in Fig. 5.2. The production by Diatoms shows an early spring bloom starting in

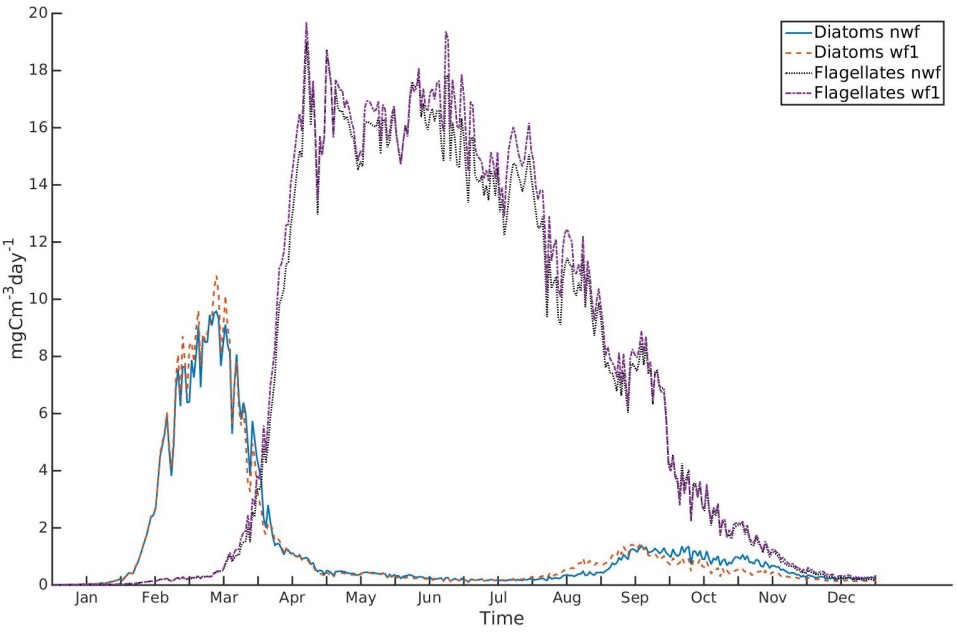

Figure 5.2: Seasonal dynamics of primary production $[mgCm^{-3}day^{-1}]$ in the North Sea for daily vertically averaged values of Diatoms and Flagellates throughout year 2008. The blue solid curve represents Diatoms from run nwf, the red dashed curve the Diatoms from wf1, the black dotted curve the Flagellates from wf1 and the purple dash-dotted curve the Flagellates from wf1.

February with a maximum value of 9.6 $mgCm^{-3}day^{-1}$ in March and a decline during April. In August the production again starts to increase to a second maximum value in

September of 1.4 $mgCm^{-3}day^{-1}$, followed by a decline which continues throughout the rest of the year. Run wf1 shows lager peaks in the Diatom spring bloom with a maximum of 10.8 $mgCm^{-3}day^{-1}$. Larger values were found in run wf1 in the start of the second bloom in late summer, with a maximum of 1.5 $mgCm^{-3}day^{-1}$, followed by less production in run wf1 for the rest of the year, compared to the reference run. The production by Flagellates in run nwf is characterized by a spring bloom starting in March, increasing until the end of April having a large production of about 16 $mgCm^{-3}day^{-1}$ from April to June, with a maximum of 19 $mgCm^{-3}day^{-1}$ before it declines nearly linearly throughout the rest of the year. Run wf1 has larger peaks than the reference run nwf from May to September, with a maximum of 19.7 $mgCm^{-3}day^{-1}$.

The difference between run nwf and wf1 of the total averaged primary production in the North Sea for daily vertically averaged values of Diatoms and Flagellates is presented in Fig. 5.3, to clearly see the difference in distribution of seasonal dynamics of primary production, between the run including wind farms and the reference run. The change

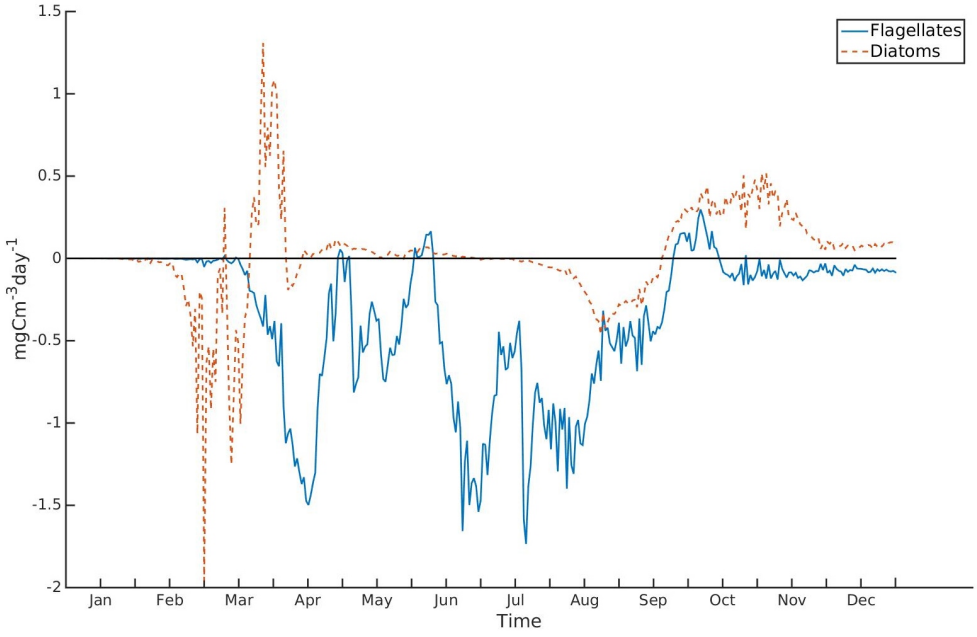

Figure 5.3: The difference between the two runs nwf and wf1 of the total averaged primary production [$mgCm^{-3}day^{-1}$] in the North Sea for daily vertically averaged values of Diatoms and Flagellates. The blue curve represents Flagellates and the red curve represents Diatoms.

in production by Diatoms is negative during the spring bloom, hence the production is larger in run wf1, with a maximum increase of 2 $mgCm^{-3}day^{-1}$. At the end of the bloom in March and April the change is positive, hence the production is smaller in run wf1, with a maximum decrease of 1.3 $mgCm^{-3}day^{-1}$. During the summer months the difference is small between the two runs. In the start of the second bloom in August the values of run wf1 are larger than the reference run, with a maximum increase of 0.5 $mgCm^{-3}day^{-1}$, followed by a smaller production in run wf1 from September with a maximum decrease of 0.5 $mgCm^{-3}day^{-1}$, lasting throughout the year. For Flagellates the difference between the two runs are negative during most of the year, hence the production in run wf1 is larger than the reference run. Run wf1 has a maximum value of larger production than nwf of 1.7 $mgCm^{-3}day^{-1}$ and a maximum value of smaller production of 0.3 $mgCm^{-3}day^{-1}$.

5.1.3 Monthly spatial change

Monthly averaged values of primary production by Flagellates and Diatoms is investigated to show the seasonal distribution of spatial change throughout the year between the run influenced by wind farms and the reference run. The result of production by Diatoms is shown for all months during the year, January to June (Fig. 5.4) and from July to December (Fig. 5.5). For run nwf (left column of figures) production in the early spring bloom, is found in the Southern Bight and off the shallow coastline of Britain in February, at the shallow coastlines of the continental Europe and Britain and over Dogger Bank in March and at a point on the coastline of Britain west of the Inner Silver Pit in April. From May to August production by Diatoms is low and located in the central and northern North Sea. During the late summer bloom in September and October production is found in the central North Sea, while in November and December production is found in the Southern Bight and at Dogger Bank. Production by Diatoms from run wf1 (middle column of figures) show a slightly different pattern than the reference run. The difference between run wf1 and nwf (right column of figures) show a change in distribution for all months. During the spring bloom from February to April the largest difference is found at the shallow coastal area off Britain with less production in run wf1 in March. At the start of the second bloom in August, larger production in run wf1 is

found south and west of Dogger Bank and in September more production is found at Dogger Bank, with less production west of it. From October to December a large change is found of up to maximum 100 % both larger and smaller production in run wf1 compared to nwf. A large change of less production is also found from March to May, with a maximum between 90 and 100 %. The maximum change between the two runs are showed in Table 5.1 for all months.

The result for production by Flagellates is shown for all months during the year, January to June (Fig. 5.6) and for July to December (Fig. 5.7). For run nwf (left column of figures) some production is found in the Southern Bight and along the shallow coast of continental Europe and Britain from January to March, followed by the spring bloom in April where a wider belt of production is found along the coast of the continental Europe and Britain, continuing until September. From October to December a smaller production is found in the same area and at Dogger Bank production is found from April to December. For run wf1 similar pattern of production by Flagellates is shown (middle column of figures), although with some differences from the reference run. The difference between the two runs (right column of the figures) show that change in production is present for all months, but with a general smaller maximum change than for Diatoms, shown in Table 5.1. At the start of the spring bloom in March less production is found south in the Southern Bight and more production is found north in the Southern Bight for run wf1. From April to July the general distribution of change in production is characterized by less production in the northern Southern Bight, while from April to October the general distribution shows larger production over Dogger Bank and south-west towards the British coast, while less production is found off the coast of Denmark and northern part of Germany. From August and throughout the year larger production is found in large parts of the Southern Bight.

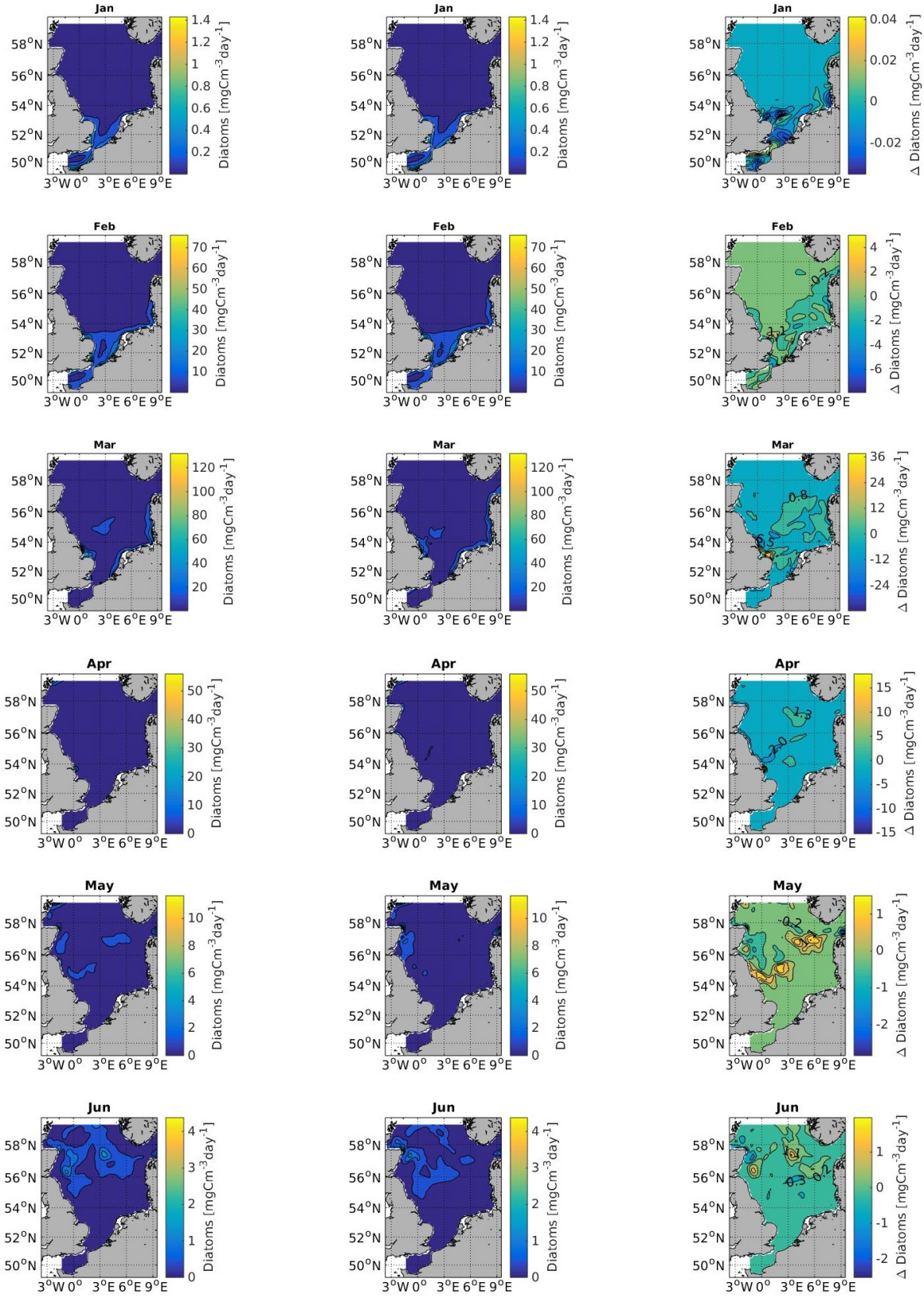

Figure 5.4: Monthly mean vertically averaged primary production [$mgCm^{-3}day^{-1}$] by Diatoms from January to June. Left: run nwf, middle: wf1 and right: (nwf-wf1).

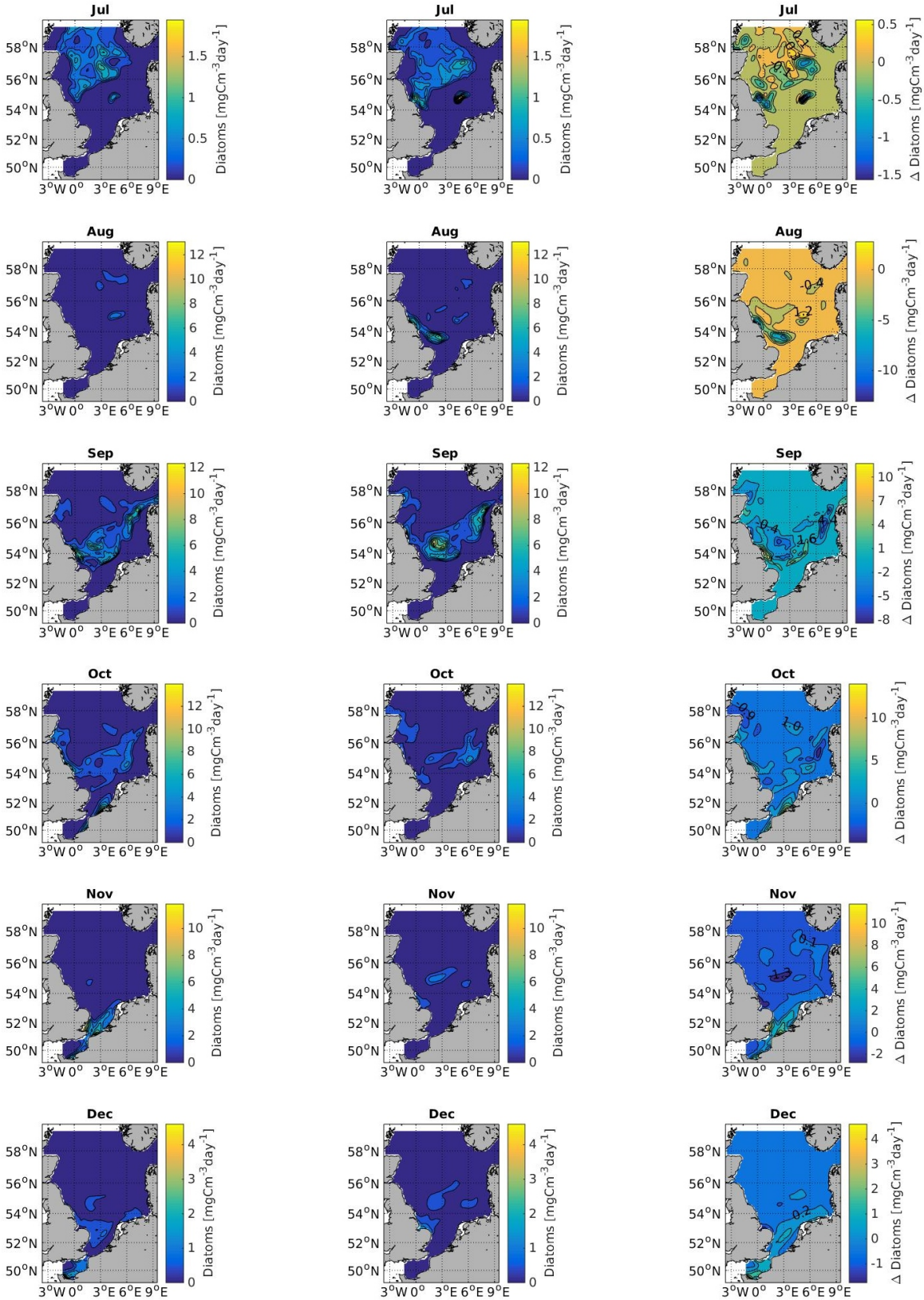

Figure 5.5: Monthly mean vertically averaged primary production $[mgCm^{-3}day^{-1}]$ by Diatoms from July to December. Left: run nwf, middle: wf1 and right: (nwf-wf1).

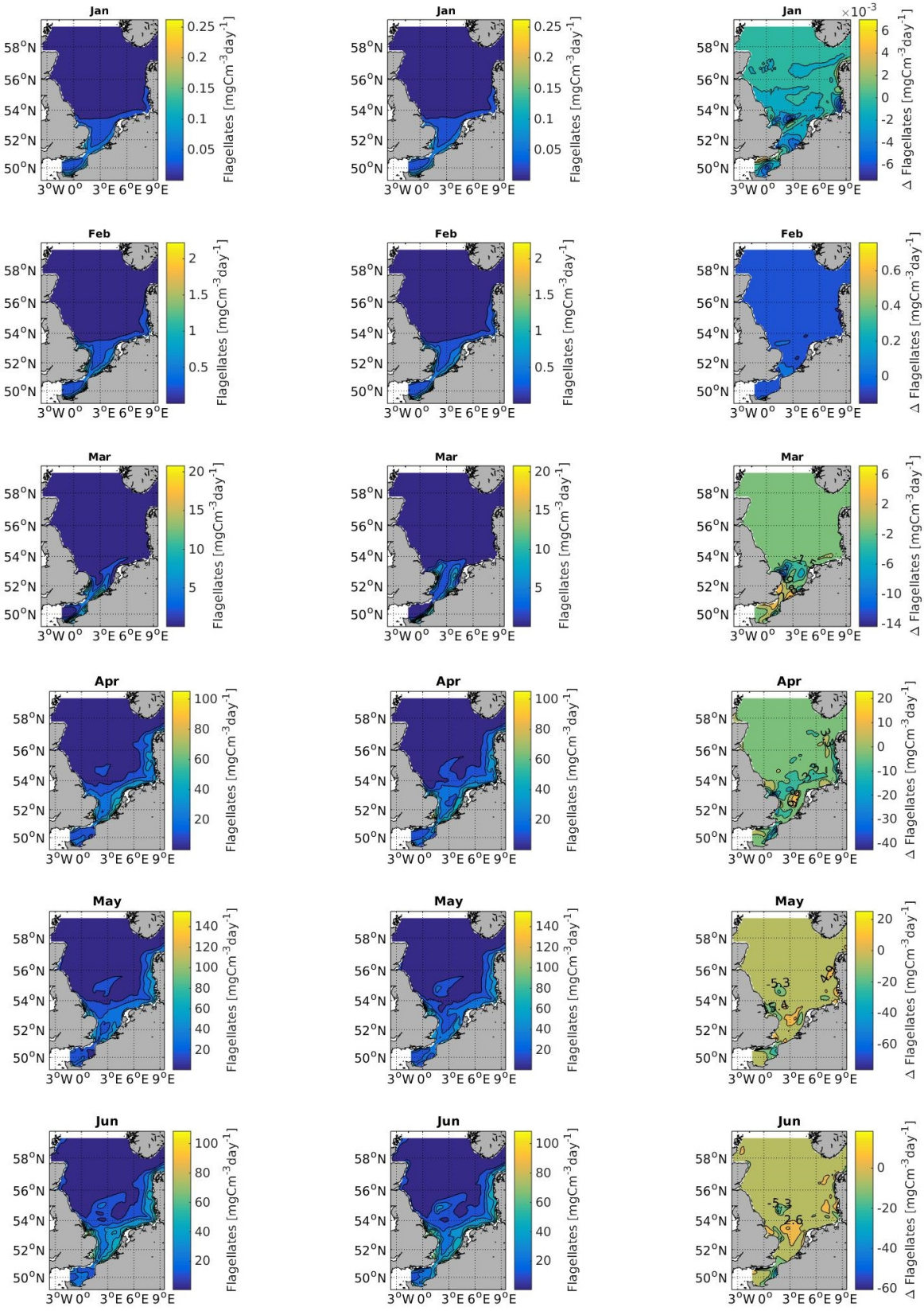

Figure 5.6: Monthly mean vertically averaged primary production $[mgCm^{-3}day^{-1}]$ by Flagellates for January to June. Left: run nwf, middle: wf1 and right: (nwf-wf1).

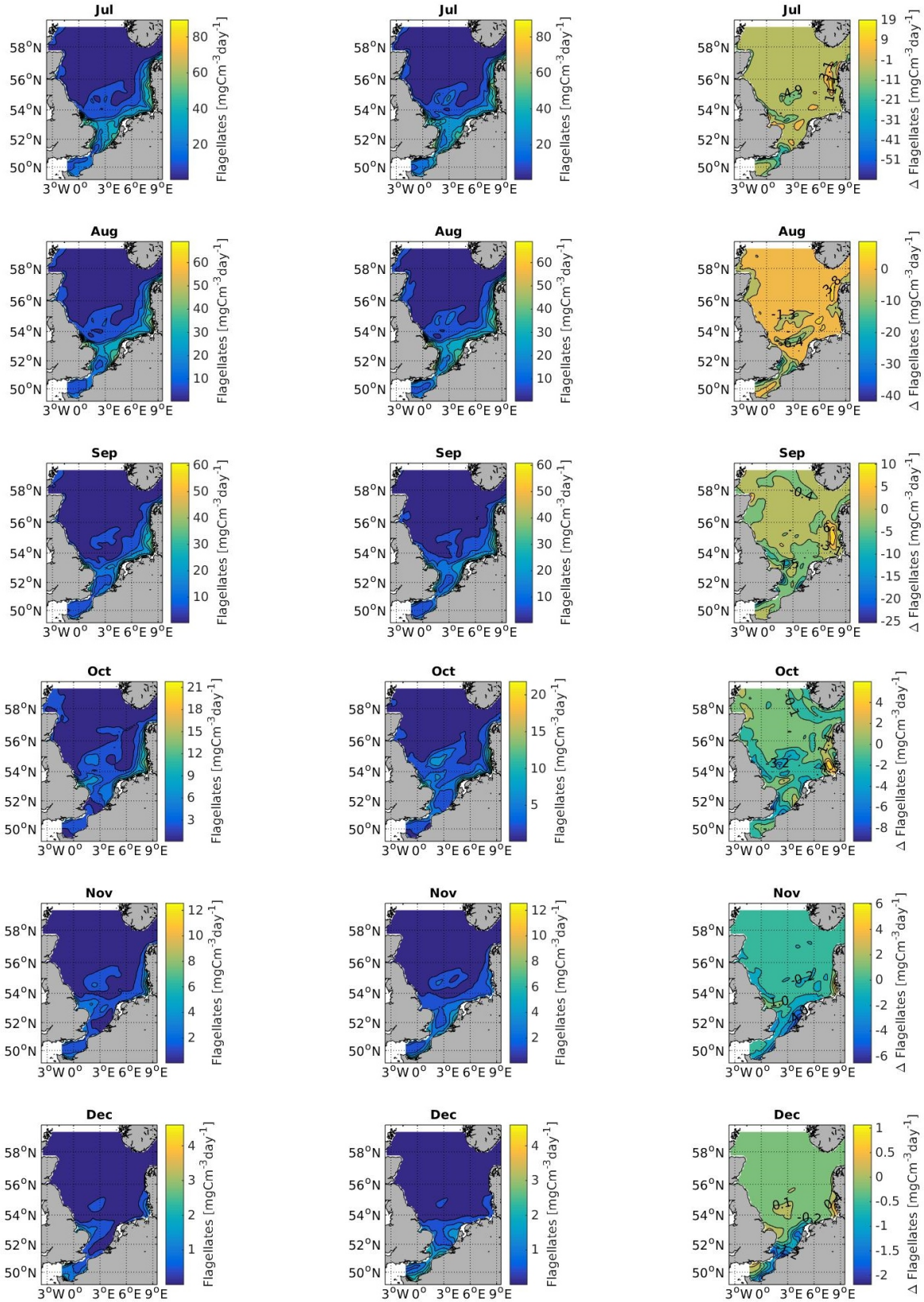

Figure 5.7: Monthly mean vertically averaged primary production $[mgCm^{-3}day^{-1}]$ by Flagellates from July to December. Left: run nwf, middle: wf1 and right: (nwf-wf1).

To see the distribution of maximum difference between run wf1 and the reference run throughout the year Table 5.1 shows maximum increase and decrease in primary production in wf1. The results of primary production, from the run including wind farm implementation compared to the reference run, shows that reduction in wind stress by wind farms in the North Sea will effect the primary production by Flagellates and Diatoms. Change in distribution of production was shown, in addition to a small change in total production.

	Month	01	02	03	04	05	06	07	08	09	10	11	12
D	Max increase [%]	32	28.6	61.4	27.2	29.3	57.7	80.5	100	81	99.2	91.9	88.8
D	Max decrease [%]	7.8	13.2	94.7	100	99.3	69.2	59.6	75.2	95	100	100	100
F	Max increase [%]	18.8	6.9	91	54.7	71.2	78	68	60.5	58.2	83.9	81.8	73.6
F	Max decrease [%]	6.3	34.7	78.9	39.2	29.7	27.6	53.4	54.5	42.5	59	62.8	30.4

Table 5.1: Seasonal distribution of maximum difference in primary production [%] between run wf1 and nwf by D: Diatoms and F: Flagellates.

5.2 Physical factors determining primary production

In this section physical factors driving phytoplankton production and dynamics are presented as possible explanations for change in primary production under influence of wind farm implementation. As described in Section 2.2.2 and 3.2 primary production is controlled by nutrients and light, where limitations of these factors will effect the production. Factors controlling the nutrient content in the euphotic zone are vertical mixing by winds and convection, upwelling and horizontal transport. Therefore the stratification of the water column is important when investigating control of primary production. Since wind stress is the modified factor in the model run influenced by wind farms, oceanic processes dependent on wind-induced turbulent mixing are further investigated. Wind conditions and stratification, including MLD and PEA, are presented in the following sections, first for the reference run nwf, then run wf1 is presented and compared to the reference run.

5.2.1 Undisturbed wind conditions and stratification

The wind speed in the North Sea changes during the year dependent of season, with higher wind speeds in the winter months. Fig. 5.8a) shows monthly averaged 10-m wind speed and Fig. 5.8b) shows monthly averaged wind direction throughout the year at the location of Alpha Ventus wind farm in the German Bight (location given in Fig. 4.2). The yearly averaged wind speed in the location of Alpha Ventus was 7.7 ms^{-1} in 2008,

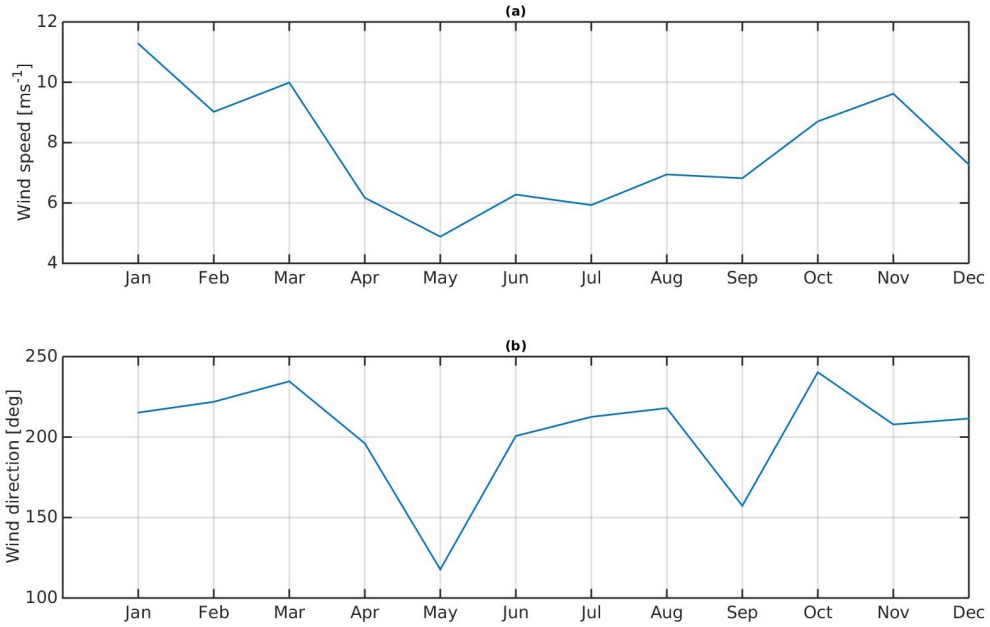

Figure 5.8: Monthly averaged (a) 10-meter wind speed [ms^{-1}) and (b) direction [Deg] at the location of Alpha Ventus wind farm in 2008. Direction zero degrees represent easterly winds and 90 degrees northerly winds.

while the annual averaged wind direction was 201 degrees, a nearly westerly wind. The wind speed has a minimum averaged value of 4.9 ms^{-1} in May and increases to 6.1 ms^{-1} during the summer until September. The summer months from June to September are usually characterized by less intense wind forcing than the rest of the year (Schrum et al., 2003). A climatic study for wind energy in the North Sea, (Geyer et al., 2015), showed an annual mean of 10.6 ms^{-1} at 100 m height in the south-western German Bight in 2008, which corresponds to a 10 m wind speed of 7.6 ms^{-1} calculated from the geostrophic wind Equations 2.9 and 2.10. Year 2008 was the second year out of two with maximum wind speeds from 1958-2012.

The wind direction (Fig. 5.8b) has a monthly mean between 200 and 250 degrees in all months except May and September, where the direction is 118 and 157 degrees respectively. Compared to a study investigating decadal variations in hydrodynamics in the North Sea (Schrum et al., 2003), the main wind directions from year 2008 in this thesis corresponds well to the seasonal variability of south-westerly winds in winter, all directions in May and westerly winds in summer, given as the seasonal variability by Schrum et al. (2003). The distribution of wind direction is shown in Fig. 5.9, where the largest distribution for wind directions lie between 200 and 290 degrees, corresponding to south-westerly and southerly winds.

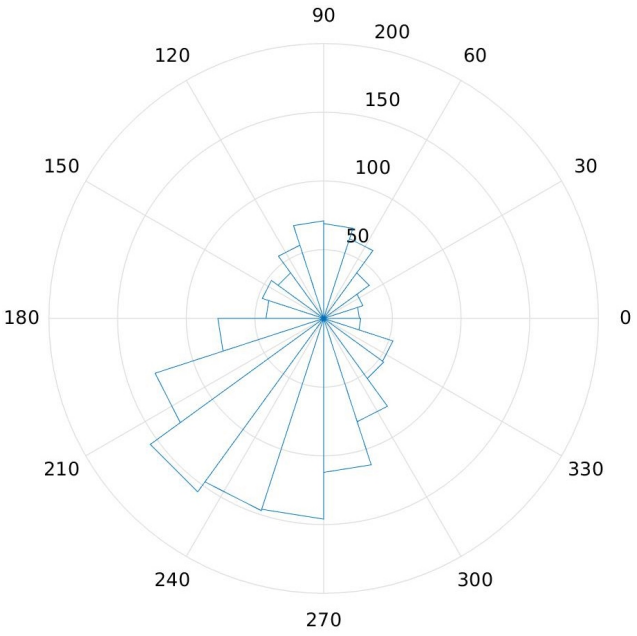

Figure 5.9: Distribution of wind directions [Deg] during year 2008, where zero degrees corresponds to a easterly wind, 90 degrees a northerly wind, 180 degrees a westerly wind and 270 degrees a southerly wind.

The stratification in the North Sea also varies with the seasonal cycle. The seasonal MLD is dependent on wind speed and convection, explained in Section 2.1.2. The monthly mean stratification pattern in the North Sea was calculated based on the location of the thermocline by using a gradient method. The threshold for the existence of a thermocline of a gradient lager than 0.5 °C between each level, was used for the upper 48 m to investigate the surface levels. The location of the thermocline was set to the

level having the strongest gradient within the threshold. However the calculation of the stratification is inaccurate due to the vertical grid resolution of 5 m in the upper surface levels investigated (8 m in the deepest level). The result for the undisturbed reference run is shown from the start of the development in April to the end of stratification in October (Fig. 5.10). For the remaining winter months the water in the North Sea is fully

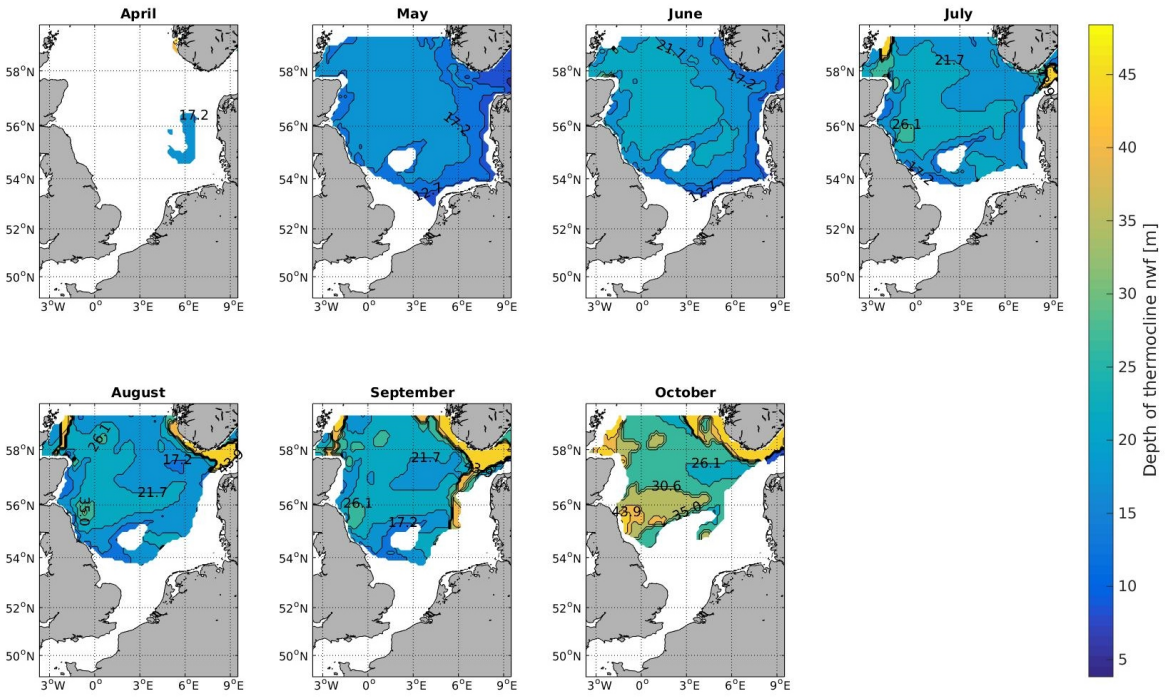

Figure 5.10: Stratification given by the location of the strongest gradient of the thermocline from the surface [m] for the reference run, nwf, calculated for the stratified months from April to October.

mixed by convection and wind mixing. In April the stratification starts to develop, while in May and June it is at its greatest extent before it decreases from July to October. The areas having no stratification throughout the year, the shallow Dogger Bank, the Southern Bight and the area north of it between the British and the Dutch coast, has fully mixed water columns. The stratification based on the thermocline was compared to the stratification pattern showed for the period 1958-1997 in (Schrum et al., 2003) and gave similar results, except larger stratified areas in the north-west part of the model domain for this thesis.

While Fig. 5.10 shows the location of the strongest gradient of the thermocline, the

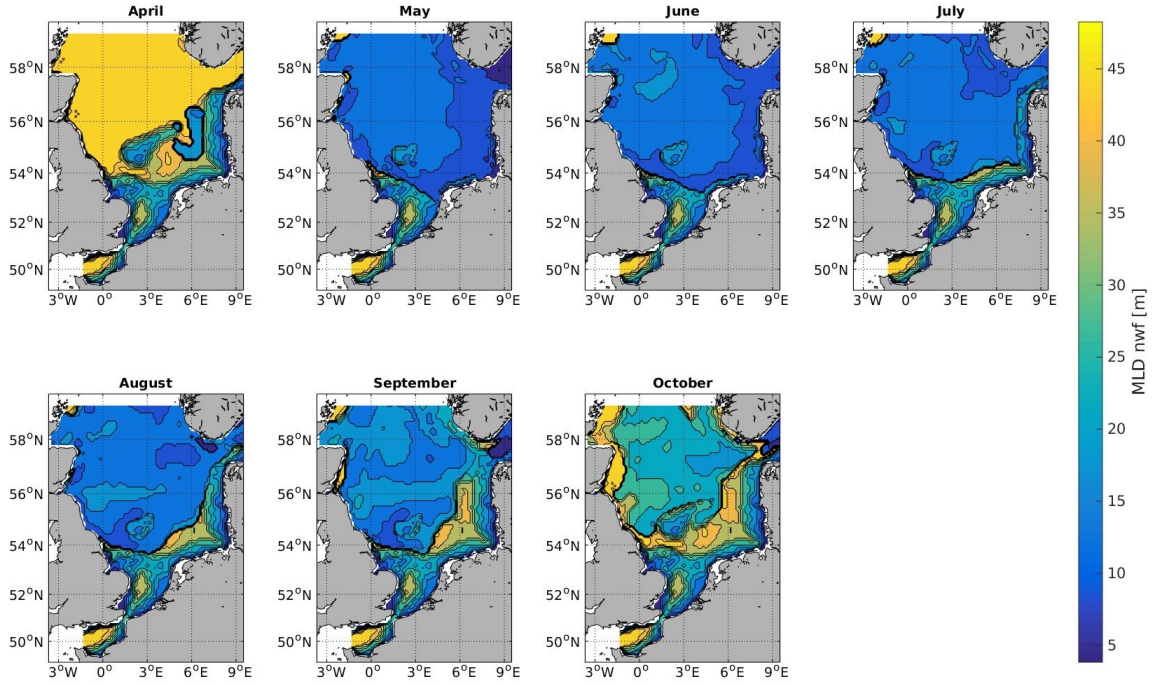

Figure 5.11: Location of the MLD given by the upper level of the thermocline from the surface [m] for the reference run, nwf, calculated for the stratified months April to October.

seasonal mixed layer depth (Fig. 5.11) was set to the location of the uppermost level of the thermocline, which was calculated for the upper 48 m for the stratified months. Where the whole water depth is fully mixed, the depth of the mixed layer follows the topography. In April large areas has a MLD that reaches the maximum depth investigated or the bottom topography. During all months the ML reaches the bottom topography in the Southern Bight, the Norfolk Banks and the Dogger Bank. From mid summer the ML reaches the bottom also in the Oyster Grounds, the German Bight and the area offshore of Denmark.

Monthly means of calculated PEA for run nwf (Fig. 5.12) was calculated using Equation 2.11, to get information on how strong the stratifications is. If the PEA is zero, the water column is fully mixed and requires no extra energy for mixing. The more negative value of the PEA, the more energy is required to fully mix the water. The upper parts of the North Sea including the deep Norwegian Trench and Skagerrak is neglected to get a more detailed plot of the south and central North Sea. In April the PEA is almost zero

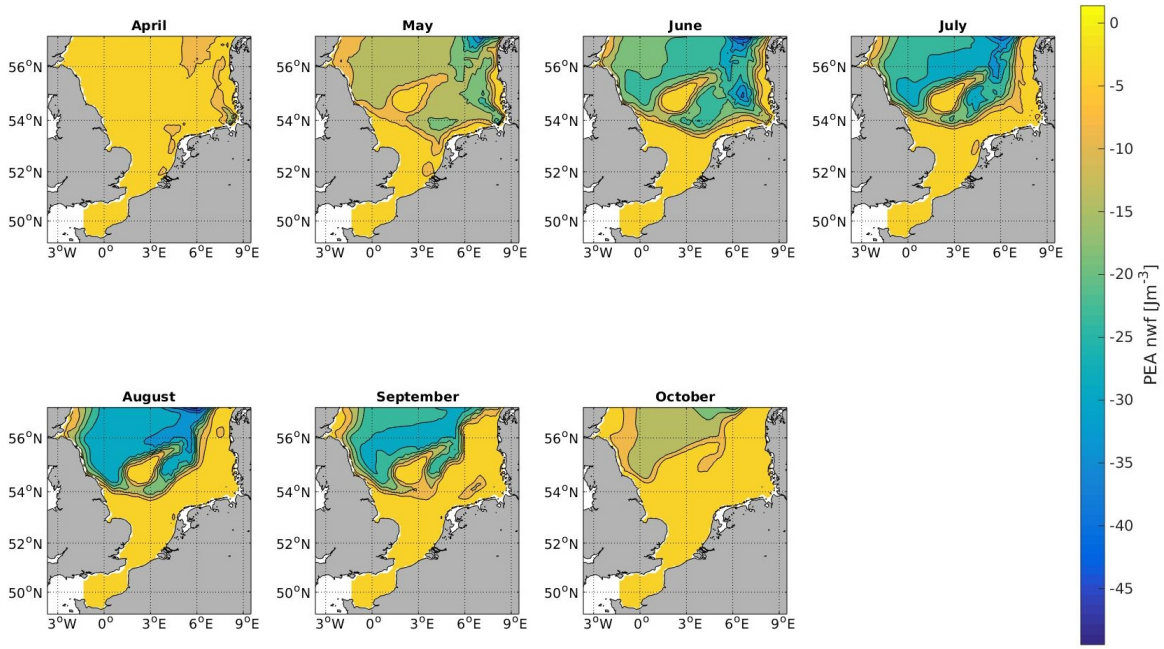

Figure 5.12: PEA $[Jm^{-3}]$ of the reference run nwf for the stratified months April to October.

for the North Sea and requires no energy for mixing, while the value gets more negative during the summer months where more energy is required to fully mix the water, before larger areas again is zero in October. The strongest stratification, is found offshore of Denmark and Germany in June and July, while in August and September it is found in the central and Northern part of the North Sea. The Dogger Bank, the Norfolk Banks and most parts of the Southern Bight are fully mixed and have zero PEA during all months.

5.2.2 Disturbed wind stress

When comparing the wind stress of the run including wind farm parameterization, wf1, and the reference run, nwf, a similar pattern of resulting wind stress deficit is found as in run cwf (Sec. 4.3). An example of a situation with high wind speed in January for a period of 6h, case 1, is shown for run nwf (Fig. 5.13a), wf1 (Fig. 5.13b) and the difference between the two runs (Fig. 5.13c), where a pattern of wind stress deficit is visible. A maximum difference in the resulting wind stress of 0.25 Pa is shown, where the point of maximum reduction has an undisturbed wind stress of 0.6 Pa and a disturbed wind

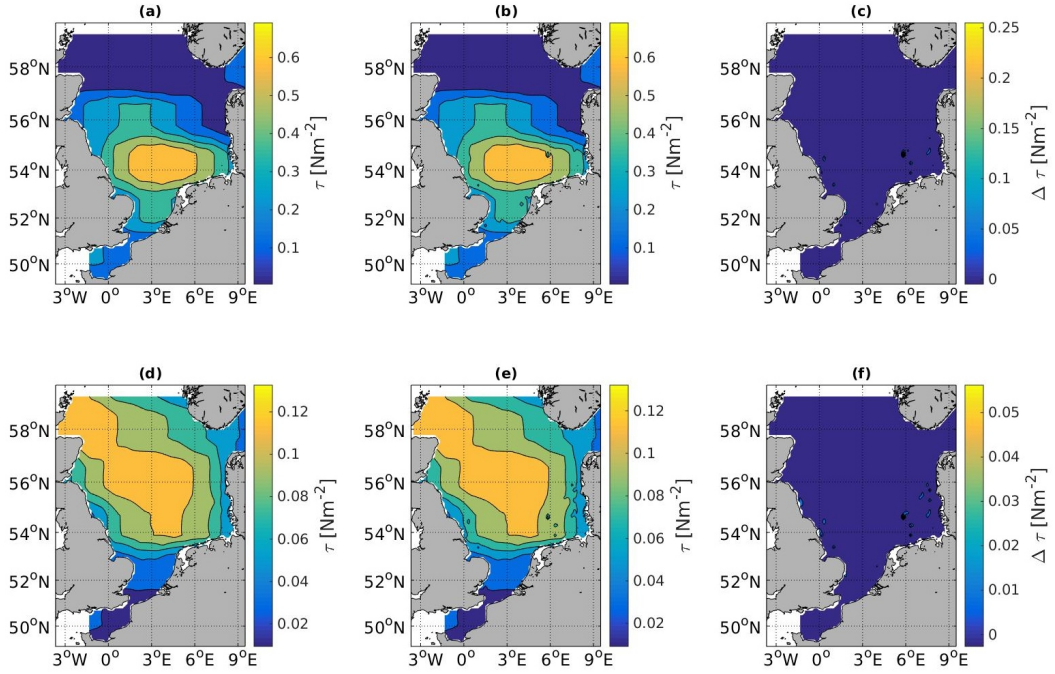

Figure 5.13: Wind stress $[Nm^{-2}]$ at the sea surface in the North Sea presented for a) run nwf, b) run wf1 and c) the difference between the two runs (nwf-wf1), during a period of 6 h in January with high wind speed, case 1. For 6 h of a day in June with lower wind speed, case 2, d) shows run nwf, e) run wf1 and f) the difference between the two runs.

stress of 0.35 Pa. The wind stress with full reduction was 57.5% of the initial wind stress, which gives a maximum reduction in wind stress of 42.5 %. The difference in percent is calculated at the grid point of maximum reduction in wind stress. A period of 6h in June with lower wind stress, case 2, is shown in Fig. 5.13d) for run nwf and in Fig. 5.13e) for run wf1 , where the resulting maximum difference in wind stress between wf1 and nwf (Fig. 5.13f) is 0.056 Pa, a maximum change of 53.13 % in the given point with an undisturbed wind stress of 0.11 Pa and disturbed wind stress of 0.05 Pa.

Run	Case	Max $\Delta\tau_x$ [Pa]	Undisturbed τ_x [Pa]	Disturbed τ_x [Pa]	Max $\Delta\tau_x$ [%]
wf1	1	0.25	0.6	0.35	42.5
wf1	2	0.056	0.11	0.05	53.13

Table 5.2: Examples of resulting maximum wind stress deficit from run wf1 for a period of 6 h in January with high wind speed, case 1, and a period of 6 h in June with lower wind speed, case 2.

5.2.3 Change in stratification and mixing layer

As for the undisturbed stratification of the North Sea from run nwf, the stratification in run wf1 (Fig. 5.14), was calculated using the same method as for run nwf, based on the gradient of the thermocline. Compared to the undisturbed case (Fig. 5.10), the disturbed stratification shows a small change in extent of the stratified water visible in April, where the stratified area is larger, and in July, where the stratification reaches closer to the coast in the Helgoland Bight. However in May and June the stratification west of Dogger Bank is more shallow, while in July to September the stratification is deeper in run wf1. Along the coast of the British Isles the stratification is found at more shallow depths from June to October, while at the central north parts of the North Sea the stratification is deeper in run wf1 from June to October.

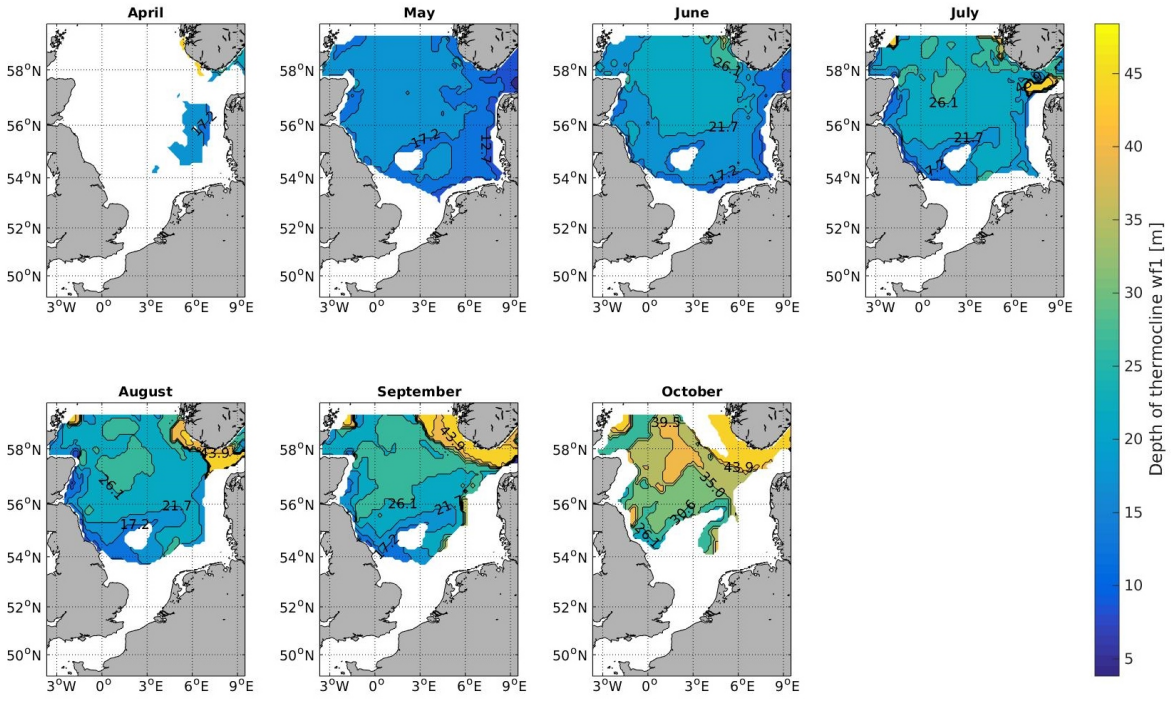

Figure 5.14: The stratification of run wf1 given by the depth of the strongest gradient of the thermocline from the surface [m] for April to October.

The monthly averaged MLD for run wf1 (Fig. 5.15), was calculated for the stratified months based on the same threshold of the thermocline as described for the MLD of the reference run and show similar result. The difference between run wf1 and the reference

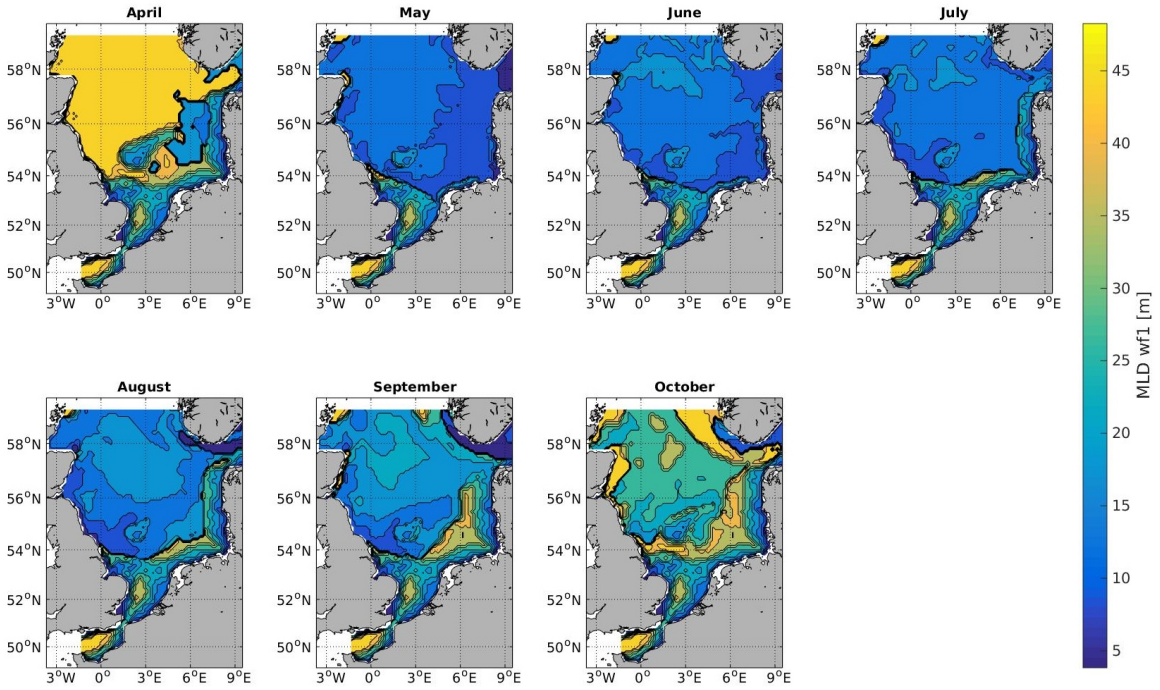

Figure 5.15: Location of the MLD [m] given by the upper level of the thermocline from the surface for run wf1, from April to October.

run (Fig. 5.16) was calculated to clearly see the change in MLD due to a reduced wind stress pattern. A difference in MLD is found for all months having stratified water. In April positive change of about 12-21 m, representing a more shallow MLD in run wf1, is found offshore of Denmark and Germany. For the remaining stratified months a change is found along the border of the stratified water and the well mixed tidal banks in the south of the North Sea. In May a deepening of the MLD in wf1 by 6.5 to 24.7 m is found between the British and Dutch coast. In June more shallow MLD in wf1 by a change of up to 30 m is found south-west of Dogger Bank. In July a more shallow MLD in wf1 by a change of up to 11.8 m was found from the coast of Britain to the Helgoland Bight. Here a deepening of 6.5 m is found along the Danish and northern German coast in run wf1. A similar pattern is found in August, but with larger changes and the more shallow area in the German Bight reaching further north in run wf1. In September and October most of the interface between the stratified and mixed water show a more shallow MLD. Some more shallow areas are also found in the central North Sea during the stratification period and some deeper areas are found in the north parts of the North Sea in late

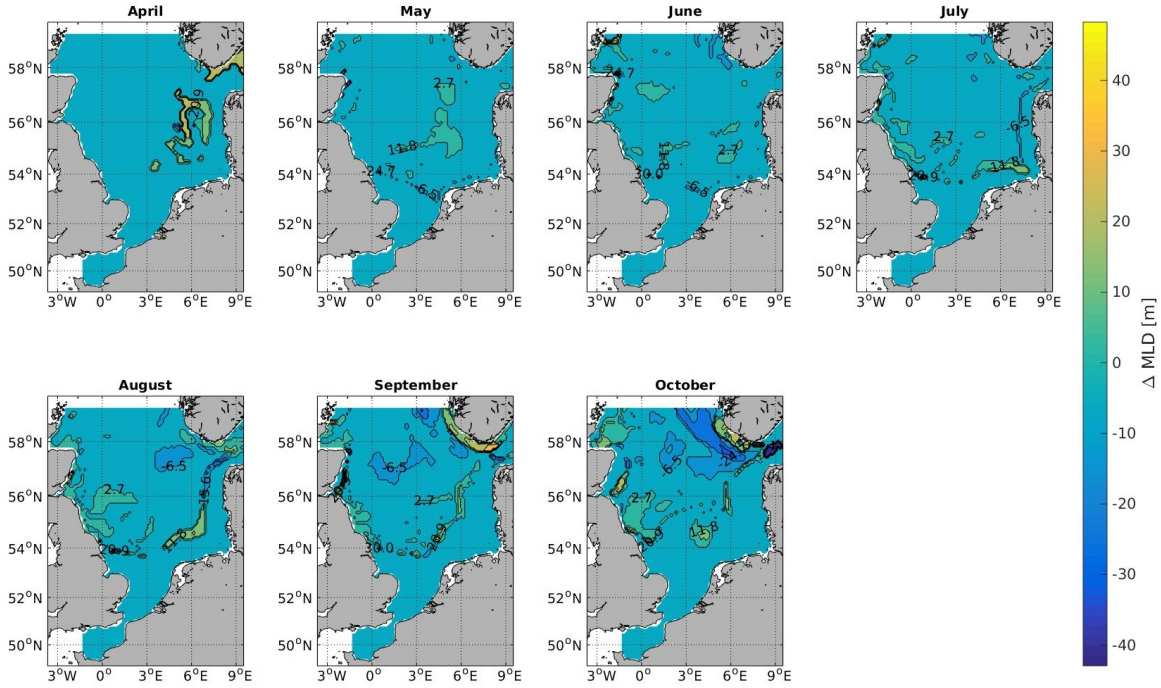

Figure 5.16: Difference in MLD [m] between wf1 and the reference run (nwf-wf1) from April to October.

summer. Ludewig (2015) investigated the Alpha Ventus wind farm in the German Bight (location given in Fig. 4.2) and found a maximum change of the thermocline of 10 m. In this thesis the change in MLD is up to 11.8 m decrease and up to 6.5 m increase in the German Bight.

The change in MLD based on the location of the pycnocline was also calculated. This includes the influence of fresher water in the south of the North sea. As for the thermocline, the pycnocline was calculated using a gradient method with a threshold of 0.125 kgm^{-3}, with the MLD located at the depth of the upper level of the pycnocline. Density was calculated from values of temperature and salinity by using a seawater property function in matlab (Moataz, 2011). Figure 5.17 show similar pattern of change as the MLD based on the thermocline, but with some differences. During the stratified months the change in upper layer of the pycnocline show larger areas of deepening of the MLD in run wf1 for all months and more changes closer to the coast of the European continent, but show similar values of change.

The monthly means of PEA of run wf1 (Fig. 5.18) shows similar pattern as for the ref-

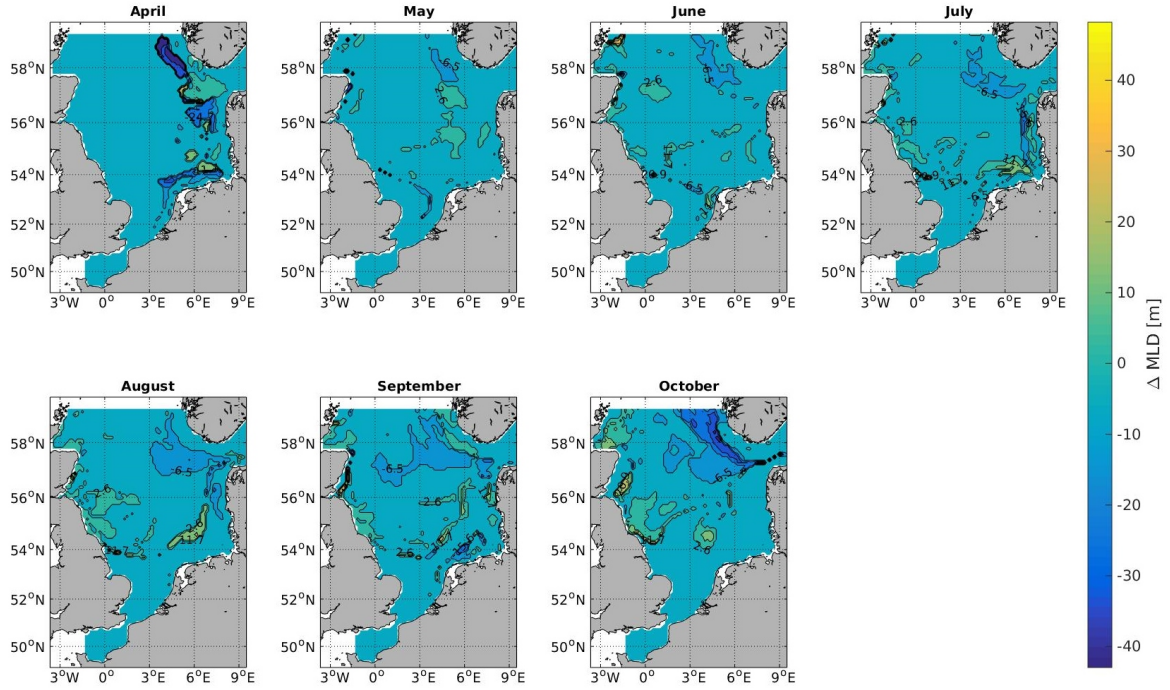

Figure 5.17: Change in MLD [m] (nwf-wf1) calculated from the location of the upper level of the pycnocline from April to October.

erence run (Fig. 5.12), but some changes are shown in the calculated difference between the two runs (Fig. 5.19), calculated to show how the reduced wind stress field effects the energy required to fully mix the water column, thus the change in strength of the stratification between the two runs. It is calculated by subtracting the values of wf1 from nwf. Since all the PEA values are negative, less negative values in run wf1 than nwf gives a negative difference where less energy is needed for the water to be fully mixed. More negative values in wf1 than nwf gives a positive difference where more energy is needed to fully mix the water. More energy is needed to fully mix the water in central and south parts of the North Sea from July to October for run wf1. In May and June some areas off the continental European coast show that less energy is required to fully mix the water in run wf1.

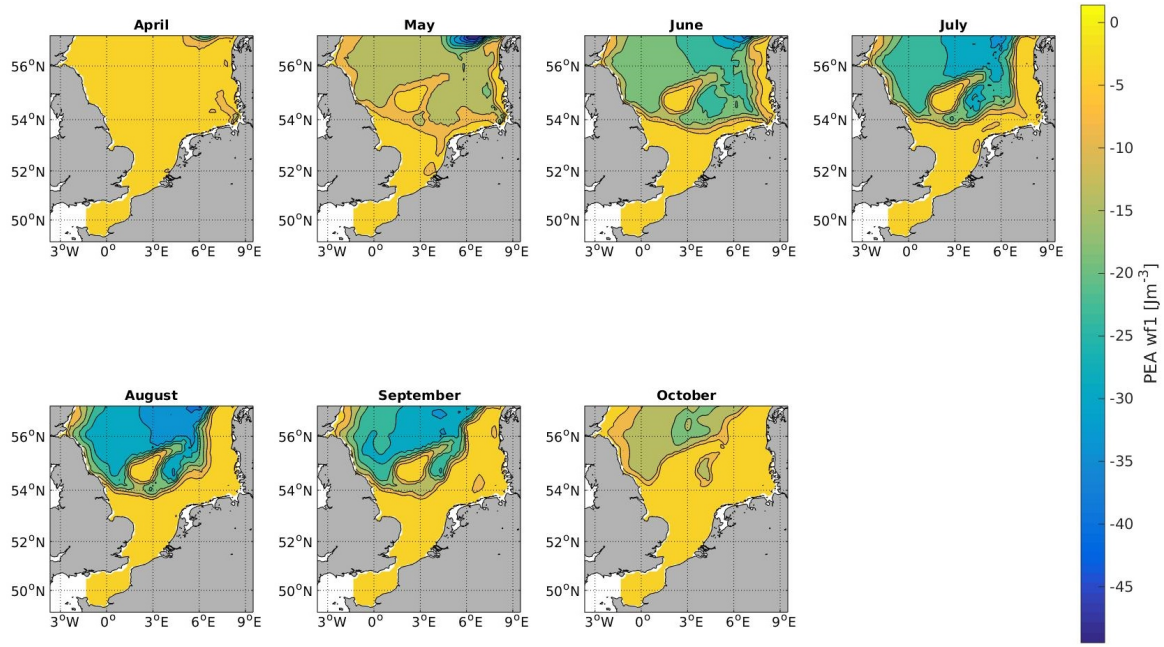

Figure 5.18: PEA [Jm^{-3}] for run wf1 from April to October.

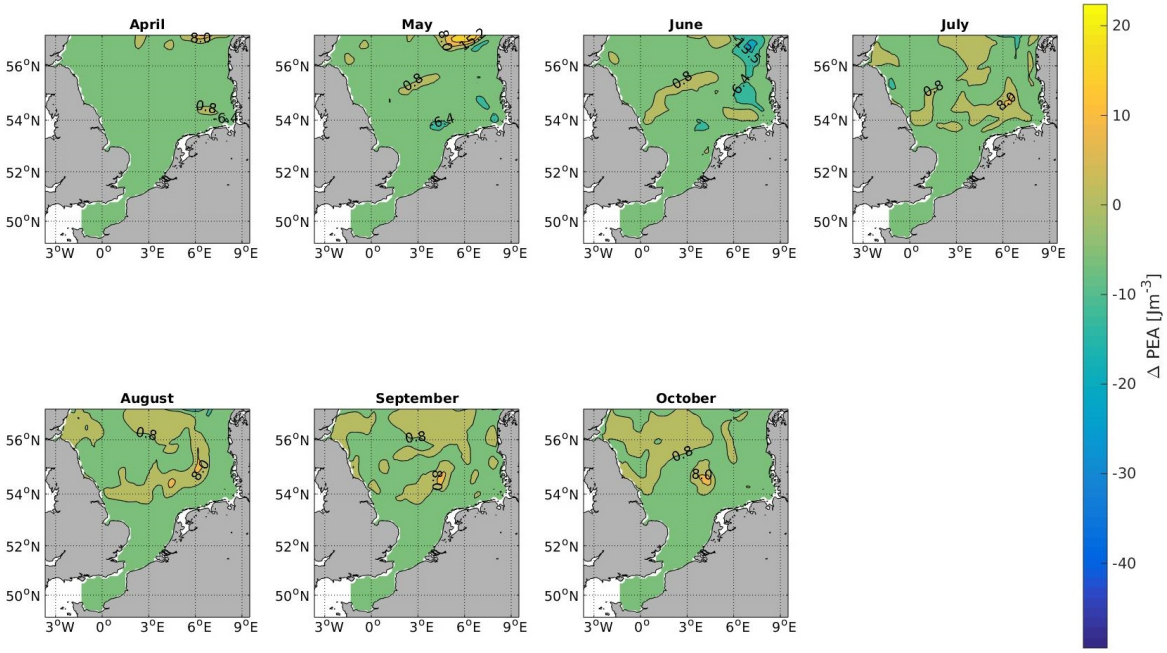

Figure 5.19: Difference in PEA [Jm^{-3}] between the two runs (nwf-wf1) for April to October.

5.3 Other effects

The temperature is not included as a state parameter that controls production in ECOSMO, however vertical gradient of temperature controls stratification which affects production. The temperature itself affects higher trophic levels, and is hence presented for annual means. Annual vertically averaged temperature for run nwf (Fig. 5.20a) shows inflow of warm water from the English Channel that continues along the coast of the European continent, and colder water from the Atlantic inflow at the Northern boundary, which continues south along the coast of the British Isles. The total averaged temperature in the model area was 9.7 °C in run nwf and 9.6 °C in run wf1, showing a difference between the two runs with a lower temperature in run wf1. The temperature from run wf1 (Fig. 5.20b) show similar inflow pattern as run nwf. However the annual averaged difference between the two runs (Fig. 5.20c) show a maximum temperature increase of 1.1 °C and a maximum decrease of 1.2 °C in run wf1. The distribution of change in temperature show a lower temperature along the British Isles and higher temperature in the Southern Bight, north of the Southern Bight, offshore of Denmark and the northern part of Germany and in the north-west part of the North Sea. Thus the temperature show a change of both total averaged temperature and in distribution.

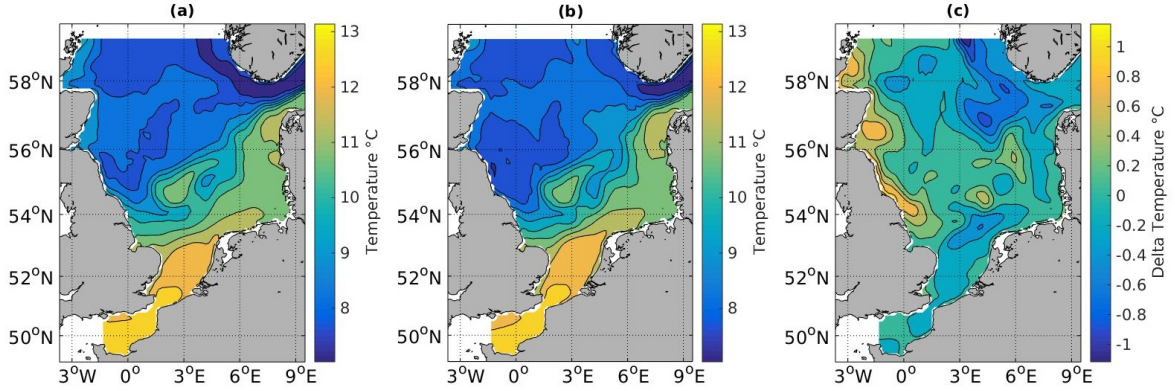

Figure 5.20: Annual vertically averaged temperature [°C] during year 2008.

5.4 Examples of daily changes in production by Flagellates

Daily averaged changes in primary production by Flagellates and physical state parameters related to wind-induced turbulent mixing is also investigated, where the focus is on Flagellates since the main production is found within the stratified months, compared to Diatoms which have the largest production before the onset of seasonal stratification. Two days showing different change in primary production by Flagellates and having different wind direction are presented in this section.

A day with large difference in primary production by Flagellates between run nwf and wf1 in July, day 206, was chosen to be compared with a day close in time, day 215 in August, because of the smaller change in production found by Flagellates. These days were chosen to be able to compare possible factors influencing the change in primary production. Day 206 has a maximum increase in vertically averaged production of 1.1 $gCm^{-2}day^{-1}$ and a maximum decrease of 0.9 $gCm^{-2}day^{-1}$ in wf1, compared to the reference run. Day 215 has a maximum increase in vertically integrated production of 0.7 $gCm^{-2}day^{-1}$ and a maximum decrease of 0.7 $gCm^{-2}day^{-1}$ in wf1, compared to the reference run. The wind direction of the two days was a northerly wind of 92° in day 206 and a south-westerly wind of 227° in day 215. First day 206 is presented.

The wind conditions in day 206 was characterized by wind from north as mentioned above, with a wind speed of 6.4 ms^{-1} at both the locations of Alpha ventus wind farm in the German Bight and at Sheringham Shoal wind farm east of Britain (location given in Fig. 4.2). The wind stress has a resulting maximum deficit of 56 %.

The pattern of vertically integrated daily production by Flagellates in day 206 for run nwf (Fig. 5.21a) shows high production along the continental European coast, the shallow British coast and in northern parts of the Southern Bight. Production from run wf1 (Fig. 5.21b) show a similar pattern with production at coastal areas, but with some differences from the reference run. The difference between the two runs (Fig. 5.21c) show patterns of positive and negative change. Less production (positive values) is found offshore of the Danish coast and in the German Bight. More production in run wf1 (negative values) is found surrounding Dogger Bank and stretching from the British to the Dutch coast. A larger production is also found close to shore in the Helgoland Bight and south in the Southern Bight. When comparing the change in production in day 206 to

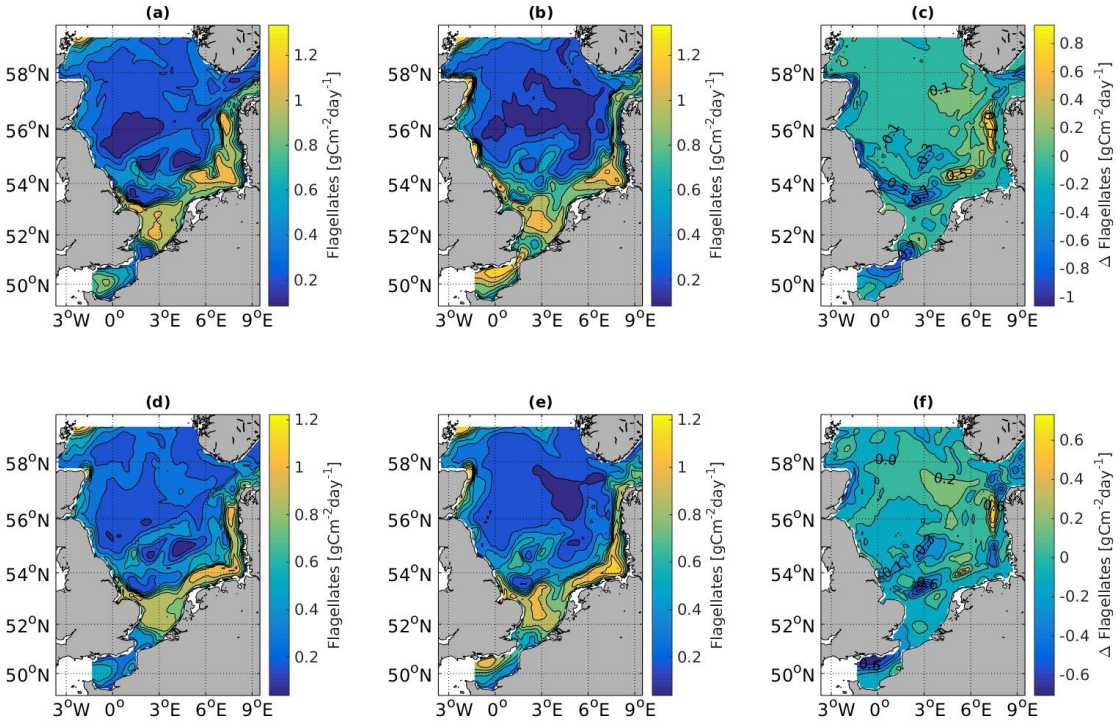

Figure 5.21: Vertically integrated daily primary production $gCm^{-2}day^{-1}$ by Flagellates for day 206 in July for a) run nwf, b) run wf1 and c) the difference between the two runs (nwf-wf1), and for day 215 in August for d) run nwf, e) run wf1 and f) the difference between the two runs (nwf-wf1).

the yearly and monthly averaged production by Flagellates of year 2008 and July respectively, areas of larger production at Dogger Bank and south of it and smaller production off the Danish and north part of the German coast, are found in both the yearly and monthly average, although with smaller extension.

The stratification in day 206, calculated from the temperature gradient criterion, showed a difference between the reference run and run wf1 (Fig. 5.22). In the reference run (Fig. 5.22a) the water column is fully mixed outside the coast of Denmark, in large areas of the German Bight and the Oyster Grounds, over the shallow Norfolk Banks outside the coast of Britain, Dogger Bank and in the Southern Bight. In the run wf1 (Fig. 5.22b) a lager extent of the stratified waters is found in the German Bight and the Oyster Grounds. Compared to the monthly averaged stratification for July, the stratification in day 206 is less extended than the monthly mean for wf1 and similar to the monthly mean for nwf.

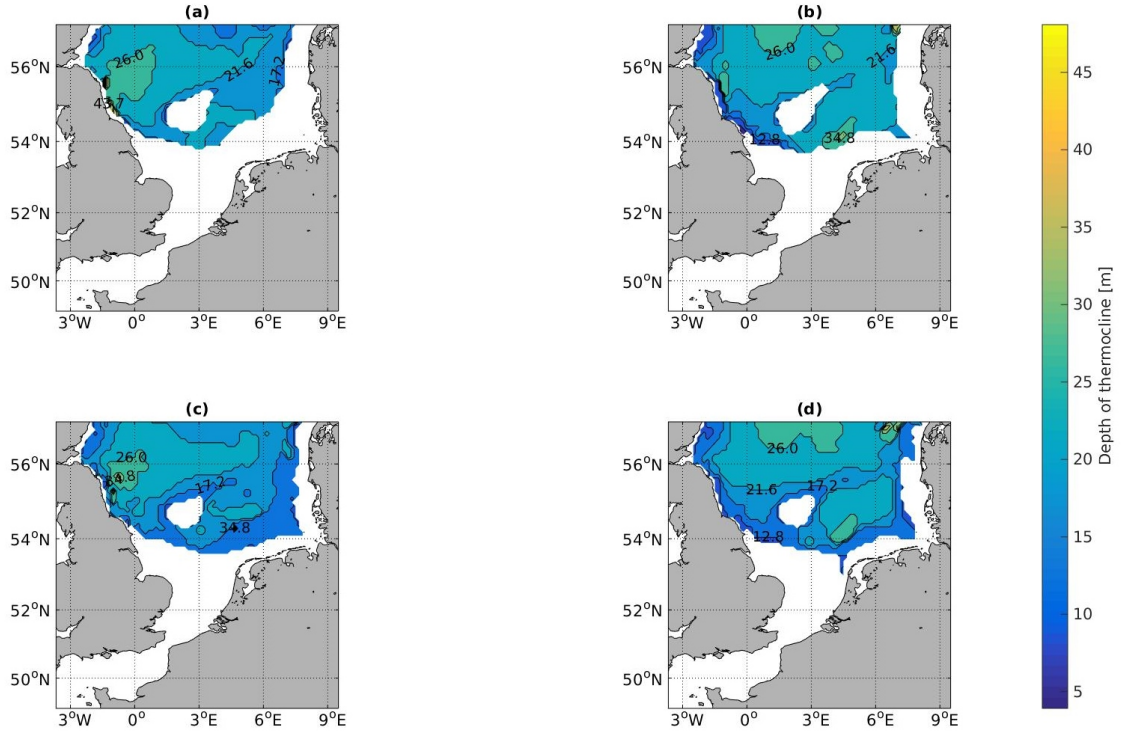

Figure 5.22: Stratification based on the largest gradient of the thermocline from the surface [m] for day 206 in July from a) run nwf and b) run wf1, and for day 215 in August from c) nwf and d) wf1.

The MLD for day 206 shows to have less areas of a MLD reaching the bottom topography in the German Bight for run wf1 (Fig. 5.23b) than run nwf (Fig. 5.23a). The change in MLD between the two runs (Fig. 5.23c) shows positive difference, hence more shallow MLD in run wf1, offshore of Germany and the Netherlands continuing towards the British Isles along the boarder of the stratified area. A negative change, deeper MLD in in run wf1, is found south and north of Dogger Bank and in the east part of central North Sea. Compared to the monthly mean stratification for July the change look similar, but with smaller extent.

The PEA for day 206 show to have large negative values east of Dogger Bank for run nwf (Fig. 5.24a) and similar pattern for run wf1 (Fig. 5.24b), but with some differences between the two runs, shown in figure (Fig. 5.24c). The negative values of change represent areas of less negative values in run wf1 than in nwf, where the water needs less energy to mix. The positive difference represents areas of more negative values in run

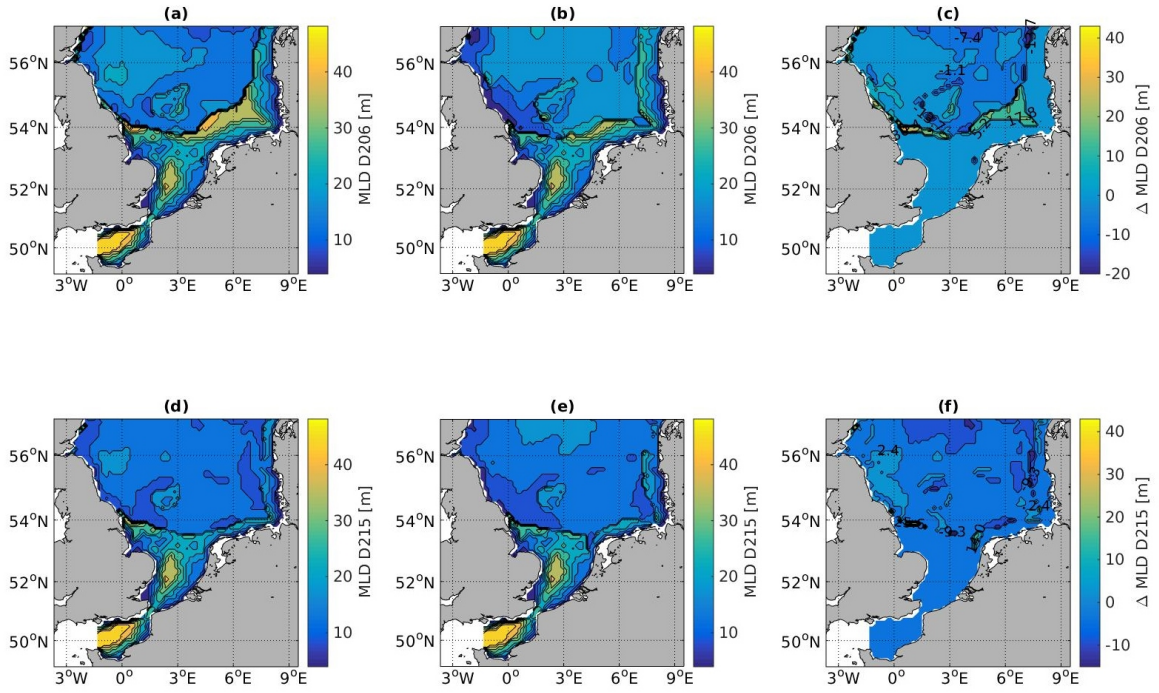

Figure 5.23: Location of the MLD given by the upper level of the thermocline from the surface [m] for day 206 in July from a) run nwf, b) run wf1 and c) the difference between the two runs (nwf-wf1) and for day 215 in August from d) nwf, e) wf1 and f) the difference between the two runs.

wf1 than in nwf, where the water needs more energy to mix. Positive difference is found in large parts of the German Bight, the Oyster Grounds and close to Dogger Bank. Pattern of negative change is found in the Southern Bight close to the Dutch coast, off the Northern German coast and the Danish coast, where a positive change is found closer to shore. Compared to the monthly mean PEA for July more negative change, where less energy is required for mixing, is found in run wf1 for day 206.

Day 215 has wind conditions characterized by wind from south west as mentioned above, a wind speed of 7.2 ms^{-1} at the Alpha Ventus wind farm and 6.4 ms^{-1} at the Sheringham Shoal wind farm. The wind stress was reduced by a resulting maximum deficit of 52 % of the wind stress in the reference case at the given grid point. The distribution of production by Flagellates in day 215 show a similar pattern as day 206. A more shallow belt of production is found outside the Danish, German and Dutch coast compared to day 206 for both run nwf (Fig. 5.21d) and wf1 (Fig. 5.21e). Outside the coast of Den-

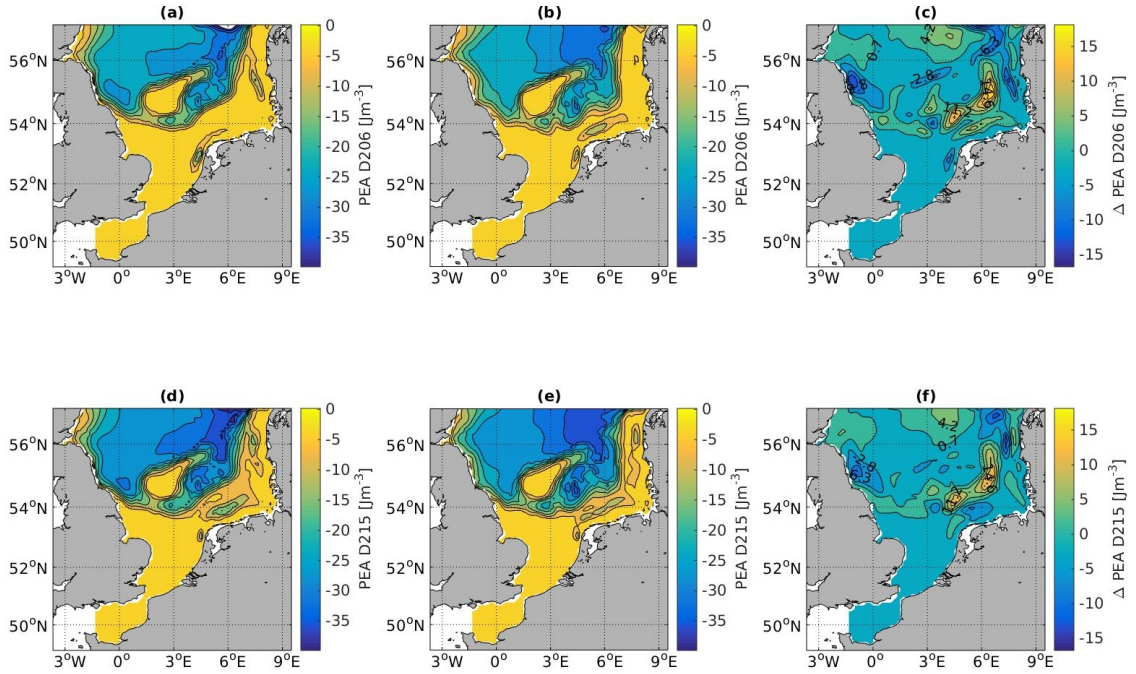

Figure 5.24: PEA $[Jm^{-3}]$ for day 206 in July from a) run nwf, b) run wf1 and c) the difference between the two runs (nwf-wf1) and for day 215 in August from d) run nwf, e) wf1 and f) the difference between the two runs.

mark less production in wf1, compared to the reference run, is found at the north part of the coast, with a larger production further South. More production is found in the area South of Dogger Bank and in the Southern Bight. The following pattern of change in production (Fig. 5.21f) shows less production offshore of the south part of the Danish coast and more production at the north part of the Danish coast in run wf1. Off the coast of Germany north of Helgoland Bight, less production is found close to shore with more production further offshore in run wf1. North of the Dutch coast less production is found and at Dogger Bank and the surrounding area both positive and negative change is found for run wf1. Compared to the yearly and monthly averaged production by Flagellates for 2008 and August respectively, the pattern of less production off the coast of Denmark and the larger production south of Dogger Bank is also found for the yearly and monthly mean.

The stratification in day 215 calculated from the thermocline, show large extent of the stratification for both wf1 (Fig. 5.22c) and nwf (Fig. 5.22d). Compared to the monthly

mean stratification for August larger stratified areas are found in day 215 for both run nwf and wf1.

The MLD for day 215 based on the thermocline reaches the bottom topography in the Southern Bight for both run nwf (Fig. 5.23d) and wf1 (Fig. 5.23e). The difference between the the two runs (Fig. 5.23f) show difference at the border between the stratified water and the fully mixed water, with positive change off the British and Dutch coast and a negative change further east off the Dutch coast and off coast close to the German and Danish boarder. A positive change and larger production are also found in the Helgoland Bight and off the north parts of the Danish coast. Compared to the monthly averaged change in MLD for August (Fig. 5.16), the pattern of positive change off the German coast and negative change of the Danish coast is different than for day 215.

The PEA for day 215 for run nwf (Fig. 5.24d) and wf1 (Fig. 5.24e) show similar patterns as day 206. The change between run nwf and wf1 (Fig. 5.22c) show similar pattern as for the change in day 206, except a negative change, where less energy is required to fully mix the water in run wf1, offshore of the Netherlands and positive values are found offshore of the north part of Germany, where more energy is required to fully mix the water.

5.5 Reduced maximum wind stress deficit run wf2

This section presents results of the response of a smaller wind stress deficit on primary production and physical state parameters related to wind-induced turbulent mixing. Run wf2, including the alternative wind farm parameterization P2, with a smaller maximum specified wind stress deficit than run wf1, is compared to run wf1 for primary production, stratification, MLD and PEA to see if the strength of reduction in wind stress effects the results.

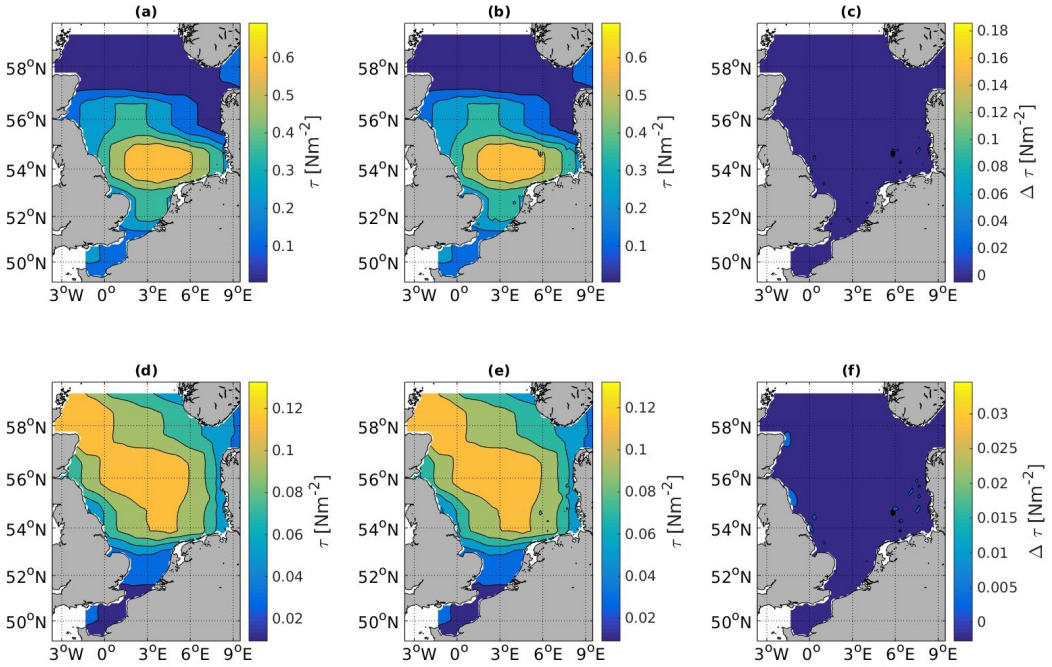

Figure 5.25: Wind stress [Nm^{-2}] at the sea surface in the North Sea presented for a) run nwf, b) run wf2 and c) the difference between the two runs (nwf-wf2), during a period of 6 h in January with high wind speed, case 1. For 6 h in June with lower wind speed, case 2, d) shows run nwf, e) run wf2 and f) the difference between the two runs.

5.5.1 Disturbed wind stress

As for wf1 (Sec. 5.2.2), the same period of 6h with high wind speed in January shows change in resulting wind stress downstream of the wind farms (Fig. 5.25) with a resulting maximum difference in wind stress of 0.19 Pa, where the point of maximum reduction has an undisturbed wind stress of 0.6 Pa and a disturbed wind stress of 0.41 Pa. The wind stress with full reduction is 69 % of the initial wind stress so that the reduction in wind stress is 31 %. For the period of 6h in June with lower wind speed, the resulting maximum deficit is 0.03 Pa, where the point of resulting maximum reduction had an undisturbed wind stress of 0.11 Pa and a disturbed wind stress of 0.07 Pa. The wind stress with full reduction is 67.3 % of the initial wind stress so that the reduction in wind stress is 32.7 %. The results are summarized in Table 5.3 and shows, as for the cwf cases (Sec. 4.3), that P1 gives larger wind stress deficit than P2.

Run	Case	Max $\Delta\tau_x$ [Pa]	Undisturbed τ_x [Pa]	Disturbed τ_x [Pa]	Max $\Delta\tau_x$ [%]
wf2	1	0.19	0.6	0.41	31
wf2	2	0.03	0.11	0.07	32.7

Table 5.3: Examples of resulting maximum wind stress deficit [Nm^{-2}] from run wf2 for a period of 6 h in January with high wind speed, case 1, and a period of 6 h in June with lower wind speed, case 2.

5.5.2 Change in primary production

Yearly averaged vertically integrated primary production by Flagellates and Diatoms was calculated for run wf2, (Fig. 5.26). The difference between run wf1 (Fig. 5.26b,e)

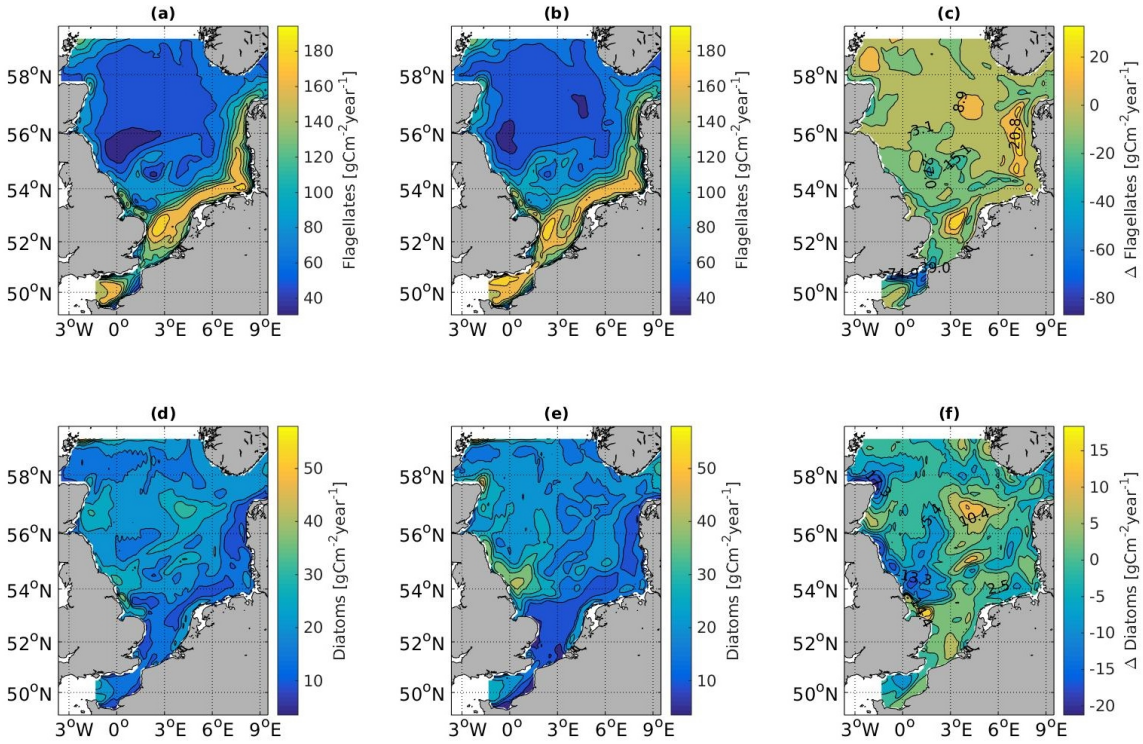

Figure 5.26: Annual vertically integrated distribution of primary production [$gCm^{-2}year^{-1}$] of a) Flagellates run nwf, b) Flagellates run wf2, c) the difference in Flagellates between the two runs (nwf-wf2), d) Diatoms run nwf, e) Diatoms run wf2 and f) the difference between Diatoms in the two runs (nwf-wf2). Notice the changing colorbar.

and the reference run nwf (Fig. 5.26a,d) for Flagellates (Fig. 5.26c) and for Diatoms (Fig.

5.26f) show no difference in distribution of change in production from run wf1 (Fig. 5.1), except some very small changes in the shape of the pattern of change in some locations. The calculated production by Flagellates has a maximum production in a grid cell of the model domain in run wf2 of 188.7 $gCm^{-2}year^{-1}$ and the total averaged production in the North Sea is 88.9 $gCm^{-2}year^{-1}$. The change in production between run wf2 and the reference run nwf, has a maximum increased production of 86.9 $gCm^{-2}year^{-1}$ in wf2 and a maximum decreased production of 32.8 $gCm^{-2}year^{-1}$ in wf2. The calculated production by Diatoms has a maximum production in a grid cell in run wf2 of 57 $gCm^{-2}year^{-1}$ and a total averaged production in the North Sea of 20.8 $gCm^{-2}year^{-1}$. The change in production between run wf2 and the reference run nwf, has a maximum increased production of 21.3 $gCm^{-2}year^{-1}$ and a maximum decreased production of 18.4 $gCm^{-2}year^{-1}$ in wf2. The values of change between run wf2 and wf1 for Flagellates (Fig. 5.27a) and Diatoms (Fig. 5.27b) show a small difference from run wf1, with both smaller and larger production in run wf2 compared to wf1.

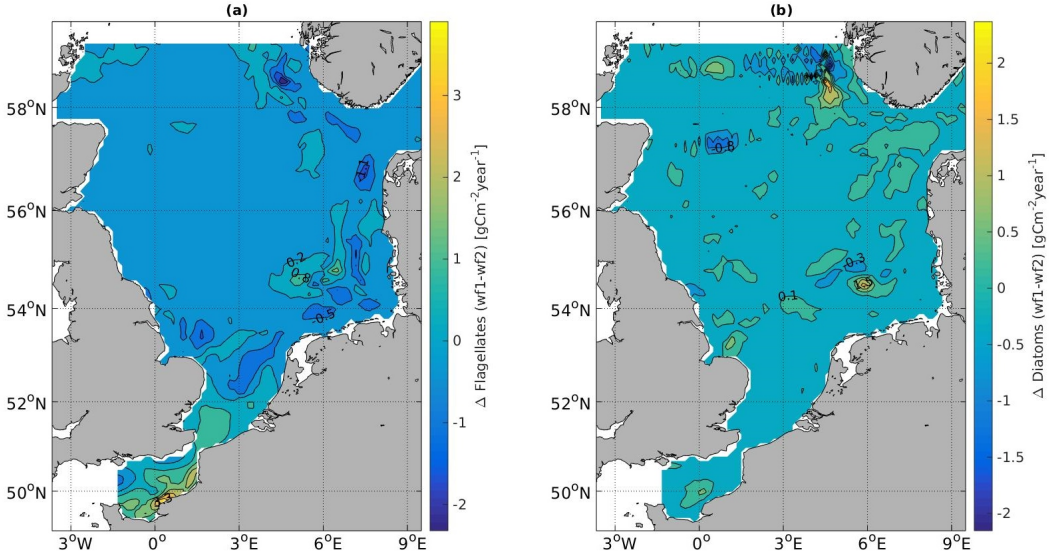

Figure 5.27: The difference in primary production $gCm^{-2}year^{-1}$ between run wf1 and wf2 (wf1-wf2), where wf2 is calculated using the wind farm parameterization P2 and wf1 using P1 for all wind farms located in the North Sea in 2015. a) shows change in production by Flagellates and b) by Diatoms.

5.5.3 Change in stratification and MLD

The location of the largest gradient of the stratification was calculated for run wf2 (Fig. 5.28), using the same threshold as for run wf1. No evident difference in stratification between run wf2 and wf1 (Fig. 5.14) is found. The MLD was calculated for run wf2, based on the upper level of the thermocline (Fig. 5.29). The difference in MLD between run wf2 and the reference run nwf (Fig. 5.30) show no evident difference in pattern of changed MLD between the two runs with different maximum specified wind stress deficit.

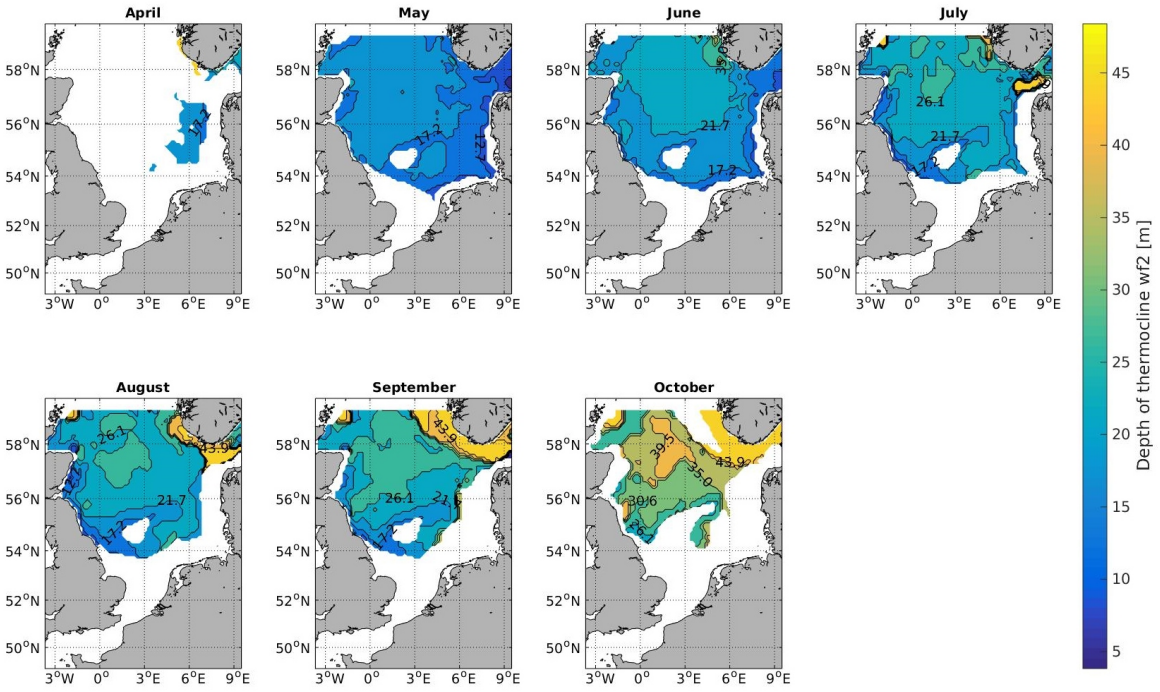

Figure 5.28: Stratification for run wf2 calculated from the location of the maximum gradient of the thermocline from the sea surface [m] from April to October.

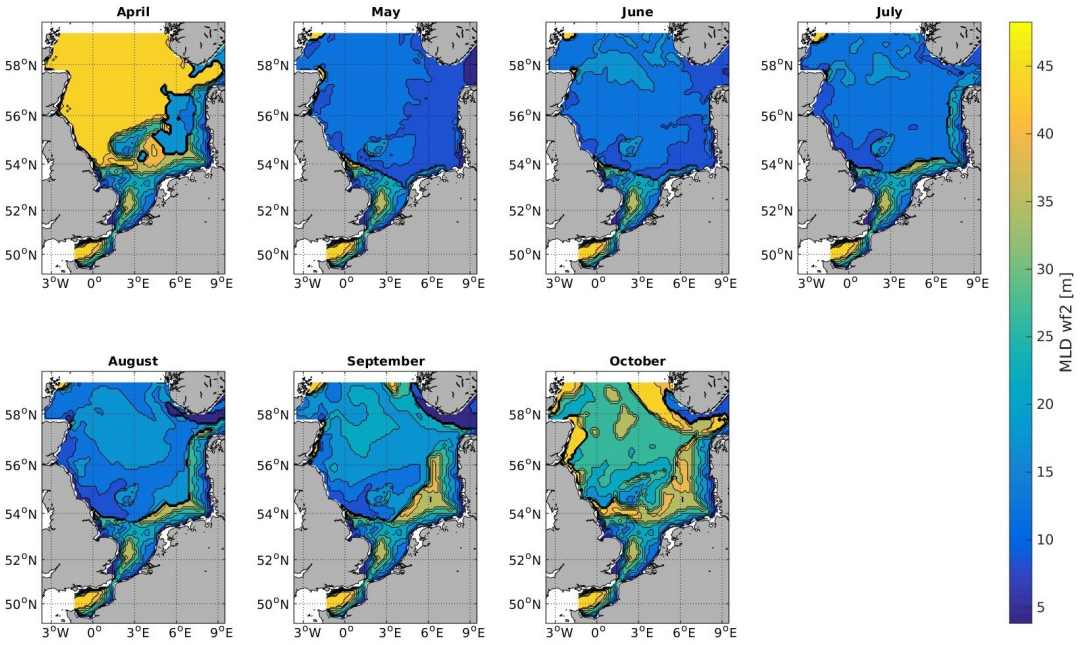

Figure 5.29: MLD [m] for run wf2 calculated from the upper level of the thermocline from April to October.

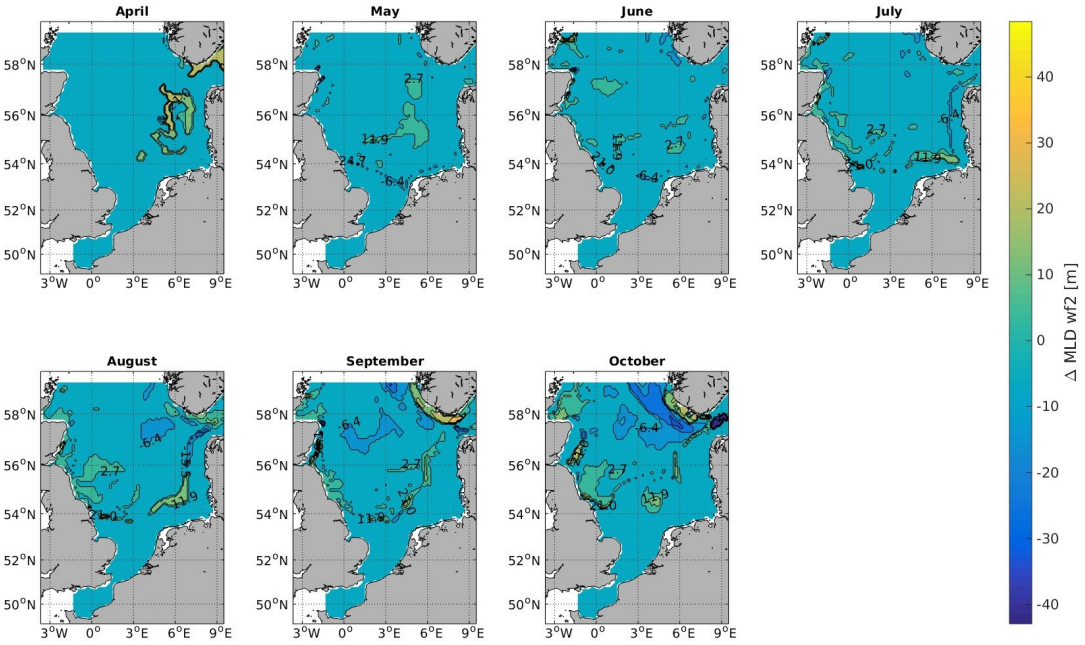

Figure 5.30: Difference in MLD [m] between run wf2 and the reference run (nwf-wf2) calculated from the upper level of the thermocline from April to October.

5.6 Future scenario of wind farm implementation run wf3

This section presents results of the response of a larger number of wind farms with larger size on primary production and physical state parameters related to wind-induced turbulent mixing. The run representing a future scenario of wind farm implementation in the North Sea, wf3, where all wind farms planned to exist in the near future are included, is compared with the runs including the operational wind farms in 2015, to see how a larger implementation of wind farms effects primary production, stratification and mixing.

5.6.1 Disturbed wind stress

The resulting wind stress comparison for run wf3 and nwf (Fig. 5.31) show similar pattern of deficit as previous cases, but with larger and more extended deficit. For the same period of 6h in January with large wind stress, case 1, the resulting maximum difference

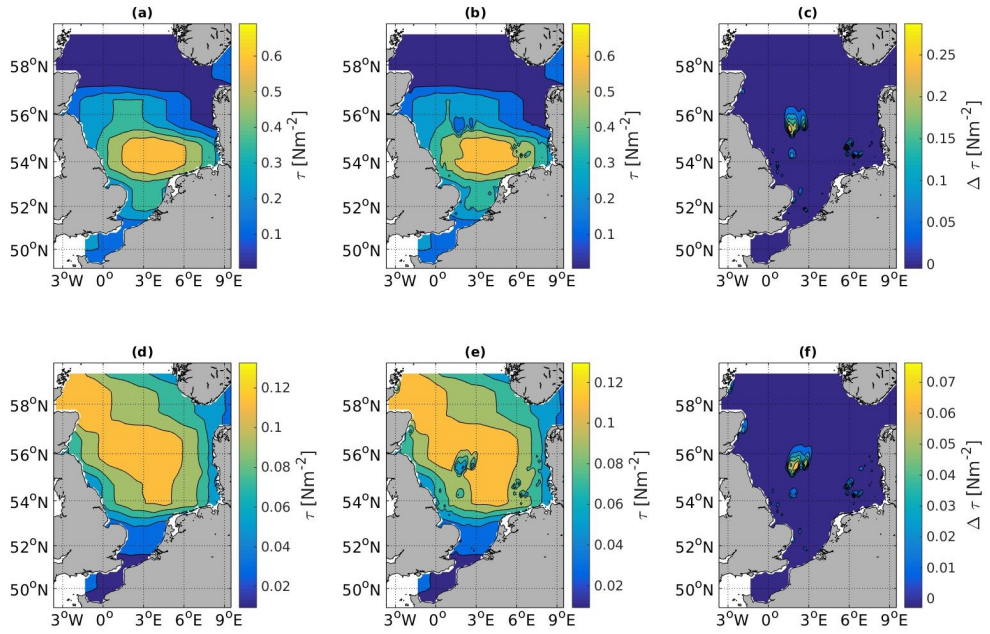

Figure 5.31: Wind stress $[Nm^{-2}]$ at the sea surface in the North Sea presented for a) run nwf, b) run wf3 and c) the difference between the two runs (nwf-wf3), during a period of 6 h of a day in January with high wind speed, case 1. For 6 h of a day in June with lower wind speed, case 2, d) shows run nwf, e) run wf3 and f) the difference between the two runs.

in wind stress between run wf3 and nwf (Fig. 5.31c) is 0.29 Pa, where the grid point of resulting maximum reduction has an undisturbed wind stress of 0.56 Pa and a disturbed wind stress of 0.27 Pa. The remaining wind stress after maximum reduction is 48.8 %, which gives a maximum reduction of 51.2 %. For the situation of lower wind stress in June, case 2, the resulting maximum difference between the two runs (Fig. 5.31f) is 0.076 Pa, where the grid point of resulting maximum reduction has an undisturbed wind stress of 0.12 Pa and a disturbed wind stress of 0.05 Pa. The remaining wind stress after maximum reduction is 37.1 %, which gives a maximum reduction of 62.9 %. The values are summarized in Table 5.4.

Run	Case	Max $\Delta\tau_x$ [Pa]	Undisturbed τ_x [Pa]	Disturbed τ_x [Pa]	Max $\Delta\tau_x$ [%]
wf3	1	0.29	0.56	0.27	51.2
wf3	2	0.076	0.12	0.05	62.9

Table 5.4: Examples of resulting maximum wind stress deficit [Nm^{-2}] from run wf3 for a period of 6 h in January with high wind speed, case 1, and a period of 6 h in June with lower wind speed, case 2.

5.6.2 Change in primary production

Primary production was calculated for Flagellates and Diatoms from run nwf and wf3 (Fig. 5.33). The difference in production was calculated between the two runs for Flagellates (Fig. 5.33c) and Diatoms (Fig. 5.33f), where the pattern of change is similar as for the previous runs. The calculated production by Flagellates has a maximum production in a grid cell of the model domain in run wf3 of 189.5 $gCm^{-2}year^{-1}$ and the total averaged production in the North Sea in run wf3 is 88.4 $gCm^{-2}year^{-1}$. The change in production between run wf3 and the reference run nwf, has a maximum increase in production of 87.2 $gCm^{-2}year^{-1}$ and a maximum decrease production of 32.4 $gCm^{-2}year^{-1}$ in wf3. The calculated production by Diatoms has a maximum production in run wf3 of 56.7 $gCm^{-2}year^{-1}$ and the total averaged production in the North Sea is 20.7 $gCm^{-2}year^{-1}$. The change in production between run wf3 and the reference run nwf, has a maximum increased production of 18.8 $gCm^{-2}year^{-1}$ and a maximum decreased production of 18.5 $gCm^{-2}year^{-1}$ in wf3. When comparing the change in primary production between

run wf3 and wf1 (Fig. 5.32) with the change between wf2 and wf1 (Fig. 5.27), lager values of increased and decreased production is found for wf3.

Information on annual primary production from the runs nwf, wf1, wf2 and wf3 are summarized in Table 5.5 for comparison.

Run	nwf	wf1	wf2	wf3
Max production Flagellates	194.2	189.3	188.7	189.5
Total averaged production Flagellates	86.2	88.9	88.9	88.4
Max Δ production increase Flagellates	-	87.2	86.9	87.3
Max Δ production decrease Flagellates	-	32.4	32.8	32.4
Max production Diatoms	57.9	57	57	56.7
Total averaged production Diatoms	20.6	20.8	20.8	20.7
Max Δ production increase Diatoms	-	21.3	21.3	18.8
Max Δ production decrease Diatoms	-	18.3	18.4	18.5

Table 5.5: Information on annual primary production $[gCm^{-2}year^{-1}]$ by Flagellates and Diatoms in the reference run nwf, run wf1, wf2 and wf3.

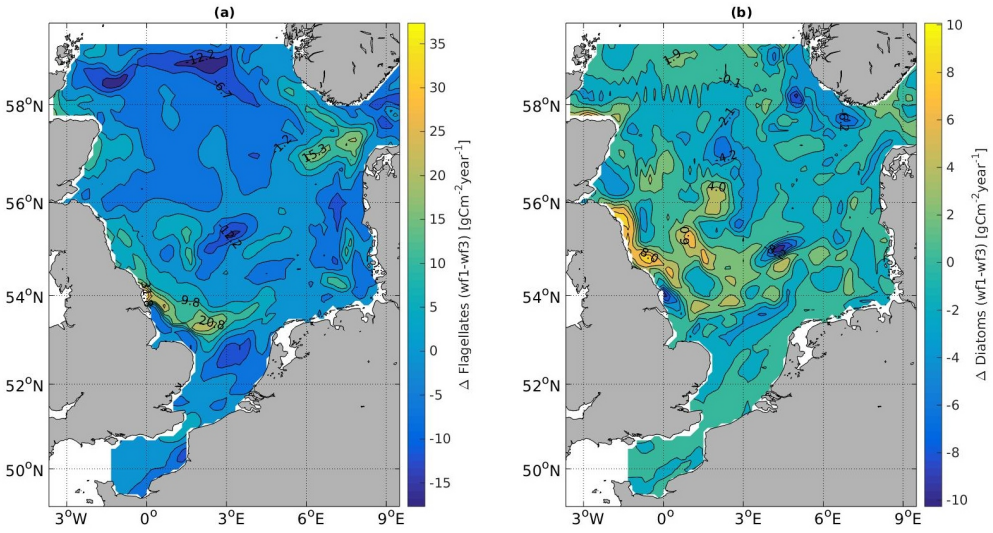

Figure 5.32: The difference in primary production $[gCm^{-2}year^{-1}]$ by a) Flagellates and b) by Diatoms between run wf1 and wf3.

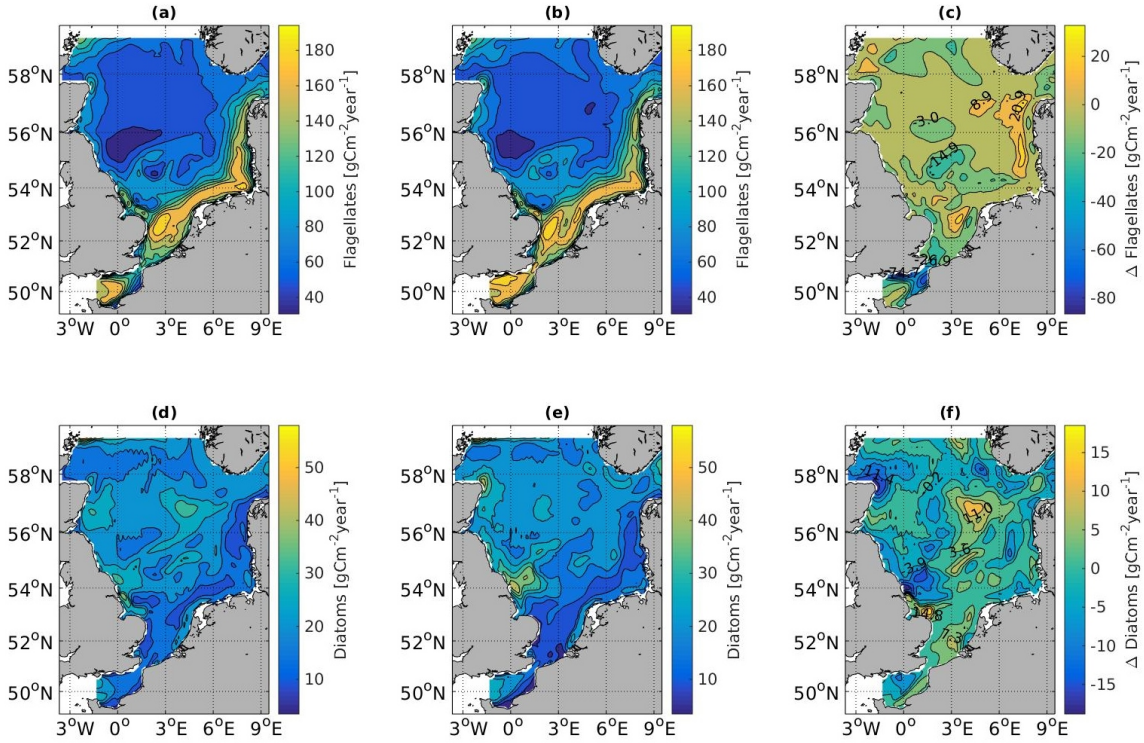

Figure 5.33: Annual vertically integrated distribution of primary production $[gCm^{-2}year^{-1}]$ by a) Flagellates run nwf, b) Flagellates run wf3, c) the difference in Flagellates between the two runs, nwf-wf3 d) Diatoms run nwf, e) Diatoms run wf3 and f) the difference between Diatoms in the two runs, nwf-wf3.

5.6.3 Change in stratification and MLD

For run wf3, the stratification was calculated using the same method as for run wf1 (Fig. 5.34). Compared to the difference in MLD from run wf1 (Fig. 5.16), the deepest stratification is found for smaller areas of the North Sea from June to October in run wf3.

The MLD for run wf3 was calculated by the same method as for run wf1 (Fig. 5.35). The difference between the MLD of run wf3 (Fig. 5.36) and the reference run nwf (Fig. 5.11), shows some differences in distribution of changed MLD than for run wf1, but with the same main pattern of change.

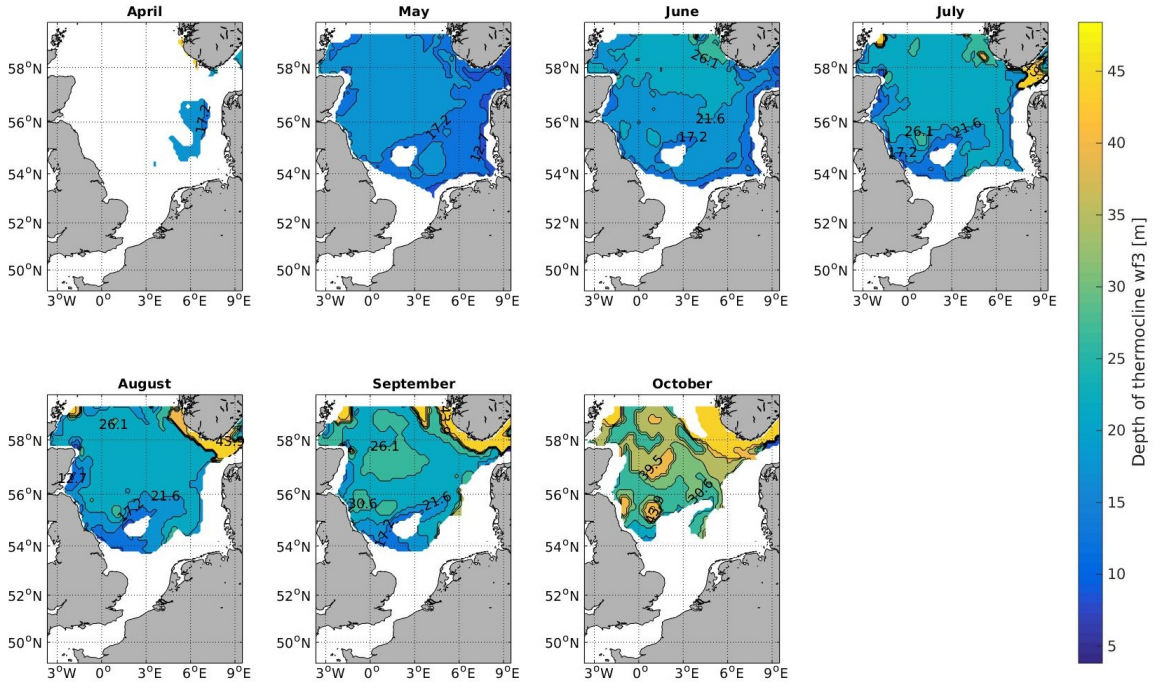

Figure 5.34: Stratification for run wf3 calculated from the location of the maximum gradient of the thermocline from the sea surface [m] from April to October.

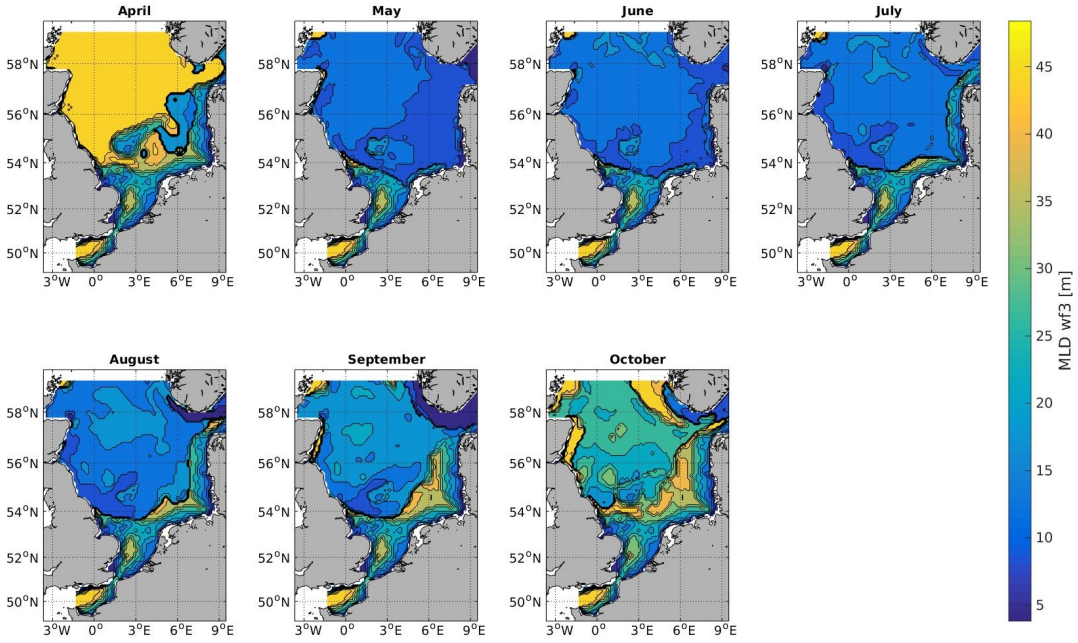

Figure 5.35: MLD [m] for run wf3 calculated from the upper level of the thermocline from April to October.

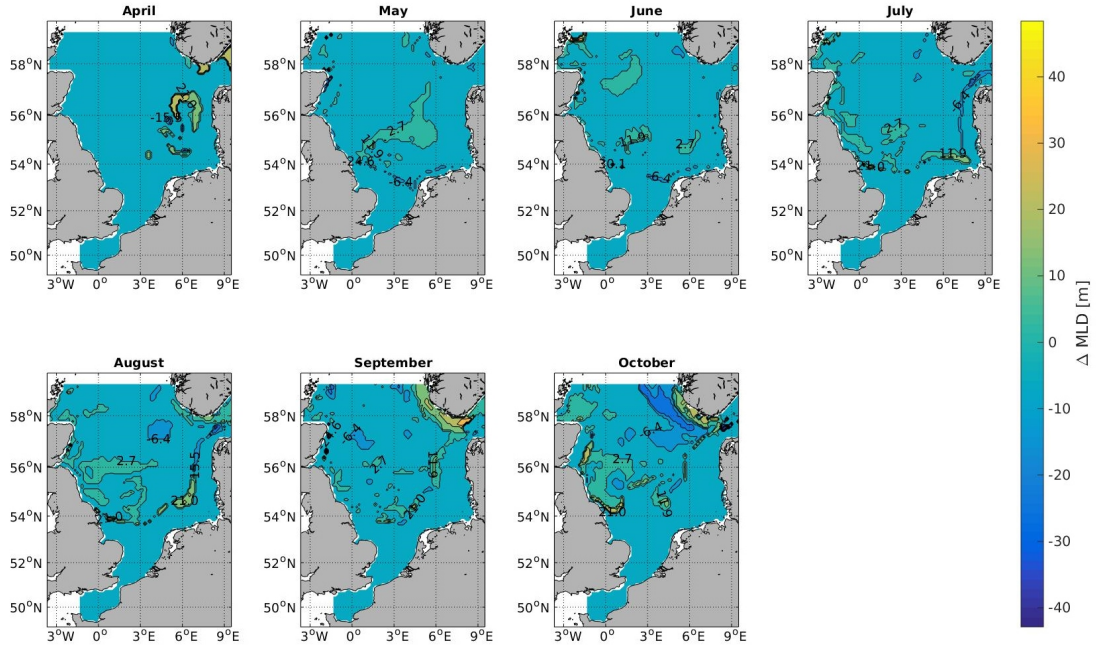

Figure 5.36: Difference in MLD [m] between run wf3 and the reference run (nwf-wf3) calculated from the upper level of the thermocline from April to October.

Chapter 6

Discussion

In this chapter the presented results of changes in primary production and related physical processes due to reduced wind stress by wind farm implementation in the North Sea are discussed. In the previous chapter, the presented yearly means of change in vertically averaged primary production between run wf1 and the reference run nwf, shows a total increase in production by Flagellates of 3 % in run wf1 and a total increase in production by Diatoms of 1 % in run wf1, in addition to changes in distribution of both smaller and larger production. Hence the yearly averaged total primary production in the North Sea is only weakly affected by the change in wind stress by a few percent (Tab. 5.5). However there are geographical variations of change up to order 80 %. Hypotheses of processes in the North Sea as explanation for this change in primary production will be discussed.

6.1 Modelled effect of change in stratification and mixing layer

Reduced wind stress due to power extraction by OWFs in the North Sea was expected to result in less energy received by the water. The smaller amount of energy available for mixing was expected to result in less mixing of the upper surface levels, a more shallow MLD and less nutrient supply from deeper stratified water where nutrient depletion can occur (Sec. 2.2.2). The difference in monthly averaged PEA between run wf1 and the reference run (Fig. 5.19) generally shows that more energy is required to fully mix the water in the south and central North Sea in run wf1 compared to the reference run.

The change in MLD of monthly means in the model domain is larger than expected, with a maximum difference in a grid cell of 40 m (Fig. 5.16). Along the tidal mixing front the largest difference is found at the north part of the shallow tidal bank of the British coast west of Dogger Bank, of up to 30 m more shallow MLD from June to October. Along the European continental coast a more shallow MLD of up to 21 m and a deepening of up to 6.5 m is found. These changes are larger than what was found by (Ludewig, 2015) and (Paskyabi and Fer, 2012). However in the German Bight the change was similar to the maximum 10 m change found by (Ludewig, 2015). A possible reason for areas of large change in MLD may be due to the topography of the North Sea. The surface mixed layer may become connected to the bottom mixed layer by tidal streams in areas with a deepening of the MLD. Areas with a more shallow MLD may become disconnected from the bottom mixed layer.

6.1.1 Change in extent of stratification in the German Bight

Modelled daily changes of day 206 and day 215 with contrasting wind directions, shows different extent of stratification due to a reduced wind stress field (Fig. 5.22). For day 206 in July, with stratification in run wf1 extended closer to the European continent compared to the reference run, a more shallow MLD (Fig. 5.23) is found in large parts of the German Bight. More energy is also required to fully mix the water in this area (Fig. 5.24). The less expansive belt of production along the Dutch, German and Danish coast in run wf1 (Fig. 5.21) may possibly be explained by less mixing in the areas of extended stratification and less nutrients entering the euphotic zone through vertical mixing (Sec. 2.2.2).

While day 206 has less extended stratification than the monthly mean of July for nwf and similar for run wf1, day 215 has an extended stratification compared to the monthly mean of August, for both wf1 and nwf. With the extended stratification in the reference run day 215, a less expansive belt of production along the coastlines is found compared to day 206, possibly explained by a limited supply of nutrients in the euphotic zone. Hence the modelled change in production due to reduced wind stress is smaller for day 215, most likely because of the similar extension of stratification for both run wf1 and the reference run in day 215. However the geographical change is still large.

By comparing modelled monthly mean stratification in run nwf (Fig. 5.10) and run wf1 (Fig. 5.14), it is shown that the large change in extension of the stratification found between the two runs in day 206 is not visible for monthly means of stratification in July, except a small extension towards the Helgoland Bight. This can imply that only some days in summer have a more extended stratification, which is expected to be dependent on wind forcing. The extended stratification found in the German Bight for run wf1 day 206 (Fig. 5.22) is found under northerly wind conditions. The more energy required for mixing in this area shown by the PEA, may indicate that the decrease in wind stress southward downstream of the wind farms results in a more extended stratification in run wf1.

6.1.2 Change in stratification and MLD for the rest of the North Sea

The difference in monthly mean MLD between the runs wf1 and the reference run (Fig. 5.16) shows both deeper and more shallow MLD for run wf1. A pattern of change along the tidal mixing front between the well mixed and the stratified water is found for all stratified months, where the change in MLD generally is more shallow for run wf1. The MLD given by the pycnocline (Fig. 5.17) shows more areas of a deeper MLD in run wf1. A more shallow MLD can imply less mixing in the vertical and hence less nutrients mixed into the euphotic zone, where a smaller production is expected. A deepening of the MLD can imply larger entrainment of nutrients to the euphotic zone where more production is expected. There is also a displacement of the location of the deepest stratification further north-east in the model domain from July to October (Fig. 5.16). However there is no change in wind stress in this northern area so this must be due to other causes than wind mixing.

For both daily and monthly means, geographical changes in primary production by Flagellates is also found in areas where there is no direct link to changes in stratification and MLD, for the stratified months April to October.

6.1.3 Change due to advection

The modelled daily change in primary production by Flagellates day 206, in parts of the German Bight with less primary production in run wf1, was explained by a stronger stratification and less mixing in the given area (Sec. 6.1.1). Further north along the German and Danish coast a deepening of the MLD (Fig. 5.23) and a lower value of PEA (Fig. 5.24) in wf1 is found for parts of this area, even though less production is found (Fig. 5.21). This may be explained by the cyclonic residual circulation in the North Sea from Atlantic water entering at the northern boundary with strong tidal streams along the coast of Britain and the European continental coastline. The residual current are less strong along the Danish coast than in the southern parts of the sea, however if less nutrients are available for production in the German Bight, the cyclonic circulation might transport less nutrient rich water further north and the smaller production is hence found further north despite the deeper MLD. Further north in Skagerrak, the production is again larger in run wf1, which may be explained by a larger amount of nutrients transported from the area of deeper MLD further south.

The area of larger production by Flagellates in day 206 from run wf1, stretching from the coast of Britain towards the Netherlands along the tidal mixing front, is located where the change in MLD (Fig. 5.23) is more shallow and the PEA (Fig. 5.24) is larger than in the reference run where more energy is required for full mixing in large parts of the area. The stratification (Fig. 5.22) is also more shallow along the coast of the British Isles, hence less production would be expected. Further north along the British Isles both less and more energy needed to fully mix the water are found. The cyclonic residual current from tidal waves may possibly transport an increased level of nutrients from the area of more mixing southward. However combined with the more shallow stratification and MLD, it may be more likely that other factors are responsible for the increased primary production.

The wind driven circulation may also affect the advection of water with different values of nutrients due to change in stratification and mixing. Day 206 has a northerly wind direction which can possibly reverse the cyclonic wind driven circulation in the North Sea, and change the advection pattern. However no clear pattern of this was found when comparing change in primary production with change in stratification and mixing for

day 206 and further investigation on circulation is needed.

Changes in primary production is also found where the water is fully mixed by convection or tidal- and wind-induced turbulent mixing for monthly and daily means. In day 206 the area South of Dogger Bank from the coast of Britain to the Netherlands are fully mixed in both wf1 and nwf due to strong tidal streams and no change in PEA is showed. The production is found along the shallow areas outside the coast of Britain in the reference run, but stretches over the deeper areas further offshore in run wf1. South in the Southern Bight more production is found in wf1. The water column is also here fully mixed in both runs. However change in stratification and MLD in more northern parts of the sea, could affect the shallow tidal banks in the south North Sea, because of advection.

6.1.4 Uncertain results

Because of some cases of increased wind stress in the modified wind stress field by the wind farm parameterization (Sec. 4.3), parts of the results may be uncertain for some days in summer. This is the case for the area of larger production along the north part of the British Isles for day 206, where a small area of larger wind stress in run wf1 is found north off the coast of Scotland. This may result in a larger amount of nutrients being transported southward along the British coast giving an increased production, which is shown in run wf1. It may also be visible for other days with lower wind speed in summer, but is not visible for day 215, which show a smaller maximum change in primary production than day 206, but still a substantial geographical change. Hence these uncertain changes are only visible in some days of the summer, and hopefully do not effect the yearly mean change of primary production.

In the English Channel and in the Strait of Dover the largest change of increased annual production by Flagellates is found, of order 80 % change. Wind farms are located in the Southern Bight, but not in the English Channel. Transport of water mainly goes towards the North Sea, however the strong tidal waves may transport water of changed properties to the English Channel (Sec. 2.2.1). The focus in this thesis is not on the English Channel, but the large maximum values in this area is important to have in mind when looking at maximum and total changes. The values of maximum change in pri-

mary production presented in the introduction of this discussion may therefore show a larger increase of primary production than what is modelled in the North Sea north of the Strait of Dover.

6.1.5 Seasonal differences

Changes in primary production are found for all months during the year. The temporal evolution of change in production by Flagellates and Diatoms during year 2008 (Fig. 5.3) show that for Flagellates the production is larger for run wf1 for most of the year. The largest peaks of increased production is found in mid April, June and July for Flagellates (Fig. 5.3), where the maximum increase is of order 30 to 50 % and located off the shallow coast south-west of Dogger Bank for April and in the English Channel in June and July. However as explained in the section above, some of the maximum increased production in run wf1 may be uncertain and larger than production in the area of interest.

For Diatoms almost 100 % maximum change is found both for the spring bloom and the second bloom, where the changes are located in the south and central North Sea for the spring bloom and in the northern, central and southern North Sea for the late summer bloom.

The change in production by Flagellates for months without a seasonal stratification show a maximum difference of up to order 80 %, though the production is smaller than for stratified months and the change will not give a large impact on the total annual production. The change in primary production for both Flagellates and Diatoms for months fully mixed by convection, implies that other factors than seasonal stratification contributes to the change in primary production.

6.2 Effect of other factors

Change in stratification is expected to be one of the main contributors to the change in primary production, but also horizontal and vertical transport by tidal streams and upwelling respectively, effect the primary production. Variability of the wind field in the North Sea is, as well as for stratification, closely connected with circulation (Schrum et al., 2003). Changes in wind speed due to power extraction by OWFs may give changes

in the circulations pattern, but further analysis is needed to investigate this aspect.

Change in vertical transport of upwelling and downwelling induced by OWFs was found by Brostrom (2008); Paskyabi and Fer (2012); Ludewig (2015), where a change in the circulation pattern with upwelling and downwelling zones was shown in the vicinity of a wind farm. Vertical transport is not investigated in this thesis, however the increase in primary production by Flagellates south of Dogger bank found for both daily, monthly and yearly means, may be connected with increased upwelling induced by wind farms. Hence it might be expected that more nutrients are used for primary production in that area and less is left for advection to areas offshore of Germany and Denmark.

Changes in primary production by phytoplankton, which are at the bottom of the marine food chain, are expected to effect higher trophic levels. The bottom-up control (Cury and Shannon, 2004) is characterized by less primary production resulting in less food for secondary production, less abundance of secondary production resulting in less forage fish witch in the end results in a decreased abundance of predators. An increase in primary production will show the opposite response, with increased abundance of the higher trophic levels. Hence both smaller and larger abundance of secondary production are expected to be found, because both larger and smaller primary production are shown from modelled results.

Zooplankton was not investigated in this thesis, which can possibly also be directly effected by the response on changes in the wind stress field, which can lead to a so called wasp-waist effect (Cury and Shannon, 2004), where a direct change in abundance of zooplankton would effect both the lower and higher and trophic levels. Less zooplankton would result in less abundance of higher trophic levels, a bottom-up control as explained above. At the same time less zooplankton would lead to less zooplankton grazing on phytoplankton and hence a larger abundance of phytoplankton. The opposite case of a larger abundance of zooplankton would result in more forage fish and predators and less phytoplankton. Temperature does not control primary production in ECOSMO, however the geographical change in temperature (Fig. 5.20) can effect higher trophic levels from early life stages to adults (Daewel et al., 2011).

6.3 Reduced maximum wind stress deficit

For run wf2, using wind farm parameterization P2 with a smaller maximum specified wind stress deficit than in run wf1, the area of reduced wind stress shows the same extent for run wf1 (Fig. 5.13) and wf2 (Fig. 5.25), but the resulting maximum reduction has a lower value of order 10-20 % in run wf2 (Tab. 5.3) than wf1 (Tab. 5.2). The larger resulting maximum deficit in run wf1 does not give larger effects on change in primary production from the reference run, when comparing run wf1 (Fig. 5.1) and wf2 (Fig. 5.26). However the difference between primary production in run wf1 and wf2 gives a small change (Fig. 5.27). No visible difference between stratification and MLD between run wf1 and wf2 are found. This can imply that a change in the strength of the reduction in wind stress of order 10-20 % for the same affected area is insignificant for the response on the upper ocean.

6.4 Future scenario of wind farm implementation

Run wf3, representing a future situation including all wind farms planned for implementation in the North Sea, shows a considerable extent of wind stress deficit for large wind farms at Dogger Bank compared to smaller wind farms (Fig. 5.31c,f) and a larger maximum wind stress deficit (Tab. 5.4), than wf1 (Tab. 5.2) of order 9 %.

Total averaged production is larger for run wf3 than the reference run of order 2.5 % for Flagellates and 1 % for Diatoms, but smaller than run wf1 and wf2 of order 0.5 % (Tab. 5.5). The stratification in run wf3 shown to have smaller areas of the deepest stratification in north and central parts of the North Sea, than in run wf1, which coincide with larger areas of reduced wind stress in these areas. This can explain the smaller total averaged production found in run wf3, with a more shallow stratification leading to smaller amount of nutrients entering the euphotic zone due to vertical mixing (Sec. 2.2.2).

It is found that a larger number of wind farms and of larger size will give larger areas of wind stress deficit and with increased maximum deficit, compared to run wf1. Hence the number of wind farms and the size of the wind farms seams to play a larger role on effects on the upper ocean than the strength of the wind stress reduction alone.

6.5 The North Sea and OWF implementation

6.5.1 Other years than 2008

Year 2008 was a year of high average wind speed, also in the summer months (Sec. 5.2.1). Only one year was investigated in this thesis, but it is expected that a high wind speed during summer is necessary to create the geographical changes in distribution of primary production for Flagellates. Other years having a lower average wind speed with low wind speed during the whole summer, may still be expected to show a change in geographical distribution of primary production since a change was shown for all months with different wind speeds in year 2008. However lower values of change may be expected, due to the lower winds in summer when the largest production is found. The prevailing wind direction for year 2008 was from south-west (Sec. 5.2.1). Years of other prevailing wind speeds may be expected to have a different extent of stratification and therefore an effect on the primary production (Schrum et al., 2003).

6.5.2 Other geographical locations

The North Sea is a shallow and well mixed sea, where OWE is suitable because of the shallow depth. At the same time the shelf sea has high productivity (Sec. 2.2). From a perspective of marine ecosystem conservation on the co-existence of OWFs and the marine ecosystems, it could be expected that the well mixed water with high productivity along the tidal banks south in the North Sea could be preferable areas for OWE production, with little effect on the ecosystem due to the well mixed water by strong tidal streams. However the large geographical variations in primary production found in this study, is expected to effect the ecosystem dynamics of the North Sea.

In deeper water and areas with weaker tidal currents where wind stress is the main driver of vertical mixing, a larger effect of OWF implementation may be expected.

Chapter 7

Conclusion and outlook

7.1 Main achievements

The less studied effect of OWFs on the marine ecosystem was investigated in this thesis by studying response on primary production. The numerical model ECOSMO, including a wind farm parameterization of reduced wind stress pattern downstream of OWFs, was used to compare runs of different disturbed wind stress with a reference run for year 2008. Physical state parameters related to dynamics of primary production was investigated, with main focus on seasonal stratification. By comparing the main run wf1, representing the present setup of wind farms in the North Sea in 2015, with the reference run nwf, the difference between the two runs was studied for the primary producers Flagellates and Diatoms, and for the temperature and salinity dependent stratification, MLD and PEA. Two other runs with different change in wind stress deficit, a smaller maximum specified wind stress deficit for the present wind farms in the North Sea, wf2, and a future scenario of wind farm implementation in the North Sea, wf3, was compared to the main run. As far as we know this is the first study of its kind modelling OWF effects on primary production using ECOSMO.

In order to be able to do this study a tool for investigation of OWF implementation in the bio-physical model ECOSMO has been developed. It is based on a theoretical approach by Brostrom (2008) in combination with published results of maximum wind speed deficit due to a wind farm as modelled by Ludewig (2015). The theoreti-

cal formula for reduction in wind stress is used for a variable wind field with different wind speed and direction for each wind farm. The wind farm parameterization calculates the desired wind stress pattern based on (Brostrom, 2008) and it calculates a wider and stronger wake for larger wind farms, which is consistent with findings in (Ludewig, 2015). It also calculates the wind stress downstream of the wind farms for different wind directions and wind intensity.

The investigation shows a small change in total averaged primary production by a few percent and a larger change in geographical distribution of up to order 80 %. Hence the total primary production in the North Sea will most likely only be weakly affected by OWF implementation. However the geographical changes in primary production can be expected to give considerable local changes in primary production. Since primary production is at the bottom of the food chain, higher trophic levels are dependent on the amount of phytoplankton available, and hence ecosystem dynamics may change for the entire food web. The geographical changes in primary production show both increase and decrease in production by Flagellates and Diatoms of about equal amount in the areas of interest, but with a larger maximum increase in production for some areas explained in Section 6.1.4. These changes may lead to conflicts if parts of the North Sea gets less primary production and a following change in higher trophic levels. Political and economical issues may arise between countries affected and responsible for the changes.

Change in reduction of wind stress forcing by using a lower maximum wind stress deficit of order 10-20 % in run wf2 compared to wf1, does not show a significant change in primary production when the same setup of OWFs are used for both runs. However a larger number of wind farms and wind farms of larger size gives a different pattern of change in primary production than for a smaller amount of wind farms of smaller size. Hence the modelled results shows that a change in the area covered by wind stress deficit is more significant than a change in the maximum specified wind stress reduction, for response on primary production.

A reduced PEA in the North Sea shows that less energy is found in the water columns due to energy extraction by OWFs and decreased wind-induced turbulent mixing. A change in MLD is found for large parts of the North Sea for the stratified months with

a pattern of change along the tidal mixing front south in the North Sea. The difference here varies between a deepening of 6.5 m to a more shallow MLD of up to 30 m. For daily means of day 206 in July, an extended stratification in the German Bight due to OWE, may explain a decreased primary production by Flagellates in the same area. Change in stratification and mixing due to reduced wind stress may be part of the explanation for changes in distribution of primary production in the North Sea. However large parts of the modelled change in primary production do not show a direct link to change in stratification and MLD. Hence other factors in the North Sea needs further investigation.

7.2 Suggestion for further work

After the work in this thesis it is clear that further studies of response on the marine ecosystem from OWF implementation in the North Sea is needed. Further analysis of the results of this work could be to investigate possible change in circulation pattern for both horizontal and vertical circulation. The horizontal circulation would give more knowledge on horizontal advection of change in primary production, while the vertical circulation would give information about change in upwelling and downwelling patterns induced by OWFs.

Further analysis of production could be a more detailed investigation of Diatoms and investigation of phytoplankton biomass and secondary production by zooplankton. Primary production by Diatoms are characterized having an early spring bloom in the North Sea, before the seasonal stratification occurs. To be able to analyse the change in production possibly due to a diurnal MLD, a detailed analysis of the modelled time evolution during the diurnal cycle would be needed to investigate this aspect. Investigation of phytoplankton biomass in comparison with the primary production could be analysed to verify that less modelled biomass is found in areas where the stratification is extended and less mixing energy is found. Investigation of zooplankton secondary production would also be of interest to see how the higher trophic levels responds to changes in wind stress and distribution of primary production.

However the cases of increased wind stress in a few locations visible for some days in summer, should be studied further to make sure these events do not influence the

results presented in this thesis. A possible solution could be to modify the code to calculate the maximum specified wind stress deficit $\Delta\tau_x$ (Eq. 4.1) for every grid point within the loop of wind stress deficit calculation, and not only for the center grid point of the wind farm.

Further studies using the wind farm parameterization could include investigation of several different wind stress reductions, starting with a small reduction, to investigate whether there is a limit to the reduced wind stress effect for the given OWF setup, on stratification and primary production in the North Sea.

Investigation of other years than 2008, would be of interest to see how a year with lower mean wind speed and particularly lower wind speeds during summer would affect the total and geographical change in primary production. It would also be interesting to see if a year with different prevailing wind direction would give a different distribution of change in primary production.

Other geographical locations with different characteristics could be investigated to give information on which factors that affects the change in primary production. Since ECOSMO is applied to the coupled system North Sea-Baltic Sea and OWF implementation is planned for the Baltic Sea (Global Database, 2016), the Baltic Sea is a good choice for further investigation of response on ecosystem dynamics due to OWF implementation. It is a semienclosed sea with a narrow connection to the North Sea, where tides only play a marginal role (Barthel et al., 2012). Therefore change in primary production due to OWE implementation affected by tidal currents in the North Sea could be compared to the change in primary production with insignificant tidal effects in the Baltic Sea. Effects on primary production due to OWE implementation in deeper water in the North Sea where tidal currents are weaker, could also be investigated to study effects of change in wind stress as the main driver of of vertical mixing.

Appendix A

Wind farm parameterization

A.1 Wind farm parameterization code

The following shows the fortran code for the wind farm parameterization implemented in ECOSMO.

```
      SUBROUTINE ParamNS(tx2d,ty2d,wspeed2d,diru)
      IMPLICIT NONE
! --- Program to parameretize the change in ocean wind stress affected -
!     by wind farms in the North Sea

      INTEGER :: n,m,latdegNW,latminNW,londegNW,lonminNW,latmin,lonmin,
     & i,j
      Parameter (n=207,m=177,latdegNW=65,latminNW=56,londegNW=-4,
     & lonminNW=10)
      REAL :: latddNW,londdNW,A,latddc,londdc,difflat,difflon,latsteps,
     & lonsteps,xc,yc,U10,dir,dir_grad,tetha,numgridL,Akm,Lkm,L,
     & x0,y0,tmp2,pi2,dU10,diff,dtaux_val
      REAL :: taux(m,n),xb(m,n),yb(m,n),lxb(m,n),lyb(m,n),tx2d(m,n),
     & ty2d(m,n),wspeed2d(m,n),diru(m,n),dtaux(m,n)
      REAL ::  dt2,r2,g2,dl2,dlr2,dlrh2,dln2(m),rdln2(m),rad2,dth2,
     &  dlvo2(m),dlvu2(m),gh2,rdt2,dt22,r42,
     &  coru2(m),corv2(m),dtrdln2(m),dtdlr2
      REAL :: phigrad2,yamgrad2

      common /gitter/ dt2,r2,g2,dl2,dlr2,dlrh2,dln2(m),rdln2(m),rad2,
     *  dth2,dlvo2(m),dlvu2(m),gh2,rdt2,dt22,r42,
     *  coru2(m),corv2(m),dtrdln2(m),dtdlr2

      common /begin_xy/ phigrad2,yamgrad2


! ---------------------------------------------------------------------

      pi2 = 4.*atan(1.)


! --- from degrees minutes to decimal degrees in point NW in model domain
      latddNW=latdegNW+(latminNW/60.)
      IF (londegNW.LT.0) THEN
         londdNW=londegNW-(lonminNW/60.)
      ELSE
         londdNW=londegNW+(lonminNW/60.)
      END IF

! --- taux:

         DO j=1,n
            DO i=1,m
              taux(i,j)=SQRT(tx2d(i,j)**2.+ty2d(i,j)**2.)
              taux(i,j)=ABS(taux(i,j))
            END DO
         END DO
```

```
! --- Start loop over wind farms (now: operational NS)

      OPEN(UNIT=191,FILE='/work/ioe065/ecosmo/input_windfarms/'//
     & 'WindfarmsNS_operational.txt')
  702 CONTINUE
      READ(191,*,END=192) A,latddc,londdc


! --- calculation of farm center point coordinates


          difflat=latddNW-latddc      ! distance between NWpoint and cpoint
          difflon=-londdNW+londdc

          latsteps=difflat/phigrad2     !number of grid steps from NW point [#]
          lonsteps=difflon/yamgrad2     !number of grid steps from NW point [#]

          yc=latsteps
          xc=lonsteps


! --- value of wspeed,diru in point (xc,yc)

          U10=wspeed2d(NINT(yc),NINT(xc))
          U10=ABS(U10)


          IF(U10.LT.3.5 .OR. U10.GT.25.)THEN            !within cut-in/cut-out speed
            GOTO 750
          END IF

! --- calculate dir in radians from diru in (yc,xc)

          dir_grad=diru(NINT(yc),NINT(xc))

          dir_grad=dir_grad+180.
          if(dir_grad.ge.360.)then
             dir_grad=dir_grad-360.
          end if


          dir=dir_grad*rad2


! --- Disturbed wind stress by one wind farm

          dtaux_val=0.001334*U10**2.061

           diff=taux(NINT(yc),NINT(xc))-dtaux_val
           dtaux=dtaux_val
```

```
! --- Make sure dtaux is not lager than taux
           DO j=1,n
             DO i=1,m
               IF(dtaux(i,j).GT.taux(i,j))THEN
                 dtaux(i,j)=taux(i,j)
               END IF
             END DO
           END DO


! --- Characteristics of farm - Broström coordinates

          Lkm=SQRT(A)        !Characteristic length of wind farm in Br-dir [km]

          L=Lkm*1000.          !Characteristic length of wind farm in Br-dir [m]

          numgridL=L/dln2(NINT(yc)) !number of grids L covers

          x0=xc-(numgridL/2.)*COS(dir)     !origin of Broström coordinate system
          y0=yc-(numgridL/2.)*SIN(dir)


! --- DO Loop over model domain to calculate the change in wind stress by wind farms uing
Broström calculations

          DO j=1,n
             DO i=1,m
               xb(i,j)=COS(dir)*(j-x0)-SIN(dir)*(i-y0)
               yb(i,j)=SIN(dir)*(j-x0)+COS(dir)*(i-y0)

               lxb(i,j)=xb(i,j)*dln2(i)         !distance of each step in Br.coord
               lyb(i,j)=yb(i,j)*dl2

               IF(xb(i,j).GE.0.)THEN
                 tmp2=(0.8*L+0.2*lxb(i,j))
                 taux(i,j)=taux(i,j)-dtaux(i,j)*EXP(-(2.*lyb(i,j)/tmp2)
     & **2.)*EXP((1-lxb(i,j))/L)*((lxb(i,j))/L)
                 tx2d(i,j)=taux(i,j)*COS(dir)
                 ty2d(i,j)=taux(i,j)*SIN(dir)
               END IF

             END DO
           END DO

  750 CONTINUE


      GOTO 702
  192 CONTINUE
      CLOSE(191)

      END
```

A.2 Maximum wind stress deficit of a wind farm

The METRAS-simulation of OWF effect on the wind field due to different geostrophic wind speeds from (Ludewig, 2015) are here presented. In this thesis the result was used for calculation of the maximum specified wind stress deficit of a wind farm $\Delta\tau_x$.

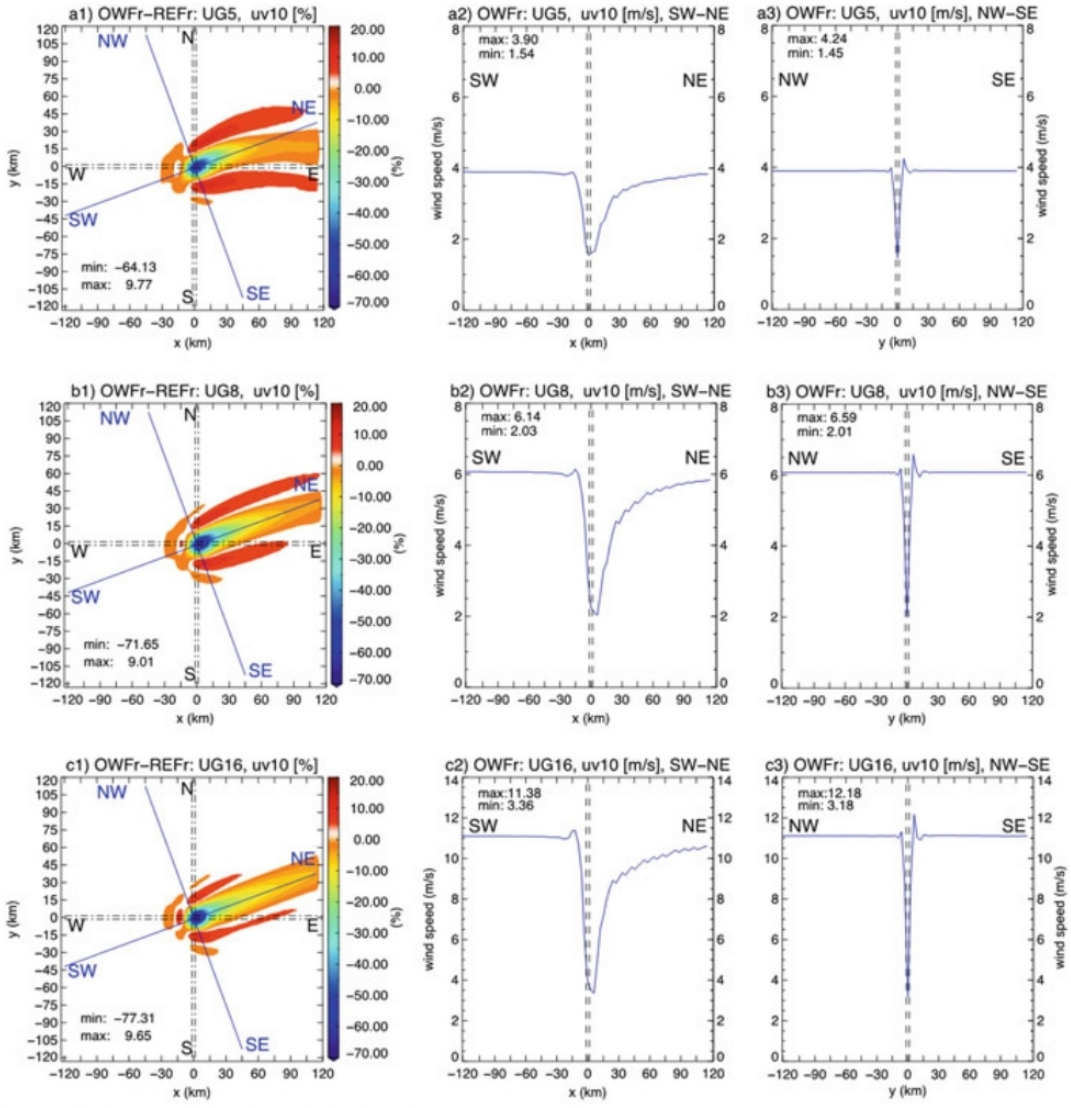

Figure A.1: Wind deficit due to a wind farm (Ludewig, 2015).

Bibliography

Arakawa, A. and Lamb, V. R. (1977). Computational design of the basic dynamical processes of the UCLA general circulation model. *Methods in computational physics*, 17:173—-265.

Backhaus, J. O. and Hainbucher, D. (1987). A Finite Difference General Circulation Model for Shelf Seas and Its Application to Low Frequency Variability on the North European Shelf. In Nihoul, J. C. J. and Jamart, B. M., editors, *Three-Dimensional Models of Marine and Estuarine Dynamics*, volume 45 of *Elsevier Oceanography Series*, pages 221–244. Elsevier.

Bailey, H., Brookes, K., and Thompson, P. (2014). Assessing environmental impacts of offshore wind farms: lessons learned and recommendations for the future. *Aquatic Biosystems*, 10(1):1–13.

Barthel, K., Daewel, U., Pushpadas, D., Schrum, C., Arthun, M., and Wehde, H. (2012). Resolving frontal structures: On the payoff using a less diffusive but computationally more expensive advection scheme. *Ocean Dynamics*, 62(10-12):1457–1470.

Boettcher, M., Hoffmann, P., Lenhart, H.-J., Schluenzen, K. H., and Schoetter, R. (2015). Influence of large offshore wind farms on North German climate. *METEOROLOGISCHE ZEITSCHRIFT*, 24(5):465–480.

Brostrom, G. (2008). On the influence of large wind farms on the upper ocean circulation. *Journal of Marine Systems*, 74(1-2):585–591.

Brown, E., Colling, A., Park, D., Phillips, J., Rothery, D., and Wright, J. (2001). Chapter 3 - Ocean currents. In Brown, E., Colling, A., Park, D., Phillips, J., Rothery, D.,

and Wright, J., editors, *Ocean Circulation (Second Edition)*, pages 37–78. Butterworth-Heinemann, Oxford.

Burton, T., editor (2011). *Wind energy handbook*. Wiley, Chichester, 2nd ed. edition.

Calaf, M., Meneveau, C., and Meyers, J. (2010). Large eddy simulation study of fully developed wind-turbine array boundary layers. *Physics of Fluids*, 22(1):1–16.

Christiansen, M. B. and Hasager, C. B. (2005). Wake effects of large offshore wind farms identified from satellite SAR. *Remote Sensing of Environment*, 98(2-3):251–268.

Coley, D. (2011). *Energy and climate change: creating a sustainable future*. John Wiley \& Sons.

Collins, S. N., James, R. S., Ray, P., Chen, K., Lassman, A., and Brownlee, J. (2013). Grids in Numerical Weather and Climate Models. *Grids in Numerical Weather and Climate Models, Climate Change and Regional/Local Responses, Dr Pallav Ray (Ed.)*.

Conkright, M., Locarnini, R., Garcia, H., O'Brien, T., Boyer, T., Stephens, C., and Antonov, J. (2002). World ocean atlas 2001: objective analyses, data statistics, and figures, CD-ROM documentation. *National Oceanographic Data Center, Silver Spring, MD*, page 17.

Cury, P. and Shannon, L. (2004). Regime shifts in upwelling ecosystems: observed changes and possible mechanisms in the northern and southern Benguela. *Progress in Oceanography*, 60(2–4):223–243.

Daewel, U. and Schrum, C. (2013). Simulating long-term dynamics of the coupled North Sea and Baltic Sea ecosystem with ECOSMO II: Model description and validation. *Journal of Marine Systems*, 119-120:30–49.

Daewel, U., Schrum, C., and Temming, A. (2011). Towards a more complete understanding of the life cycle of brown shrimp (Crangon crangon): modelling passive larvae and juvenile transport in combination with physically forced vertical juvenile migration. *FISHERIES OCEANOGRAPHY*, 20(6):479–496.

Das, A. (2014). An empirical model of power curve of a wind turbine. *Optimization, Modeling, Simulation, and Economic Aspects*, 5(3):507–518.

Davenport, A. (1963). The relationship of wind structure to wind loading: Proc. of the Conf. of Wind Effects on Building and Structures. *Teddington*, 1963:54—-102.

de Boer, G. J., Pietrzak, J. D., and Winterwerp, J. C. (2008). Using the potential energy anomaly equation to investigate tidal straining and advection of stratification in a region of freshwater influence. *Ocean Modelling*, 22(1–2):1–11.

de Boyer Montégut, C., Madec, G., Fischer, A. S., Lazar, A., and Iudicone, D. (2004). Mixed layer depth over the global ocean: An examination of profile data and a profile-based climatology. *Journal of Geophysical Research: Oceans*, 109(C12):n/a—-n/a.

Ehrlich, R. (2013). Wind Power. In *Renewable Energy: a first cource*, chapter 7, pages 183–216. CRC Press.

European Wind Energy Association (2015). Wind energy scenarios for 2030. Technical report.

Eurostat (2015). Europe 2020 indicators - climate change and energy. http://ec.europa.eu/eurostat/statistics-explained/index.php/Europe_2020_indicators_-_climate_change_and_energy#More_renewable_energy_means_fewer_EU_emissions. 23.05.2016.

Fitch, A. C., Olson, J. B., and Lundquist, J. K. (2013). Parameterization of wind farms in climate models. *Journal of Climate*, 26(17):6439–6458.

Fitch, A. C., Olson, J. B., Lundquist, J. K., Dudhia, J., Gupta, A. K., Michalakes, J., and Barstad, I. (2012). Local and Mesoscale Impacts of Wind Farms as Parameterized in a Mesoscale NWP Model. *Monthly Weather Review*, 140(9):3017–3038.

G. Monterey, S. L. (1997). Seasonal variability of mixed layer depth for the world ocean. *NOAA ATLAS NESDIS*, 14(Washington D.C.).

Geyer, B., Weisse, R., Bisling, P., and Winterfeldt, J. (2015). Climatology of North Sea wind energy derived from a model hindcast for 1958-2012. *JOURNAL OF WIND ENGINEERING AND INDUSTRIAL AERODYNAMICS*, 147:18–29.

Global Database (2016). Offshore Wind Farms. http://www.4coffshore.com/windfarms/. 11.10.2015.

Halava (2010). Map of the North Sea. https://commons.wikimedia.org/wiki/File:North_Sea_map-en.png. 01.02.2016.

Harten, A. (1983). High resolution schemes for hyperbolic conservation laws. *Journal of Computational Physics*, 49(3):357–393.

Holmes, J. D. (2015). *Wind loading of structures*. CRC Press.

Janssen, F., Schrum, C., and Backhaus, J. O. (1999). A climatological data set of temperature and salinity for the Baltic Sea and the North Sea. *Deutsche Hydrografische Zeitschrift*, 51(9):5–245.

Jongbloed, R. H., van der Wal, J. T., and Lindeboom, H. J. (2014). Identifying space for offshore wind energy in the North Sea. Consequences of scenario calculations for interactions with other marine uses. *Energy Policy*, 68:320–333.

Kalnay, E., Kanamitsu, M., Kistler, R., Collins, W., Deaven, D., Gandin, L., Iredell, M., Saha, S., White, G., Woollen, J., Zhu, Y., Chelliah, M., Ebisuzaki, W., Higgins, W., Janowiak, J., Mo, K. C., Ropelewski, C., Wang, J., Leetmaa, A., Reynolds, R., Jenne, R., and Joseph, D. (1996). The NCEP/NCAR 40-year reanalysis project. *BULLETIN OF THE AMERICAN METEOROLOGICAL SOCIETY*, 77(3):437–471.

Ludewig, E. (2015). *On the Effect of Offshore Wind Farms on the Atmosphere and Ocean Dynamics*, volume 31 of *Hamburg Studies on Maritime Affairs*. Springer International Publishing, Cham, Cham.

Mann, K. H. (2006). *Dynamics of marine ecosystems : biological-physical interactions in the oceans*. Blackwell Publ., Malden, Mass, 3rd. ed. edition.

Manwell, J. F., McGowan, J. G., and Rogers, A. L. (2010). *Wind energy explained: theory, design and application*. John Wiley \& Sons.

Marshall, J. and Plumb, R. A. (2007). *Atmosphere, Ocean and Climate Dynamics : An Introductory Text*. Academic Press, Burlington, MA, USA.

Matthias, V., Aulinger, A., and Quante, M. (2008). Adapting {CMAQ} to investigate air pollution in North Sea coastal regions. *Environmental Modelling & Software*, 23(3):356–368.

Moataz, M. (2011). Sea Water Properties Function. http://www.mathworks.com/matlabcentral/fileexchange/31210-sea-water-properties-function/content/swp.m. 2016-01-10.

Nauw, J., De Haas, H., and Rehder, G. (2015). A review of oceanographic and meteorological controls on the North Sea circulation and hydrodynamics with a view to the fate of North Sea methane from well site 22/4b and other seabed sources. *Marine and Petroleum Geology*, 68:861.

Nielsen, M. H. and John, M. S. (2003). Inter-and intra-annual variations in the stratification, timing, and intensity of phytoplankton blooms in the Central North Sea in the 1990s. *ICES Marine Science Symposia*, 219:384—-386.

Orlanski, I. (1976). A simple boundary condition for unbounded hyperbolic flows. *Journal of Computational Physics*, 21(3):251–269.

Paskyabi, M. B. (2015). Offshore Wind Farm Wake Effect on Stratification and Coastal Upwelling. *Energy Procedia*, 80:131–140.

Paskyabi, M. B. and Fer, I. (2012). Upper Ocean Response to Large Wind Farm Effect in the Presence of Surface Gravity Waves. *Energy Procedia*, 24(0):245–254.

Pohlmann, T. (1996). Calculating the annual cycle of the vertical eddy viscosity in the North Sea with a three-dimensional baroclinic shelf sea circulation model. *Continental Shelf Research*, 16(2):147–161.

Redfield, A. C. (1934). On the proportions of organic derivatives in sea water and their relation to the composition of plankton. *University press of liverpool Liverpool, UK*.

Rodhe, J., Tett, P., and Wulff, F. (2006). THE BALTIC AND NORTH SEAS: A REGIONAL REVIEW OF SOME IMPORTANT PHYSICAL-CHEMICAL-BIOLOGICAL INTERACTION PROCESSES (20, S). *Citeseer*.

Schrum, C. (1997). Thermohaline stratification and instabilities at tidal mixing fronts: results of an eddy resolving model for the German Bight. *Continental Shelf Research*, 17(6):689–716.

Schrum, C., Alekseeva, I., and St. John, M. (2006). Development of a coupled physical–biological ecosystem model ECOSMO. *Journal of Marine Systems*, 61(1-2):79–99.

Schrum, C. and Backhaus, J. A. N. O. (1999). Sensitivity of atmosphere–ocean heat exchange and heat content in the North Sea and the Baltic Sea. *Tellus A*, 51(4):526–549.

Schrum, C., Siegismund, F., and JOHN, M. (2003). Decadal variations in the stratification and circulation patterns of the North Sea. Are the 1990s unusual. *ICES J Mar Sci, Symp Ser*, 219:121—-131.

Slagstad, D. (1992). SEA-ICE AND WIND - EFFECTS ON PRIMARY PRODUCTIVITY IN THE BARENTS SEA.

Stewart, R. H. (2008). *Introduction to physical oceanography*. Citeseer.

Stull, R. B. (1989). *An introduction to boundary layer meteorology*. Atmospheric sciences library. Kluwer Academic Publishers, Dordrecht, 2nd reprin edition.

Sündermann, J. and Pohlmann, T. (2011). A brief analysis of North Sea physics. *Oceanologia*, 53(3):663–689.

Sverdrup, H. (1953). On conditions for the vernal blooming of phytoplankton. *Journal du Conseil*, 18(3):287—-295.

Thomsen, K. E. (2012). Chapter One - What Is an Offshore Wind Farm? In Thomsen, K. E., editor, *Offshore Wind*, pages 1–7. Elsevier, Boston.

Thorpe, S. A. (2007). *An introduction to ocean turbulence*. Cambridge University Press, Cambridge.

Toba, Y. and Jones, I. S. (2001). *Wind Stress over the Ocean*. Cambridge University Press.

Vanhellemont, Q. and Ruddick, K. (2014). Turbid wakes associated with offshore wind turbines observed with Landsat 8. *Remote Sensing of Environment*, 145:105–115.